LABORATORY EVALUATION OF PILES INSTALLED WITH VIBRATORY DRIVERS

Final Report

Volume 1 of 2

Prepared for

National Cooperative Highway Research Program
Transportation Research Board
National Research Council

M. W. O'Neill and C. Vipulanandan

University of Houston
Houston, Texas
NCHRP Project 24-3

December, 1988

LABORATORY EVALUATION OF PILES INSTALLED WITH VIBRATORY DRIVERS

Final Report

Volume 1 of 2

Prepared for

National Cooperative Highway Research Program
Transportation Research Board
National Research Council

M. W. O'Neill and C. Vipulanandan

University of Houston
Houston, Texas
NCHRP Project 24-3

December, 1988

TABLE OF CONTENTS

LIST OF FIGURES

LIST OF TABLES

Acknowledgments

The research reported herein was performed under NCHRP Project 24-3 by the Department of Civil Engineering of the University of Houston. It was supervised and performed by the Principal Investigators, Professors Michael W. O'Neill and Cumaraswamy Vipulanandan. They are grateful for the expert technical contributions provided by Daniel Wong and Mauricio Ochoa, Research Assistants at the University of Houston, who conducted the laboratory tests under the supervision of the principal investigators and who reduced most of the data. Appreciation is also expressed to Will Rainey and Charles Deckert of Raymond Technical Facilities, Inc, who designed the vibro-driver, to Roy Henson of the Department of Civil Engineering of the University of Houston, who developed the electronics systems and who assisted with the tests, and to numerous graduate and undergraduate students of the principal investigators, who assisted with placement, removal and drying of the sand. Recognition is also given the Waterways Experiment Station of the U. S. Army Corps of Engineers, which shared information relative to parallel studies of the behavior of piles installed by vibro-driving.

Abstract

This report presents the results of a large-scale laboratory study on the basic behavior of displacement piles installed with vibratory drivers compared to impact hammers and the influence of various soil and driver parameters on the behavior of piles. In order to achieve the desired goals, a model testing system consisting of a long sand column capable of simulating deep sand deposits, instrumented 4-in.-diameter closed-ended pile, vibratory driver and impact hammer was designed and built. Among the driver parameters investigated are frequency, bias mass and dynamic force (eccentric moment) and sand parameters such as grain size, relative density (65 and 90%) and in-situ effective stress (10 and 20 psi). Two uniform sands with effective grain sizes of 0.2 mm and 1.2 mm were selected for this study, and a total of 22 large-scale model tests were performed.

The optimum frequency for the test conditions, selected based on the maximum rate of penetration, was 20 Hz and was independent of bias mass and soil conditions. Among the variables investigated, the relative density of sand had the greatest effect on the rate of penetration during vibro-driving. Penetration rate also increased with increasing bias mass and decreasing in-situ horizontal stress. Grain size had a smaller, and variable, effect on rate of penetration and on bearing capacity. Impact-driven piles in sand with 65% relative density developed 25% higher shaft resistance and 15 to 20% higher toe resistance in compression than the vibro-driven piles, but this trend was completely reversed at 90% relative density, where the vibro-driven pile exhibited better static performance than the impact-driven pile. The uplift resistance that developed along the shaft of both vibro-driven piles and impact driven piles was 75% of the corresponding resistance developed in compression. Restriking of vibro-driven piles in sand with 65% relative density produced a very small increase in compression capacity, but there was no clear trend for relative density of 90%.

A design method has been proposed to predict the bearing capacity of a vibro-driven pile from rate of penetration, power delivered to the pile head and soil conditions. This model should be verified or modified with field data before using it in design.

Summary

In order to develop a better understanding of the behavior of vibro-driven piles, a detailed, large-scale laboratory study was undertaken. The overall objective of this study was to evaluate the load-deformation behavior of piles installed with vibratory drivers and compare their performance with impact-driven piles. Specific objectives included: (1) a comparison of load-deformation behavior of piles installed with vibratory drivers and impact hammers; (2) the identification of soil parameters that significantly affect the load-deformation behavior of piles installed with vibratory drivers; (3) a comparison of load-deformation behavior of piles installed with vibratory drivers with and without restriking using an impact hammer, to evaluate the effect of restriking; (4) the development of a predictive method to determine the bearing capacity of vibro-driven piles. In order to achieve the desired goals, a model testing system consisting of a long sand column capable of simulating deep sand deposits, an instrumented 4-in.-diameter, closed-ended pipe (displacement-type) pile, vibratory driver and impact hammer was designed and built. Among the driver parameters investigated were frequency, bias mass and dynamic force (eccentric moment) and sand parameters such as grain size, relative density and in-situ effective stress. The effective confining pressure of 10 psi and 20 psi were used to simulate pile penetrations on the order of 50 to 100 feet. Two uniform sands with effective grain sizes of 0.2 mm and 1.2 mm were selected and deposited at relative densities of 65% and 90% to simulate contraction and dilation conditions. A total of 22 large-scale model tests were performed.

The optimum frequency for the testing conditions, selected based on the maximum rate of penetration, was 20 Hz and was independent of bias mass and soil conditions. Among the variables investigated, the relative density of sand had the greatest effect on the rate of penetration during vibro-driving. The penetration rate

also increased with increasing bias mass and decreasing in-situ horizontal effective stress. Effective grain size had a less significant effect on penetration rate than did relative density or horizontal effective stress. Impact-driven piles in sand with 65% relative density sand developed 25% higher shaft resistance and 15 to 20% higher toe resistance in compression than the vibro-driven piles, but this trend was completely reversed at 90% relative density, where the vibro-driven pile exhibited better static performance than the impact-driven pile. The uplift resistance that developed along the shaft of both vibro-driven piles and impact-driven piles was 75% of the corresponding resistance developed in compression. Restriking of vibro-driven piles in sand with 65% relative density sand produced a small increase in compression capacity, but there was no clear trend for a relative density of 90%.

From the test results it was clear that the pile-head acceleration, velocity of penetration and power delivered to the pile head were important factors affecting the vibro-driving of the test piles. A candidate design method has been proposed, based on an analysis of the laboratory test data, to predict the bearing capacity of a vibro-driven displacement pile from rate of penetration, power delivered to the pile head (which is related to pile-head acceleration) and soil conditions. This method also could be used to select the vibratory driver parameters needed install a pile to achieve a desired bearing capacity. This method should be verified with field data before using it in design, however.

CHAPTER 1

Introduction and Research Approach

Piles are usually installed by impact driving or by the use of a vibrator affixed to the head of the pile. A vibrator, or "vibro-driver," depicted schematically in Fig. 1, produces a dynamic, sinusoidal, vertical forcing function at frequencies ranging from as low as 5 Hz to as high as 140 Hz. A vibratory driver typically consists of a vibrating element (eccentric moments produced by unbalanced counterrotating masses shown in Fig. 1), bias mass, isolation springs between the bias mass and the vibrating element and a means of connecting the vibrating element to the pile. The bias mass performs the function of producing a near-static compression force on the pile that, when superimposed on the dynamic force produced by the vibrating element, assists in the driving of the pile. This mass is prevented from vibrating in phase with the vibrating element by means of the isolation springs, which are of such a stiffness to assure that the resonance frequency of the bias mass-isolation spring system is considerably below the operating frequency of the vibrator. However, while the bias mass aids in pushing the pile, some of the energy generated by the vibrating element is dissipated in the production of low-frequency motion of the bias mass. The pile-vibrator connection is usually a chuck-type or pinned connection, whose detailed design is important in the prevention of damage to the pile as the vibrator is in operation and which may also be a source of energy losses.

Vibratory drivers have been used for installing piles in many parts of the world since the early 1930's as an alternative to more conventional impact hammers. In

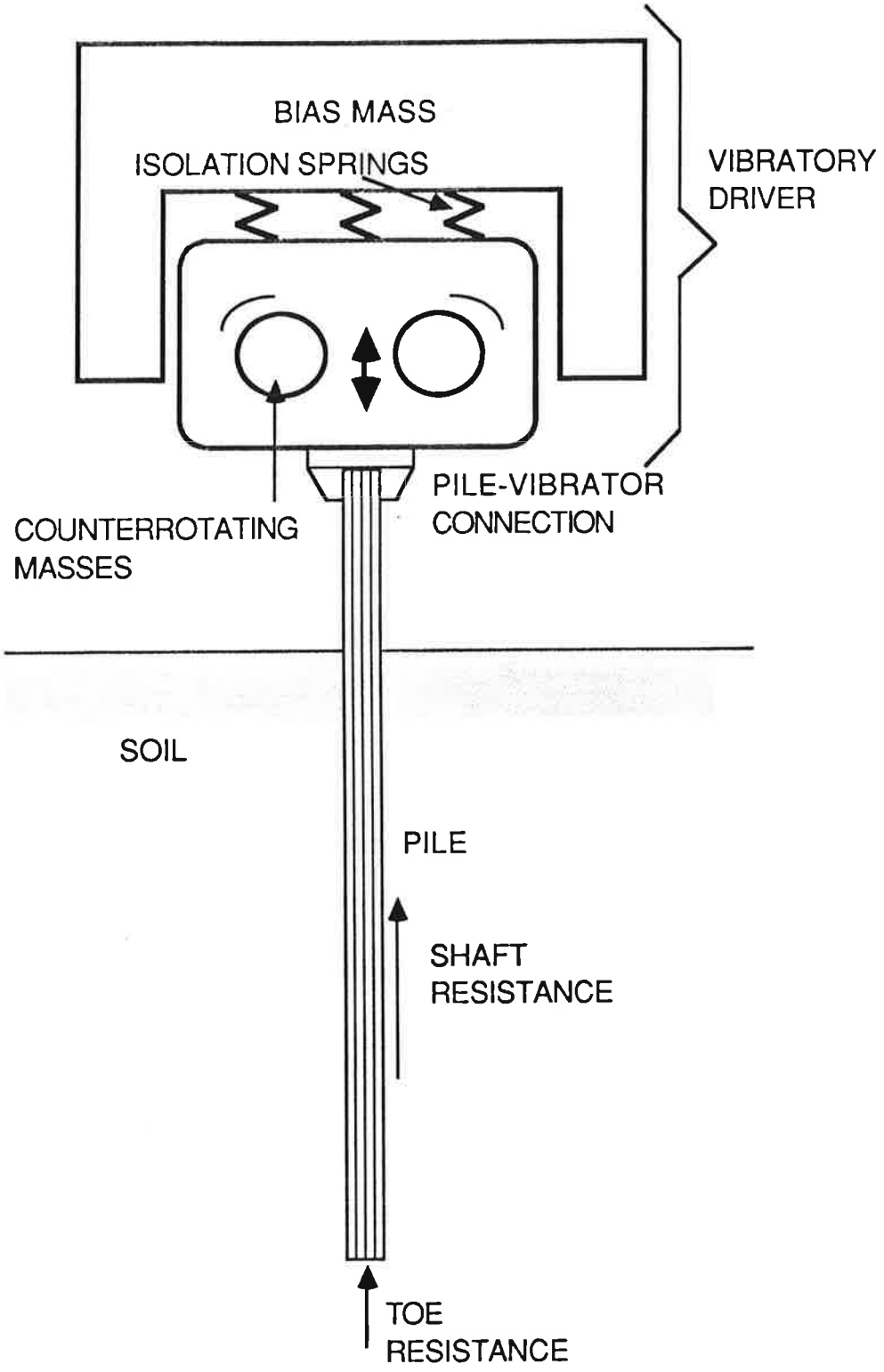

Fig. 1. Schematic of Vibro-Driver and Pile

recent years vibratory pile drivers have gained popularity with contractors relative to impact drivers because they produce less noise and less damage to piles during driving and permit significantly faster rates of penetration in favorable soil conditions (generally, cohesionless soils). Vibratory pile drivers have not gained wide acceptance in the United States, except for the installation and extraction of non-bearing piles such as sheet piles, because the engineering community is generally unfamiliar with this method of installation and because there are uncertainties regarding the estimation of ultimate bearing capacity. Due to these uncertainties, restriking a vibro-driven pile with an impact hammer is often required to assure that a pile has developed a design bearing capacity, but this process greatly reduces the economic benefits of using vibratory drivers.

A limited number of laboratory model studies and full-scale studies on vibro-driven piles have been reported in the literature, as summarized in Appendix A. These studies relate vibratory driver parameters, such as dynamic force, displacement amplitude, frequency and bias mass to the driveability (rate of penetration) and the static bearing capacity of the pile. Although past studies are important, very little has been done to investigate the influence of the soil parameters (particle size, volume change characteristics, strength) and in-situ stress conditions on the performance of vibro-driven piles. In order to develop more accurate predictive methods for the ultimate bearing capacity and load-movement behavior of vibro-driven piles, induced residual stresses and the magnitudes and distribution of shaft resistance along the pile and toe resistance (Fig. 1) must be understood in the context of the properties of the soil. As a step towards developing a better understanding of the behavior of vibro-driven piles in saturated cohesionless soil, a detailed, large-scale laboratory experimental study was undertaken.

RESEARCH PROBLEM STATEMENT AND OBJECTIVE

Research Problem Statement

State Departments of Transportation often are requested by contractors to permit the use of vibratory drivers in place of more conventional impact hammers to install piles. Vibratory pile drivers can provide substantial savings by reducing the amount of driving time to final penetration under certain soil conditions. However, the lack of a reliable dynamic method of estimating bearing capacity limits their usefulness. Presently, the most common method to determine capacity is to restrike the pile with an impact hammer, but the validity of this method is unproven, and the extra operation reduces the potential savings.

Developing a reliable method for dynamically determining bearing capacity of piles installed with vibratory drivers is a complex problem. The U.S. Army Corps of Engineers has been involved recently in the evaluation of field studies to compare the performance of vibratory drivers and impact hammers. To supplement this activity, laboratory studies are needed to provide insight into the basic behavior of piles installed with vibratory drivers compared to impact hammers and the influence of various soil parameters on the behavior of piles. Laboratory studies will also assist in the design of future field tests and provide insights into the analysis of their results.

Objectives

The overall objective of this study is to evaluate the load-deformation behavior of piles installed in the laboratory with vibratory drivers. Specific objectives include: (1) a comparison of load-deformation behavior of piles installed with vibratory drivers and impact hammers; (2) the identification of soil parameters that significantly affect load-deformation behavior of piles installed with vibratory drivers; (3) a comparison

of load-deformation behavior of piles installed with vibratory drivers with and without restriking using an impact hammer, to evaluate the effect of restriking; and (4) the development of a recommended predictive method of determining the bearing capacity for further field verification.

SCOPE OF STUDY

Vibro-drivers are generally grouped as low-frequency drivers (up to 40 Hz), which operate mainly by reducing soil resistance through excitation of the soil particles and, perhaps, simultaneous buildup of excess pore water pressure, and high-frequency drivers (between 40 Hz and 140 Hz), which often operate at the free natural frequency or second harmonic frequency of the pile, which in turn provides significant amplification of the forcing function and more rapid penetration. Neither type of driver is considered generally effective in deposits of cohesive soil, and such soil was therefore excluded from the laboratory study. The most popular drivers in operation are the low-frequency type, because they are easier to maintain mechanically, whose operating frequencies are from about 5 Hz to 40 Hz. This laboratory study was limited to investigating the performance of low-frequency vibro-drivers because of the predominance of their usage.

A reusable, instrumented, 4-inch diameter, closed-ended pipe pile was used as the test pile in this study. The effects of driving this pile with both a vibro-driver and an impact hammer into two uniformly graded sands, with effective grain sizes of 0.2 mm and 1.2 mm, confined in a test chamber were investigated. Since most piles that support transportation structures in submerged granular soils will be driven to depths in the range of 50 to 100 feet, it was decided to simulate the mean effective stresses that

occur in soil masses between the ground surface and these depths in the test chamber. Installation and loading tests were therefore conducted at effective confining pressures of 10 psi (simulating a pile with a 50-foot penetration; i. e., 25 feet to the middepth of the pile times a buoyant unit soil weight of 57.6 pcf = 1440 psf, or 10 psi) and 20 psi (simulating a pile with a 100-foot penetration) under an isotropic stress state and under conditions of K_o = 0.5 in the chamber to duplicate typical in-situ vertical and horizontal stresses. The parameters that were investigated in relation to driving and bearing capacity of vibro-driven piles were the driver frequency, weight of the bias mass, eccentric moment, soil particle size, relative density and in-situ stress conditions. Performance in static compression and uplift of piles installed with a vibratory driver was compared to piles installed with a comparable impact hammer. A method for determining the bearing capacity of vibro-driven piles was developed based on this laboratory model study, which should be verified or modified based on properly developed field experiments prior to implementation for design. An appropriate followup program is recommended in Chapter 4.

RESEARCH APPROACH

In order to achieve the desired goals, a model testing system was designed, built and appropriately instrumented. The testing system included a long sand column, pile, vibratory driver, impact hammer and data acquisition equipment. The sand column was formed in a containment vessel 30 inches in diameter and 100 inches in height. The containment vessel was designed to apply confining pressures in any selective manner to simulate various in-situ stress conditions and to submerge the sand. A reusable, instrumented, closed-ended steel pipe ("displacement pile") with a 4-inch

diameter and 0.188-inch wall thickness was repeatedly driven, floowed by the performance of compression and uplift loading tests. The test pile was instrumented to measure force and acceleration at the pile head and toe, lateral total soil and pore water pressure at the wall of the pile 1.4 diameters above the toe, total lateral soil pressure against the pile wall at the middepth of the pile, load distribution along the pile (static testing) and pile displacement. Soil particle size, volume change characteristics (contraction and dilation under shear) and internal and interface (soil-steel) friction angles and in-situ stress conditions are considered to exert the strongest influence on vibratory pile driving. Hence, two uniform siliceous sands with effective grain sizes of 0.2 mm (fine San Jacinto River Sand, or "SJR" Sand) and 1.2 mm (coarse Blasting Sand, or "BLS" Sand) were selected for testing. To represent contraction and dilation conditions, these soils were deposited in the test chamber at relative densities of 65% and 90%. This range of relative density is one of practical interest, since values of less than about 50 - 55% are rarely found in natural deposits, and values exceeding 90% are representative of deposits that normally would not require pile foundations. Confining pressures of 10 and 20 psi were used to simulate stress conditions in the soil mass.

From past studies it has been suggested that the dynamic force, displacement amplitude, frequency and static bias weight are the most important driver parameters. A hydraulically operated, rotating-mass-type model vibratory driver with operating frequency between 5 Hz and 50 Hz was designed and built to apply a maximum dynamic force amplitude of 13,000 lb., to develop a maximum eccentric moment of 300 in-lb. and to support a bias mass weighing 2000 lb. A single-acting impact hammer with a maximum rated energy of 1150 ft-lb. per blow at full stroke was used for impact driving and restriking of the vibro-driven pile, although that hammer was operated at 69 to 72% of full stroke during this study. An analog data acquisition system was used for

collecting dynamic data, and a digital system was used for static compression and tension loading tests. Further details regarding the experimental arrangements, including details of the test pile, chamber, vibro-driver and impact hammer, descriptions of the instruments, data acquisition systems and calibration procedures, data reduction techniques, results of laboratory soil property tests, and descriptions of sand deposition techniques, are given in Appendices B to J.[1]

A total of 22 model tests were performed to achieve the stated objectives. The testing program, as outlined in Tables 1, 2 and 3, included driving the closed-ended pipe pile to a penetration of about 78 inches into the pressurized chamber with both the vibro-driver and the impact hammer. In selected tests the vibrated pile was restruck with the impact hammer to investigate the effect of restriking on vibro-driven piles. During each restrike event the pile was driven a distance equal to one-half of its diameter. A detailed summary of each of the 22 tests, with comments, is provided in Appendix B.

A portion of these 22 tests comprised a parametric study to identify and quantify the driver and soil parameters that exert the strongest influence on pile penetration velocity. These tests, identified as "parameter" tests in Appendix B, were driving tests only, and no corresponding static loading tests were conducted. The remaining tests, identified as "capacity" tests, were tests in which the pile was installed either with the vibro-driver using optimum driver parameters obtained from the parameter tests or with the impact hammer. Compression loading tests, followed by uplift loading tests, were conducted during these tests, on the same day that the piles were installed, to compare performance of the vibro-driven pile to that of the impact-driven pile in static compression and uplift. As a fundamental means of making

[1] Appendices B-Q are contained in Volume 2.

Table 1. Test Program for Vibro-Driver with San Jacinto River Sand

Test No. / Variables	1a	1b	2a	2b	3a	3b	4a	4b	5	6	7	8	9*
Vibro/Impact	V	V	V	V	V	V	V	V	V	V	V	V	V
Vibro-Driver													
Frequency Constant									X	X	X	X	X
Frequency Variable	X	X	X	X	X	X	X	X					
Bias Mass Constant									X	X	X	X	X
Bias Mass Variable					X	X	X	X					
Soil													
Particle Size D_{10}=0.2mm	X	X	X	X	X	X	X	X	X	X	X	X	X
Particle Size D_{10}=1.2mm													
Relative Density 65%			X	X			X	X			X		
Relative Density 90%	X	X			X	X			X	X		X	X
In Situ Stress													
10 psi *Uniform*	X		X		X		X		X	X	X		
20 psi		X		X		X		X					X
K_o = 0.5												X	
Restrike										X	X	X	X
Load Test													
Compression									X	X	X	X	X
Uplift									X	X	X	X	X

* Wave Equation Analysis Conducted; Vibratory Driver = V; Impact Hammer = I

Note: "a" and "b" suffixes indicate that effective chamber pressure was changed during a test, so that one installation could be considered as a test of two chamber pressure conditions. Tests 1a and 1b, 2a and 2b, 3a and 3b, and 4a and 4b were each conducted during a single pile installation.

Table 2. Test Program for Vibro-Driver with Blasting Sand

Test No. / Variables	10a	10b	11a	11b	12a	12b	13a	13b	14	15	16	17*
Vibro/Impact	V	V	V	V	V	V	V	V	V	V	V	V
Vibro-Driver Constant							X		X	X	X	X
Frequency Variable	X	X	X	X	X	X		X				
Constant							X		X	X	X	X
Bias Mass Variable					X	X	X	X				
Soil D_{10}=0.2mm												
Particle Size D_{10}=1.2mm	X	X	X	X	X	X	X	X	X	X	X	X
65%			X	X			X	X			X	
Relative Density 90%	X	X			X	X			X	X		X
In Situ Stress 10 psi	X		X		X		X		X	X	X	
Uniform 20 psi		X		X		X		X				X
K_0 = 0.5												
Restrike										X	X	X
Load Test *Compression*			X				X		X	X	X	X
Uplift			X				X		X	X	X	X

* Wave Equation Analysis Conducted; Vibratory Driver = V; Impact Hammer = I

Note: "a" and "b" suffixes indicate that effective chamber pressure was changed during a test, so that one installation could be considered as a test of two chamber pressure conditions . Tests 10a and 12a, 10b and 12b, 11a and 13a, and 11b and 13b were each conducted during a single pile installation. Test 11a/13a was an exception, in that it was originally intended to be a dual parameter test but was changed during the course of testing to be a capacity test.

Table 3. Impact Hammer Test Program

Test No. / Variables	18	19	20	21*	22*
Vibro/Impact	I	I	I	I	I
Vibro-Driver					
Frequency — Constant					
Frequency — Variable					
Bias Mass — Constant					
Bias Mass — Variable					
Soil					
Particle Size — D_{10}=0.2mm	X		X	X	X
Particle Size — D_{10}=1.2mm		X			
Relative Density — 65%			X		
Relative Density — 90%	X	X		X	X
In Situ Stress					
Uniform — 10 psi	X	X	X		
Uniform — 20 psi				X	
$K_o = 0.5$					X
Restrike					
Load Test					
Compression	X	X	X	X	X
Uplift	X	X	X	X	X

* Wave Equation Analysis Conducted; Vibratory Driver = V; Impact Hammer = I

comparisons between the behavior of the pile installed by the vibro-driver, with and without restrike, and the impact driver, unit shaft and toe load transfer relationships were determined for all of the static loading tests. Furthermore, in order to arrive at a more fundamental understanding of the pattern of soil resistance during vibro-driving, shaft and toe unit load transfer relationships were derived from the dynamic data for the vibrating pile for selected conditions in which the pile was penetrating into the soil. In addition, in order to understand whether Smith-type wave equation parameters (quake, damping and distribution of resistance) that are used in the analysis of impact-driven piles can also be used for the evaluation of the behavior of piles that are vibrated into place and later restruck with an impact hammer, selected impact and restrike test data were analyzed using wave-equation computer programs.

Finally, after a complete analysis of all of the data, a simple candidate method for predicting the bearing capacity of a displacement-type, vibro-driven laboratory pile in submerged, granular soil from known driver and soil parameters was developed. A corresponding candidate procedure was also developed for the selection of a vibro-driver to install a displacement pile of desired static capacity in submerged, granular soil for a given set of soil and pile conditions.

CHAPTER 2

Results

The results of the laboratory study are described in this chapter. Details and documentation of procedures and techniques may be found in Appendices K - Q, Volume 2, and a concise summary of the significant conclusions is provided in Chapter 4. This chapter is organized as follows. First, the effects of the soil and driver variables on pile installation are described. That section is followed by a section describing parametric relationships for rate of penetration and power transmission from the driver to the pile that were derived from the tests and that will be expanded upon in Chapter 3, in which a candidate design method is proposed. The third section briefly considers water expulsion from the test chamber as a measure of potential soil volume decrease produced by installing displacement piles with vibro-drivers. The fourth section describes the results of restrike events versus continuous driving events in light of the wave equation parameters that are required to reproduce the measured results. The fifth section describes the relative static behavior of the pile installed by vibration, vibration with restrike, and impact driving. The final section describes measured dynamic load transfer characteristics from the vibration tests. These data have no direct, immediate use in design but are useful in gaining insights into the process of vibro-driving of piles and have important implications with respect to the development of advanced mathematical models for the replication of the installation of vibro-driven piles in cohesionless soils.

EFFECTS OF SOIL AND DRIVER PARAMETERS ON PILE INSTALLATION

Penetration Rates

The purpose of the "parameter " tests (Table B.1, Appendix B) was to assess the effects of bias mass, mean effective chamber pressure (representing mean in-situ soil effective pressure and, by analogy, pile penetration), effective grain size and relative density of the soil on the penetration rate of the pile. Data from all parameter tests with the vibro-driver were reduced and summarized graphically in the form of penetration rate versus driver frequency and are presented in Figs. 2 - 7.

The purpose of Fig. 2 is to indicate that the driver when configured with 50 in-lb of unbalanced moment was inadequate to drive the test pile in fine San Jacinto River ("SJR") Sand under the conditions of 90% relative density and 20 psi effective chamber pressure. A low rate of penetration was achieved at 10 psi effective chamber pressure in the frequency range of 10 to 25 Hz, with an optimum rate occurring at a frequency of about 20 Hz. The effect of increasing the unbalanced moment to 100 in-lb and increasing the bias mass are addressed in Fig. 3, which provides data for SJR Sand in the "dense" state (relative density = 90%) and at high (20 psi) effective chamber pressure. With a minimum bias mass a low rate of penetration was achieved by increasing the unbalanced moment to 100 in-lb (doubled from the condition in Fig. 2 in which refusal was met); however, the optimum rate of penetration of about 0.15 ips is probably too low to be attractive to contractors. It is also clear that increasing the bias mass provided a positive effect on driving rate. Increasing the weight of the bias mass from the minimum value of 380 lb (the permanent carriage weight) to 2000 lb (by adding 1620 lb of bias mass) caused the rate of penetration to triple at the optimum driving frequency, which was again very near 20 Hz, but the magnitude of the bias mass appeared to have relatively little effect on the optimum driving frequency.

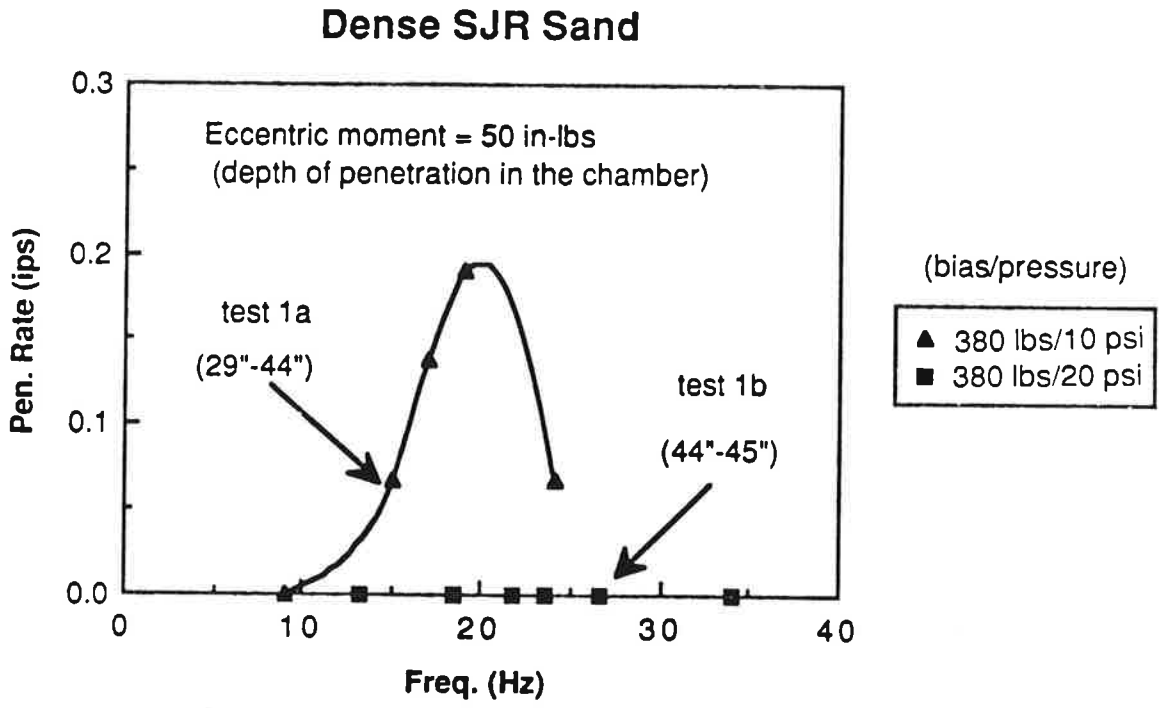

Fig. 2. Rate of Penetration for Fine (SJR) Sand at 90% Relative Density with Eccentric (Unbalanced) Moment = 50 Inch-Pounds
(Note: Bias Mass = Carriage Weight Plus Weight of Added Mass)

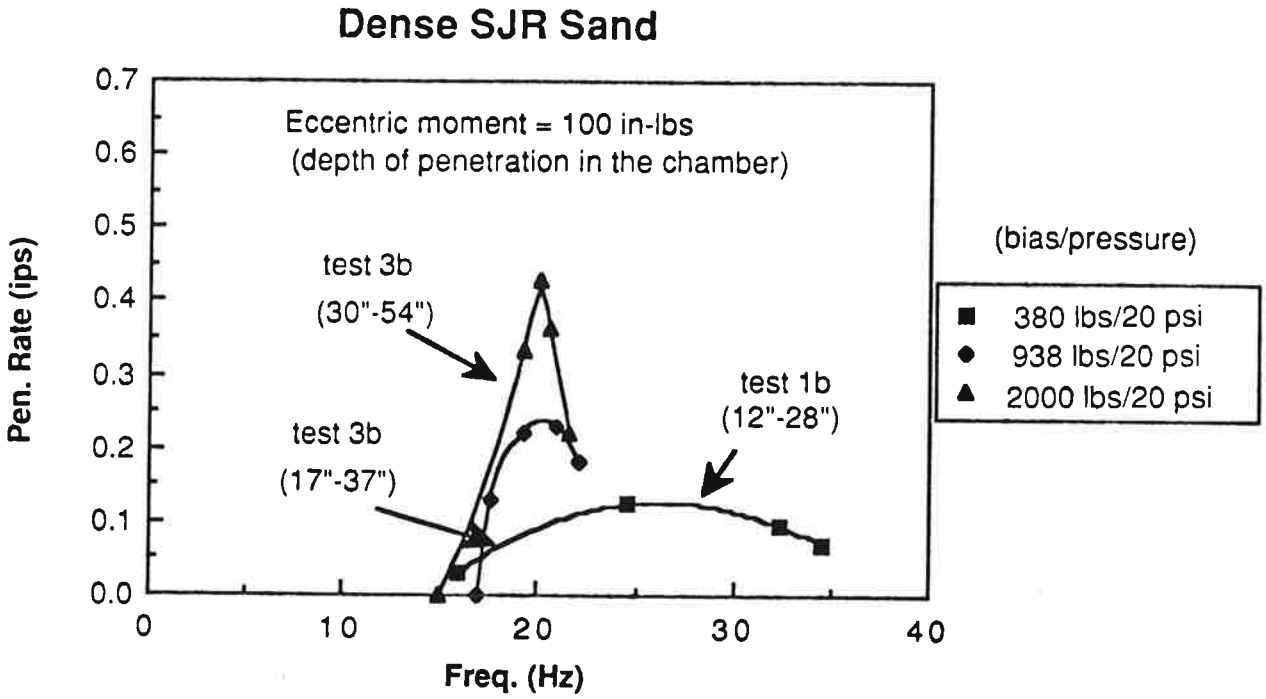

Fig. 3. Rate of Penetration for Fine (SJR) Sand at 90% Relative Density with Eccentric (Unbalanced) Moment = 100 Inch-Pounds
(Note: Bias Mass = Carriage Weight Plus Weight of Added Mass)

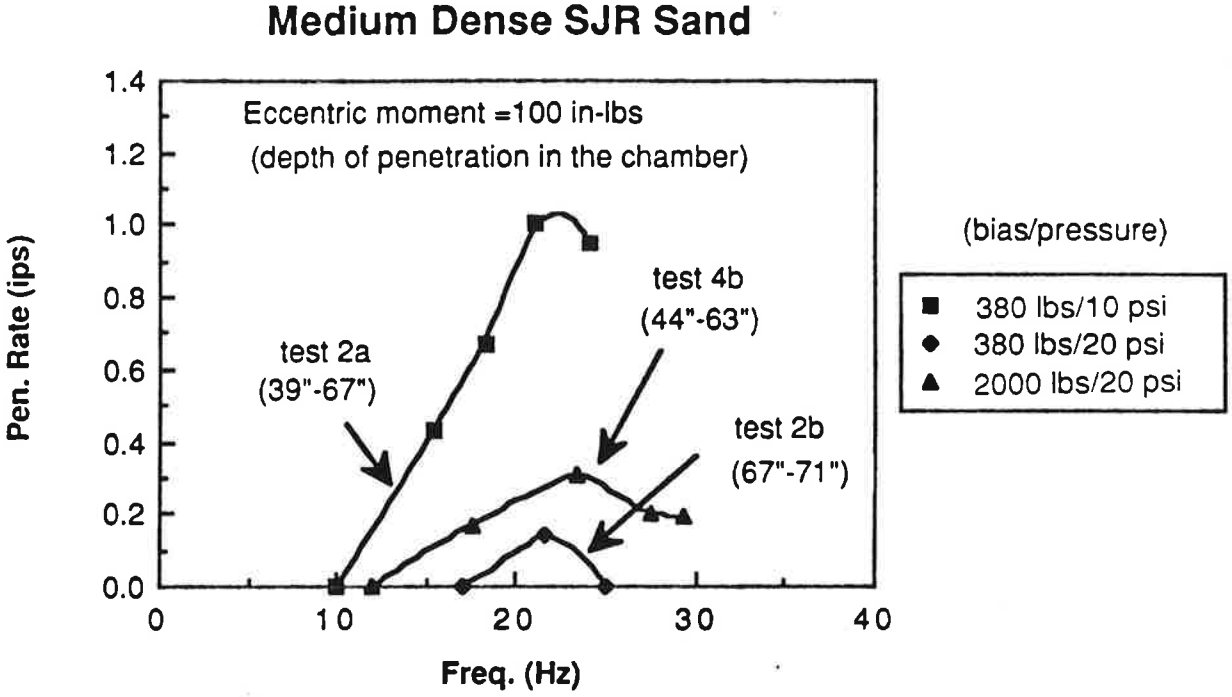

Fig. 4. Rate of Penetration for Fine (SJR) Sand at 65% Relative Density with Eccentric (Unbalanced) Moment = 100 Inch-Pounds
(Note: Bias Mass = Carriage Weight Plus Weight of Added Mass)

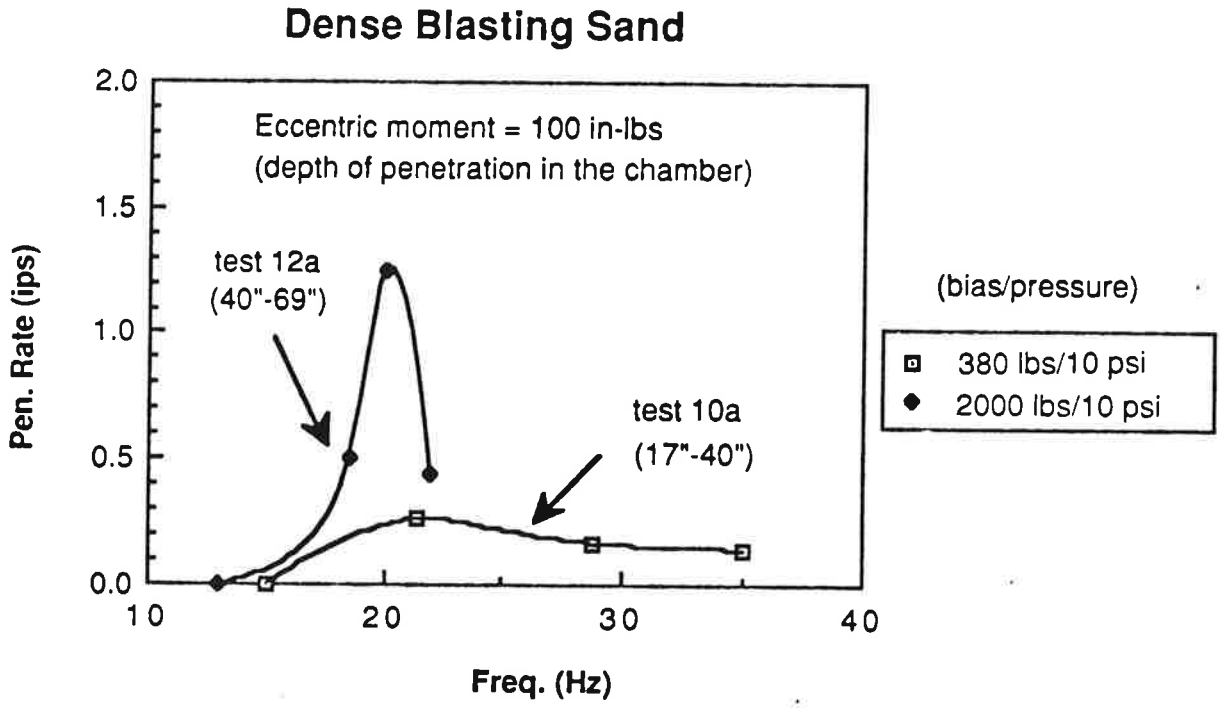

Fig. 5. Rate of Penetration for Coarse (BLS) Sand at 90% Relative Density with Eccentric (Unbalanced) Moment = 100 Inch-Pounds; Chamber Pressure = 10 psi (Note: Bias Mass = Carriage Weight Plus Weight of Added Mass)

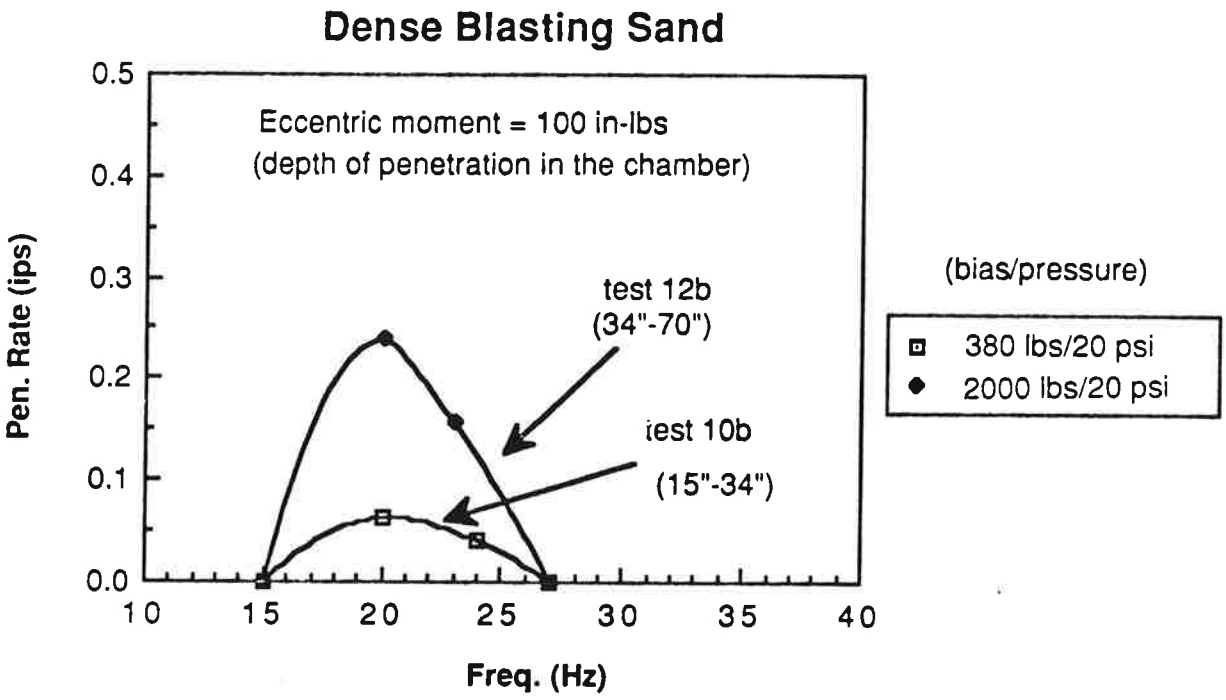

Fig. 6. Rate of Penetration for Coarse (BLS) Sand at 90% Relative Density with Eccentric (Unbalanced) Moment = 100 Inch-Pounds; Chamber Pressure = 20 psi (Note: Bias Mass = Carriage Weight Plus Weight of Added Mass)

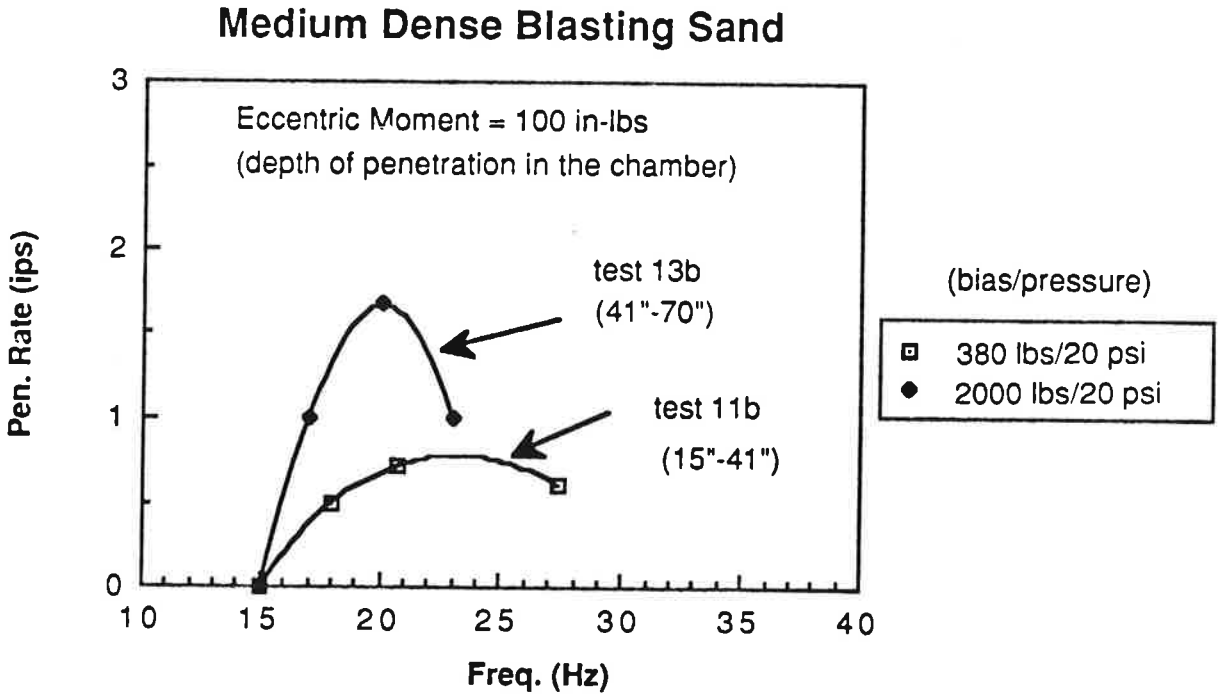

Fig. 7. Rate of Penetration for Coarse (BLS) Sand at 65% Relative Density with Eccentric (Unbalanced) Moment = 100 Inch-Pounds; Chamber Pressure = 20 psi (Note: Bias Mass = Carriage Weight Plus Weight of Added Mass)

It was decided that, because of the failure of the driver with 50 in-lb unbalanced moment to drive the pile under 20 psi chamber pressure, even for relatively shallow penetrations, an unbalanced moment of at least 100 in-lb was needed for future driving tests. Examination of the driver performance curve (Fig. E.10) reveals that the next highest discrete unbalanced moment exceeding 100 in-lb was 300 in-lb; however, that moment could not be used above 20 Hz, since it produced forces exceeding the design capacity of the driver at such frequencies. Since a frequency in the range of 20 Hz appeared to be the optimum driving frequency, it was decided not to conduct tests with 300 in-lb unbalanced moment, but to consider 100 in-lb as the optimum value. Successful installation was achieved using this unbalanced moment in all tests but two, where refusal was met prior to achieving full penetration of the pile. At f = 20 Hz, the 100 in-lb moment produces a theoretical single-amplitude dynamic force of

$$(2\pi f)^2 \text{ X (eccentric moment) / g} = 4.1 \text{ kips}.$$

Dynamic force amplitude is given for a full range of frequencies and eccentric moments in Fig. E.10. The value of 4.1 kips (k) is approximately equal to 15% of the static compression capacity of the highest-capacity pile that could be driven with this moment, and appeared, therefore, to represent a threshold eccentric moment, below which driving was ineffective. (The maximum static compression capacity measured among all piles successfully vibrated to a simulated depth of 50 or 100 feet was about 28 kips, with one exception. Static capacities will be described in detail later in this chapter.) It can be surmised from the study, therefore, that piles with static capacities exceeding about 28/4.1, or 7 times, the magnitude of the theoretical amplitude of unbalanced force would meet refusal with bias-mass weights not exceeding the maximum simulated values employed in this study (2000 lbs, or about 7% of the maximum static pile capacity in compression) and vibrator body weights of the order employed in this study (780 lbs, or about 20% of the unbalanced force). Increasing the weight of the bias mass beyond 7% of maximum static pile capacity may have permitted

the use of a ratio of unbalanced moment to pile capacity of less than 15%, but specific tests were not conducted to assess this effect. The vibrator body weight was not a variable in this study.

Figure 4 further confirms an optimum driving frequency of near 20 Hz for SJR Sand, even at the "medium dense" state (65% relative density), regardless of the magnitude of bias mass. It also reinforces the conclusion drawn previously for the dense sand condition that increasing the bias mass increases rate of penetration significantly. Furthermore, it is obvious in Figs. 2 and 4 that much higher rates of penetration were achieved under lower effective chamber pressure (simulated mean soil pressure for 50-foot penetration) than under the higher pressure (simulated 100-foot penetration).

Based on a review of Figs. 2 - 4, which apply to SJR (fine) sand, it was concluded that a driving frequency of 20 Hz, a maximum weight of bias mass of 2000 lbs and an unbalanced moment of 100 in-lb were the optimum parameters for the laboratory testing system and that these parameters would be used in future capacity-assessments tests with SJR Sand. While the optimum unbalanced moment and weight of bias mass appear to be related to the maximum static compression capacity of the pile (discussed above), which potentially represents a means of scaling the laboratory results to the field, no logic for development of a scaling rule involving bias mass and unbalanced moment could be ascertained for optimum frequency. Although the effects of wave reflections from chamber boundaries may have had some effect on optimum driving frequency in the laboratory tests, there is no indication that the optimum frequency would have been significantly different from 20 Hz in a full-scale field operation for the conditions that were simulated in the laboratory. It appears, therefore, that the optimum driving frequency is related to the development of a condition in the soil that allows for the largest reduction of impedance to driving by the soil. Mechanisms for

soil impendance reduction, deduced from the analysis of load transfer and soil pressure data, are discussed later.

Figures 5 - 7 present the results of similar parameter tests using coarse Blasting ("BLS") Sand. Identical conclusions with respect to optimum frequency, bias mass and eccentric moment can be drawn as were drawn for SJR Sand. The one difference in BLS Sand relative to SJR Sand is that for a given set of driver conditions and chamber pressures, penetration was more rapid in the coarse BLS Sand in the medium-dense state than in the fine SJR Sand in the medium-dense state, while very little difference was observed in the dense state.

One significant effect that was observed in the parameter tests that is difficult to report quantitatively is that once vibro-driving was stopped for a pile that was penetrating at a reasonable rate (as was necessary in some of the early tests in order to synchronize the motors of the driver), it was difficult to reinitiate positive penetration with the same driver parameters that had successfully kept the pile penetrating prior to the stoppage. This observation suggests that it is important not to stop driving the pile once a desirable rate of penetration has been reached, prior to achieving design penetration.

Further insight into the effect of soil conditions on penetration resistance of vibro-driven piles may be seen by observing Figs. 8 - 11, which present penetration resistance records for the "capacity" tests in which the driver and soil conditions remained constant for each test as the pile was penetrated to its full depth. Note that the penetration rate (v_p) is plotted against nondimensional penetration or depth (D/B), where D is the depth of the pile toe below the top of the chamber, and B is the diameter of the pile. One significant result is that the rate of penetration appears to be controlled by lateral effective soil pressures rather than by vertical effective pressures, since the pattern of penetration rate for K_o = 0.5 (vertical effective stress = 20 psi; lateral effective stress = 10 psi) in fine SJR Sand in Fig. 8 more closely conforms to the patterns for

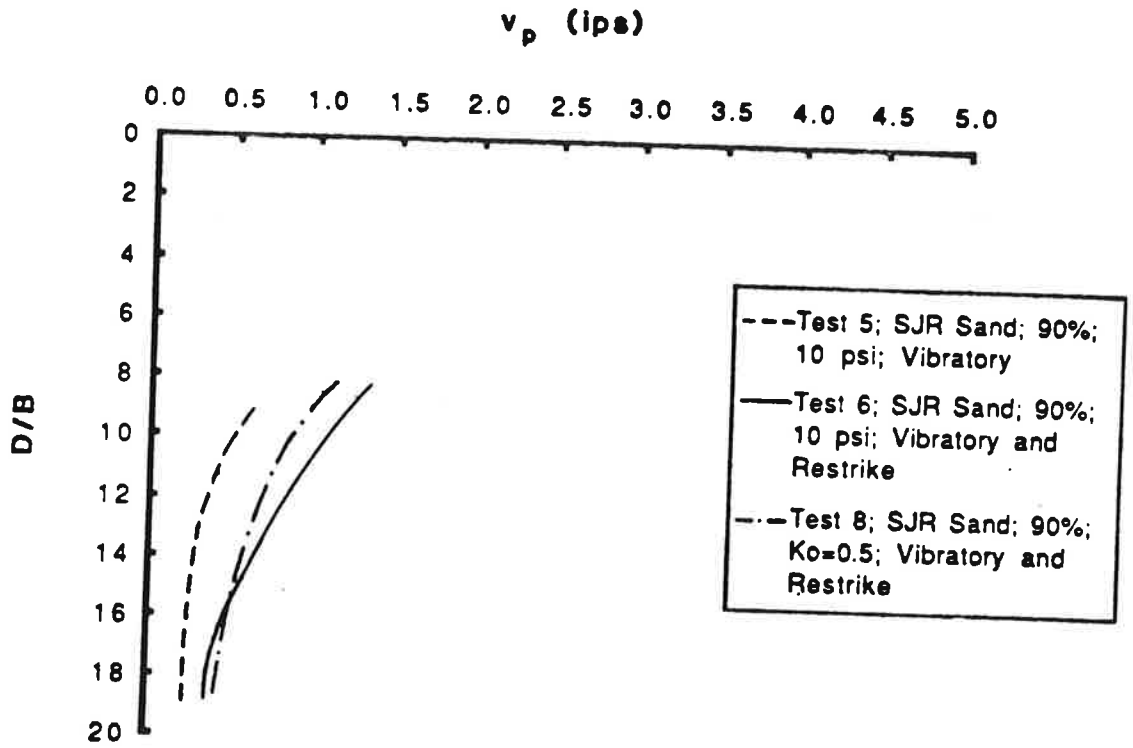

Fig. 8. Rate of Penetration Vs. Toe Depth-to-Diameter Ratio (D/B); SJR Sand at 90% Relative Density

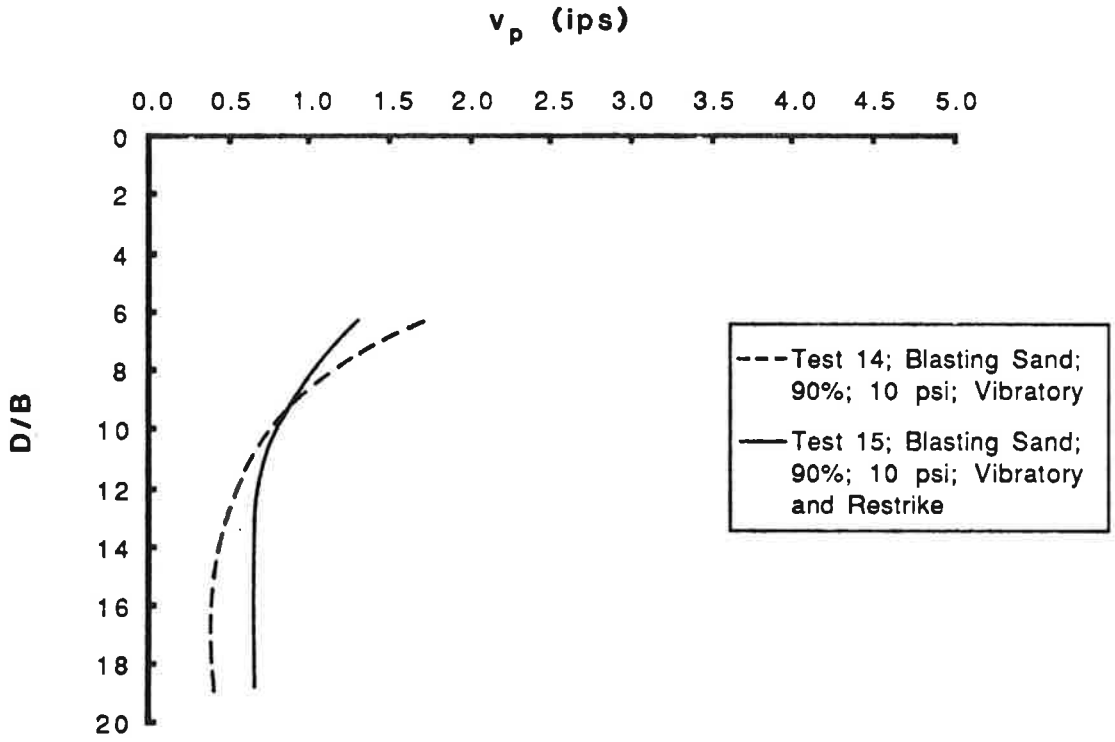

Fig. 9. Rate of Penetration Vs. Toe Depth-to-Diameter Ratio (D/B); BLS Sand at 90% Relative Density

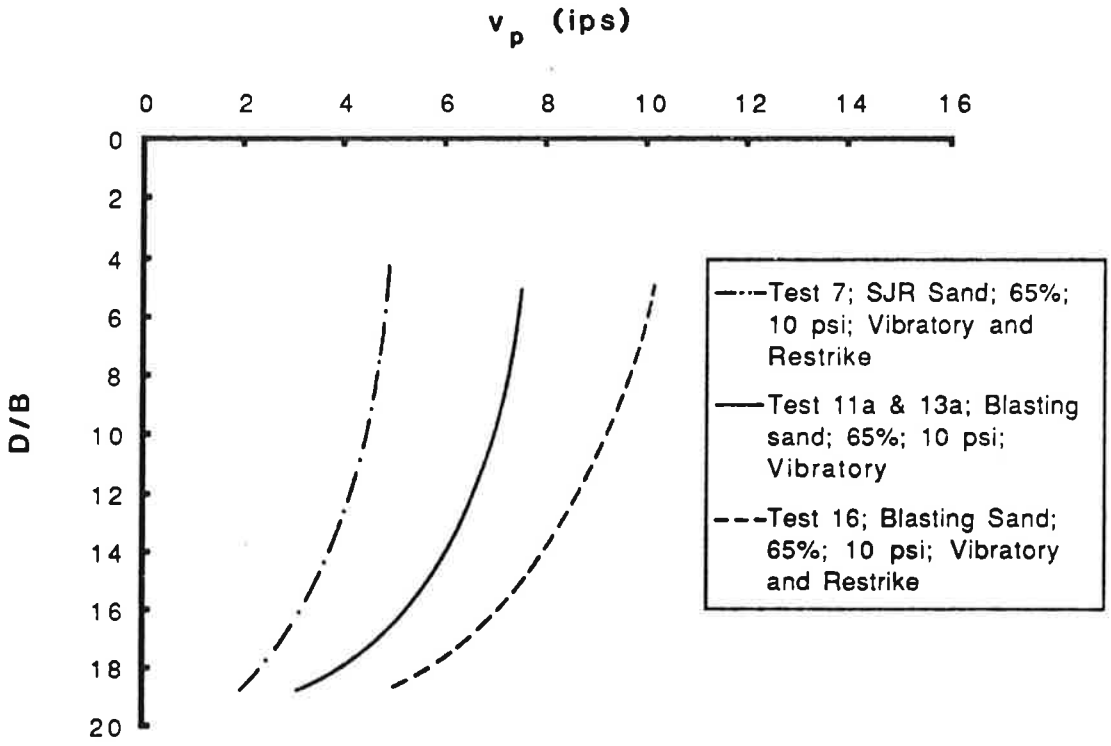

Fig. 10. Rate of Penetration Vs. Depth-to-Diameter Ratio (D/B); Comparison of Tests at 65% Relative Density and 10 psi Chamber Pressure

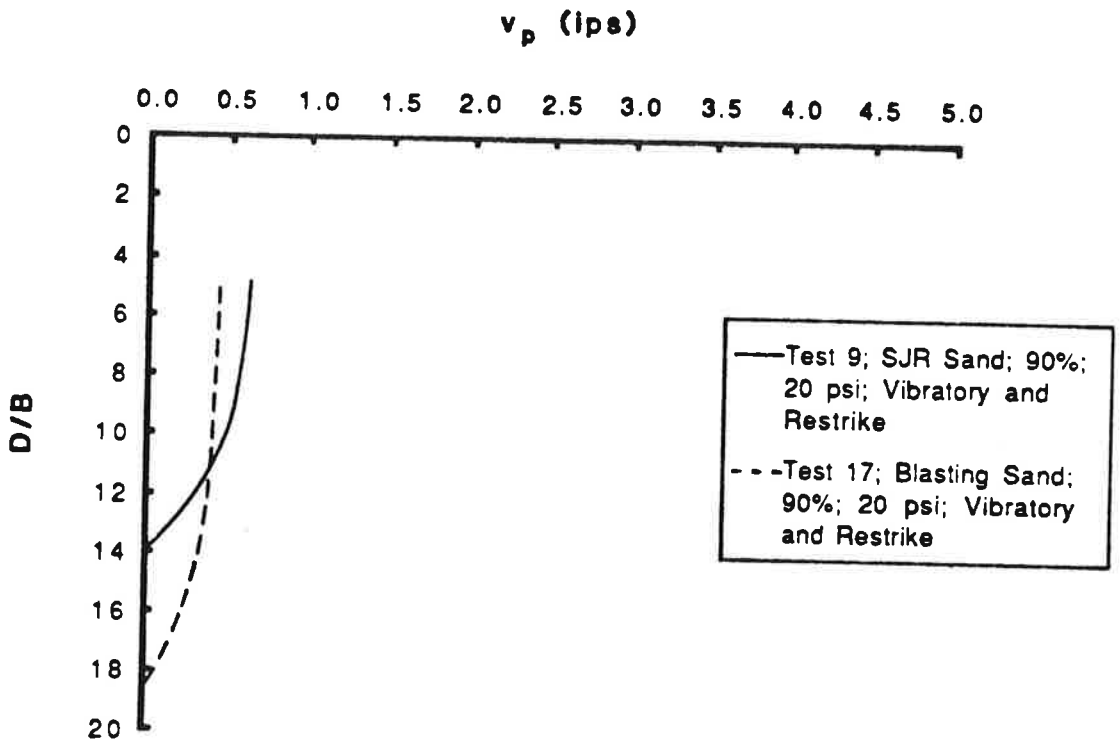

Fig. 11. Rate of Penetration Vs. Depth-to-Diameter Ratio (D/B); Comparison of Tests at 90% Relative Density and 20 psi Chamber Pressure

other pile installations in SJR Sand with 10 psi isotropic chamber pressure (also in Fig. 8) than to the patterns defined in Fig. 11 (20 psi isotropic chamber pressure). A second observation is that Fig. 9 indicates the probable bounds of error for rate of penetration with a vibro-driver, as the two tests reported were conducted under as nearly identical conditions as could be produced in the laboratory.

Significantly higher penetration rates occurred at comparable depths of penetration at 10 psi chamber pressure when the relative density was 65% compared to equivalent conditions at 90% relative density. For example, it can be observed in Fig. 10 that penetration rates ranged from 2 ips to 10 ips for medium dense sand, while penetration rates were from 0.2 ips to 2.5 ips for dense sand (Figs. 8 and 9). Increasing effective chamber pressures from 10 psi to 20 psi (doubling the simulated depth) clearly decreased the rate of penetration (Figs. 8, 9 and 11), although the effects were not as prominent as those of relative density.

A reasonable definition of refusal in the laboratory tests is a rate of penetration of 0.1 ips. At values higher than 0.1 ips it was possible to maintain a reasonably uniform rate of penetration as the pile penetrated more deeply, but once the rate was reduced below about 0.1 ips, it rapidly came to a complete stop.

Penetration resistance records for all impact driving tests are depicted in Figs. 12 and 13. Somewhat higher penetration resistances are evident for 90% relative density than for 65% relative density (Fig. 12). The increase in penetration resistance appears more prominently affected by doubling the effective chamber pressure from 10 psi to 20 psi than by increasing the relative density from 65% to 90%. This statement can be verified by comparing the results of the various tests in Fig. 12 and then comparing the results of Test 18 in Fig. 12 with Test 21 in Fig. 13. In this respect the behavior of the impact-driven piles was different from that of the vibro-driven piles. However, by comparing Test 22 in Fig. 13 with Test 21 in the same figure and Tests 18 and 19 in Fig. 12, it is seen that the penetration resistance of the impact-driven pile,

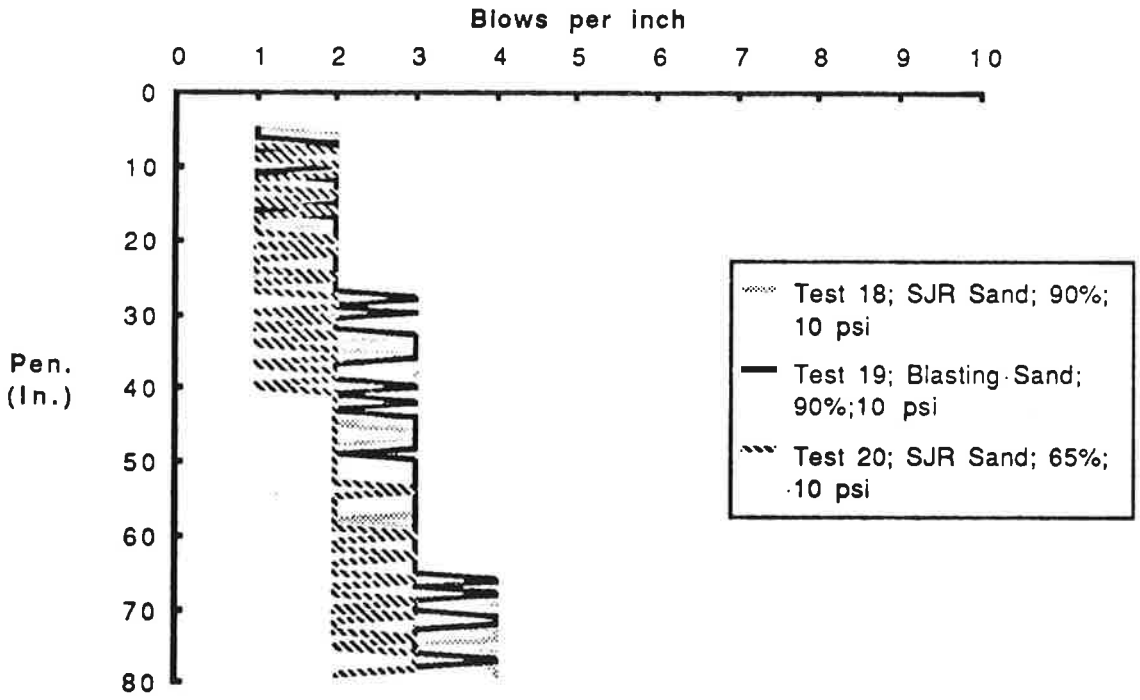

Fig. 12. Driving Records for Impact Tests Conducted at 10 psi Chamber Pressure

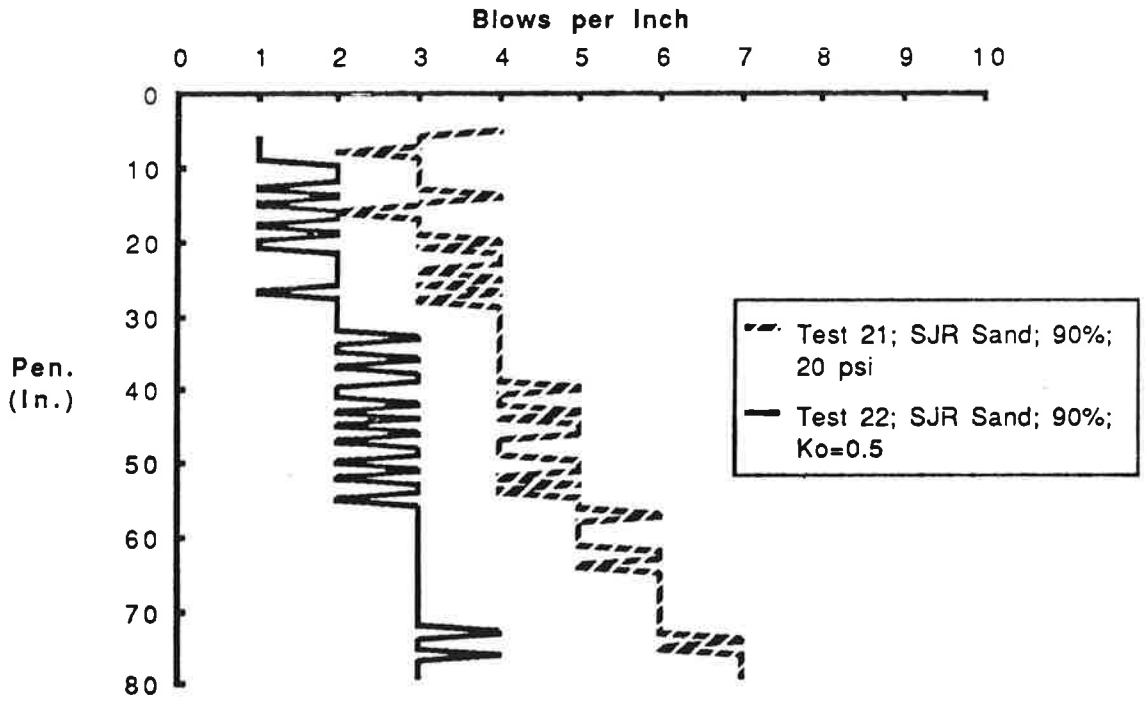

Fig. 13. Driving Records for Impact Tests Conducted in Fine (SJR) Sand at 90% Relative Density

like that of the vibro-driven pile, was much more strongly controlled by lateral effective soil pressures than by vertical effective pressures.

Penetration resistance records for all restrike events are given in Table 4. The general trends, in terms of penetration resistance during restrike as a function of chamber pressure and relative density, are consistent for both fine and coarse sand and are consistent with the trends established in the impact-driving tests relative to effective chamber pressure and relative density of the sand. The second inch of restrike offered less penetration resistance than the first inch for conditions of high density and high pressure, however.

A performance relationship between the model vibro-driver and model impact hammer used in this study was established in terms of driving rate (v_p) for the vibro-driver and blow count (blows/inch) for the impact hammer for tests where soil conditions were identical. That relationship, shown in Fig. 14, demonstrates that for a given pile, pair of drivers, pile cushioning, etc., it may be possible to convert rate of vibro-driver penetration into equivalent blow count for an impact-driven pile, which may possibly be used on a given project to verify pile capacity in granular soil. Note that the particular relationship given in Fig. 14 is only valid for driver and hammer in this laboratory study, however.

Typical Force and Velocity Time Histories for Vibro-Driven Pile

Observation of the time histories of pile-head and pile-toe forces and velocities provides further insight into the mechanisms producing penetration in vibro-driven piles. Detailed force, velocity, acceleration and lateral soil pressure time history data for all vibro-capacity tests are provided in Appendix M. A few records are also presented in this chapter in order to discuss some of the significant aspects of the behavior of the pile-soil system during vibro-installation. A few general trends that are evident in the data in Appendix M are that magnitudes of peak acceleration were greater in the coarse sand under comparable testing conditions, which may suggest that

Table 4. Blow-Counts for Restrike Events

Test No.	Relative Desnity (%)	Confining Pressure (psi)	Penetration (in.)	No. of Blows
		San Jacinto River (Fine) Sand		
6	90	10	75 - 76	4
			76 - 77	4
7	65	10	75 - 76	2
			76 - 77	2
8	90	10 (Lateral)	75 - 76	4
		20 (Vertical)	76 - 77	5
9	90	20	55 - 56	8
			56 - 57	5
		Blasting (Coarse) Sand		
15	90	10	75.5 - 76.5	4
			76.5 - 77.5	4
16	65	10	77 - 78	2
			78 - 79	1
17	90	20	74 - 75	12
			75 - 76	8

the coarser sand requires somewhat higher accelerations to produce a rate of penetration equivalent to that in fine sand. Acceleration signals tended to be more

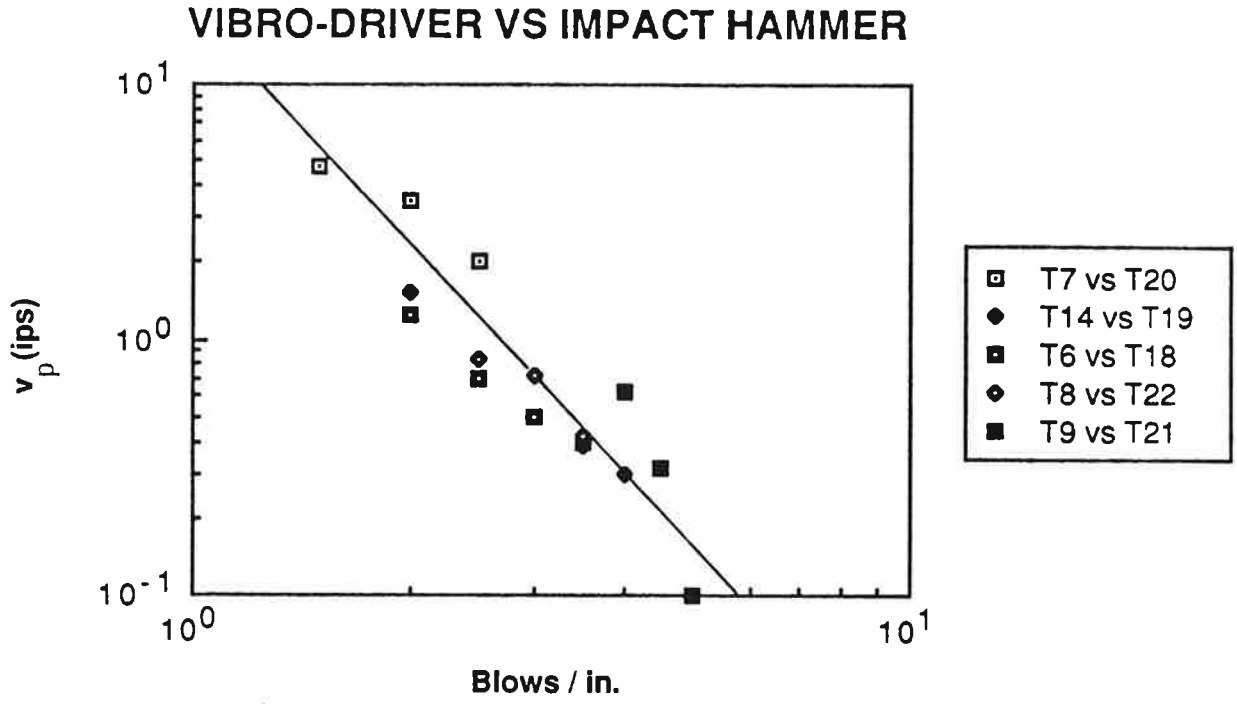

Fig. 14. Relationship Between Penetration Velocity for Vibro-Driven Piles and Driving Resistance for Impact-Driven Piles for Laboratory Study

noisy with the coarse sand than with the fine sand, perhaps due to more severe slipping of grains in the coarser sand. The range of accelerations that were found to produce penetration were 3 - 12 g, which is in general agreement with the work of Rodger and Littlejohn (1)[2]; however, in Test 9 (high density and high pressure in fine sand), in which refusal was met at a penetration of about 13 diameters, peak accelerations at the head and toe were in the range of 4 to 5 g. It appears, therefore, that the threshold acceleration required for penetration proposed by Rodger and Littlejohn (1.5 g) is too low for the most severe conditions studied herein. It is speculated that any threshold value is probably a function of confining pressure, density and grain size characteristics and was of the order of 5 g for the conditions that existed in Test 9.

Pile-head and pile-toe force and velocity time histories are presented for two separate conditions in Figs. 15 - 18. In these figures positive velocity corresponds to downward movement of the pile, and positive force corresponds to compression. Figures 15 and 16 are data from near full penetration in Test 11a/13a, which was conducted in medium-dense coarse sand at 10 psi confining pressure (50 foot simulated depth) and represents the "easy driving" end of the spectrum. In this test the histories of head and toe velocities were very similar and were very nearly sinusoidal. The head and toe forces exhibited near-sinusoidal behavior, but with magnitudes skewed toward positive (compressive) values of force. Part of the skew is explained by the presence of 2000 lb of bias compression load on the pile. Negative force peaks of about 200 lb in Fig. 16 are indicative of momentary uplift capacity of the pile in excess of the bias load, equal to the sum of the suction at the pile toe and negative shaft friction. The magnitude of peak compressive force at the toe was about 65% of that at the head. Figures 17 and 18 are data from near full penetration in Test 17, which was conducted in dense coarse sand at 20 psi confining pressure (100 foot simulated penetration) and

---

[2] References are given at the conclusion of the text.

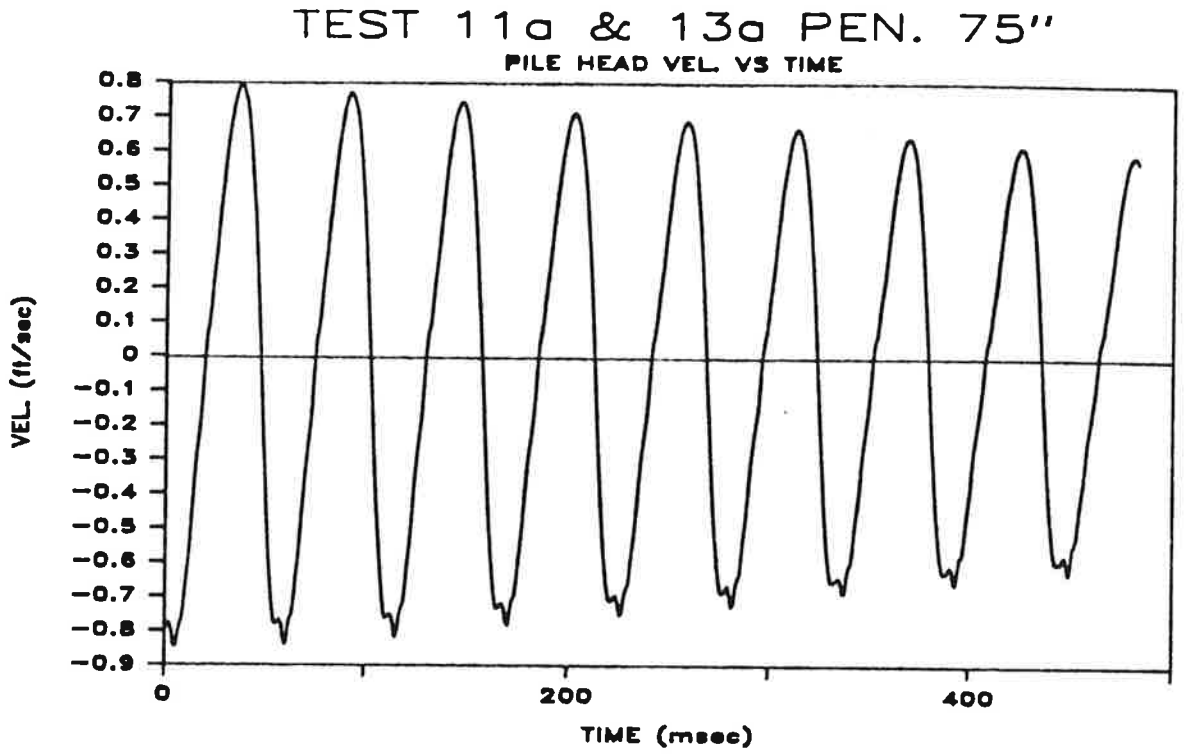

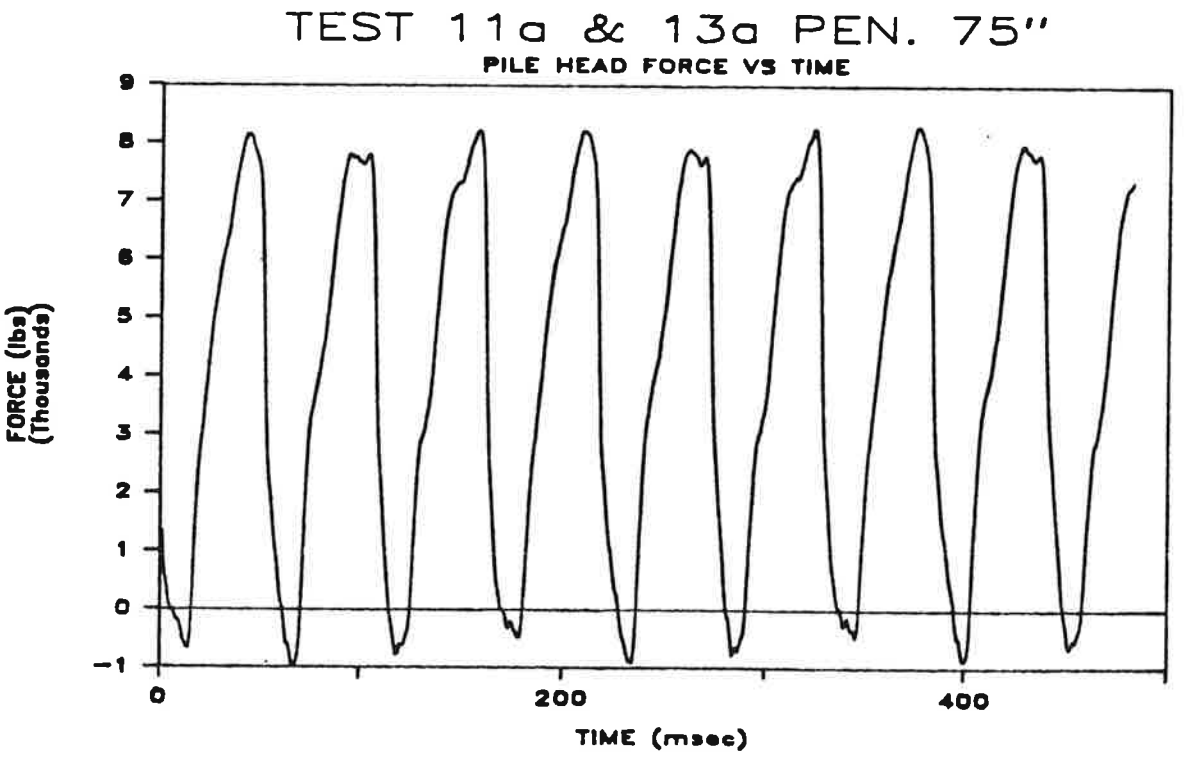

Fig. 15. Pile-Head Velocity and Force Vs. Time; Test 11a/13a
(Relative Density = 65%; Chamber Pressure = 10 psi)

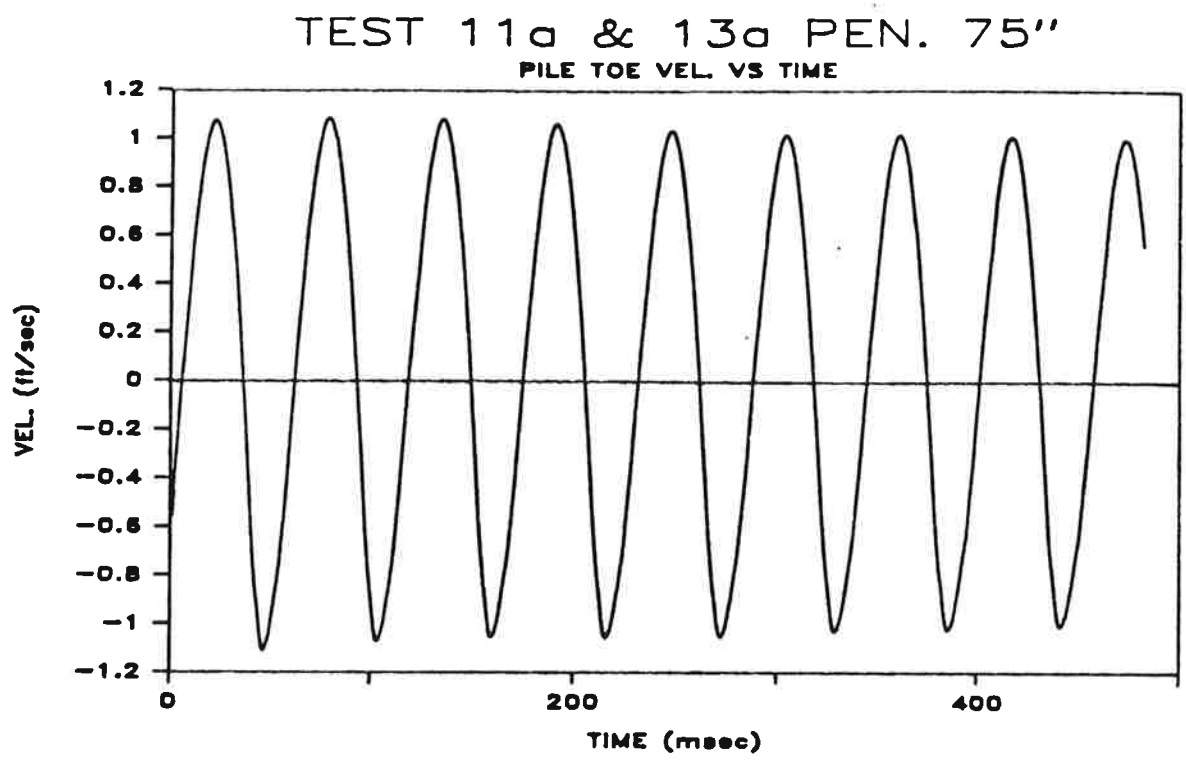

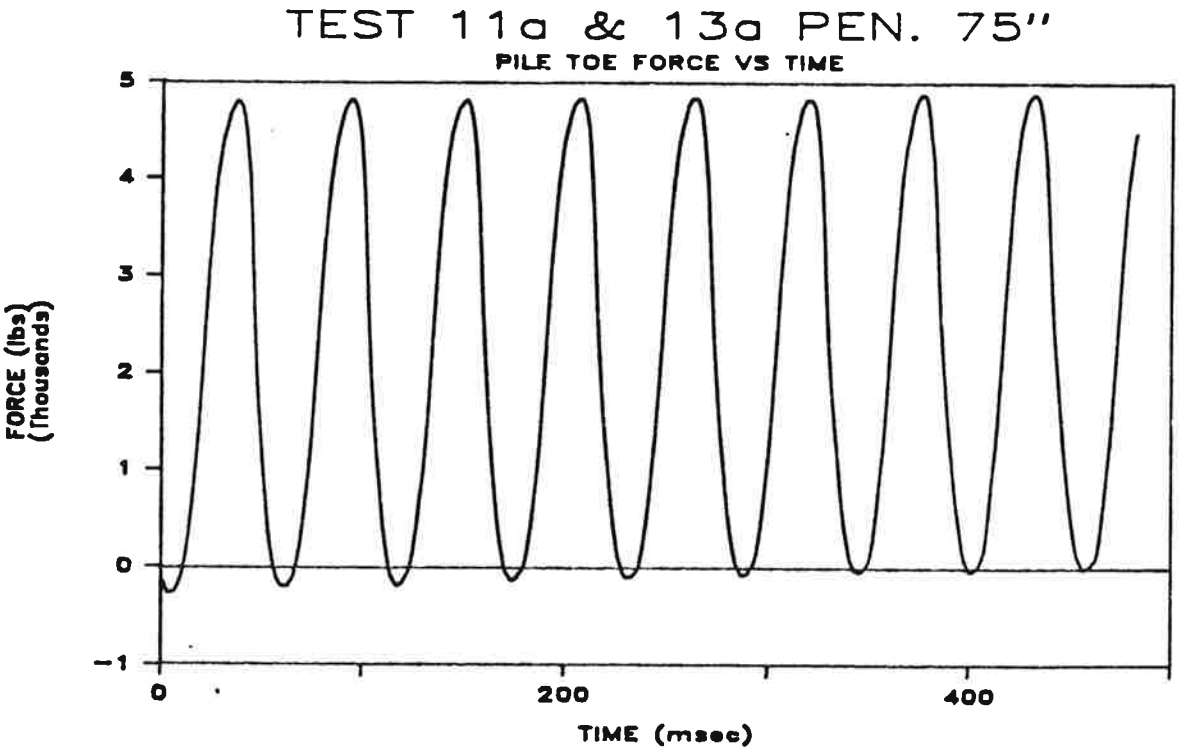

Fig. 16. Pile-Toe Velocity and Force Vs. Time; Test 11a/13a
(Relative Density = 65%; Chamber Pressure = 10 psi)

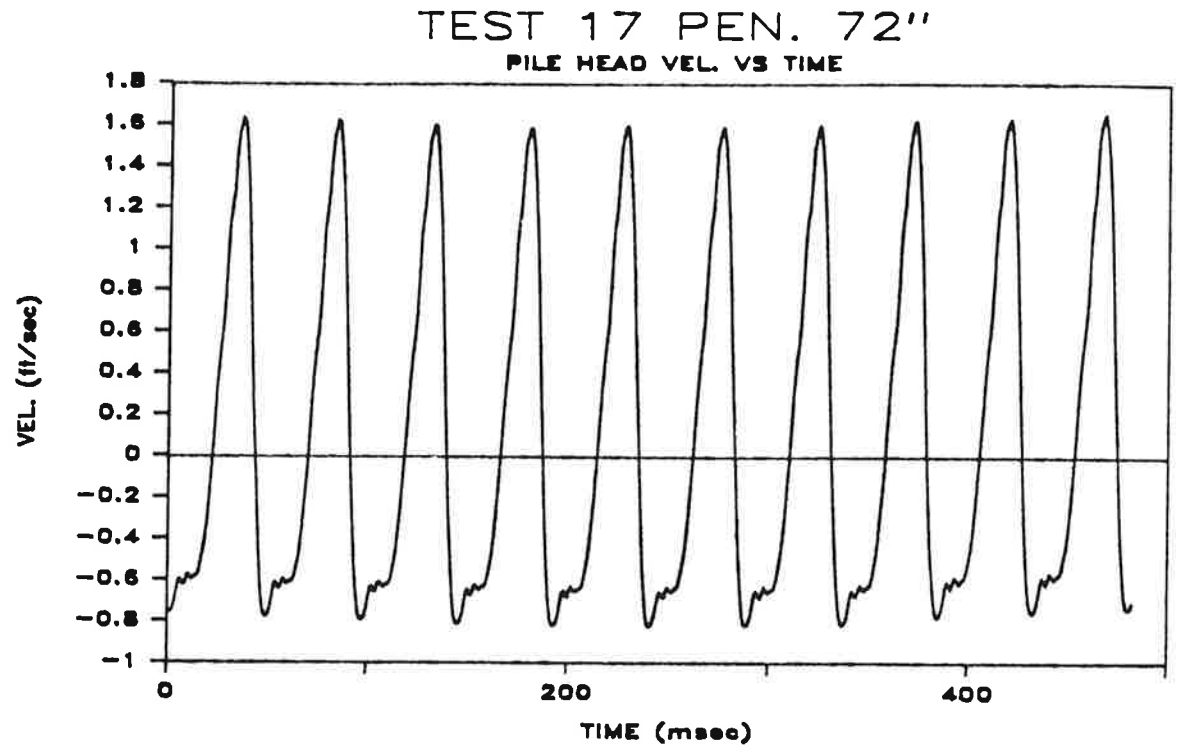

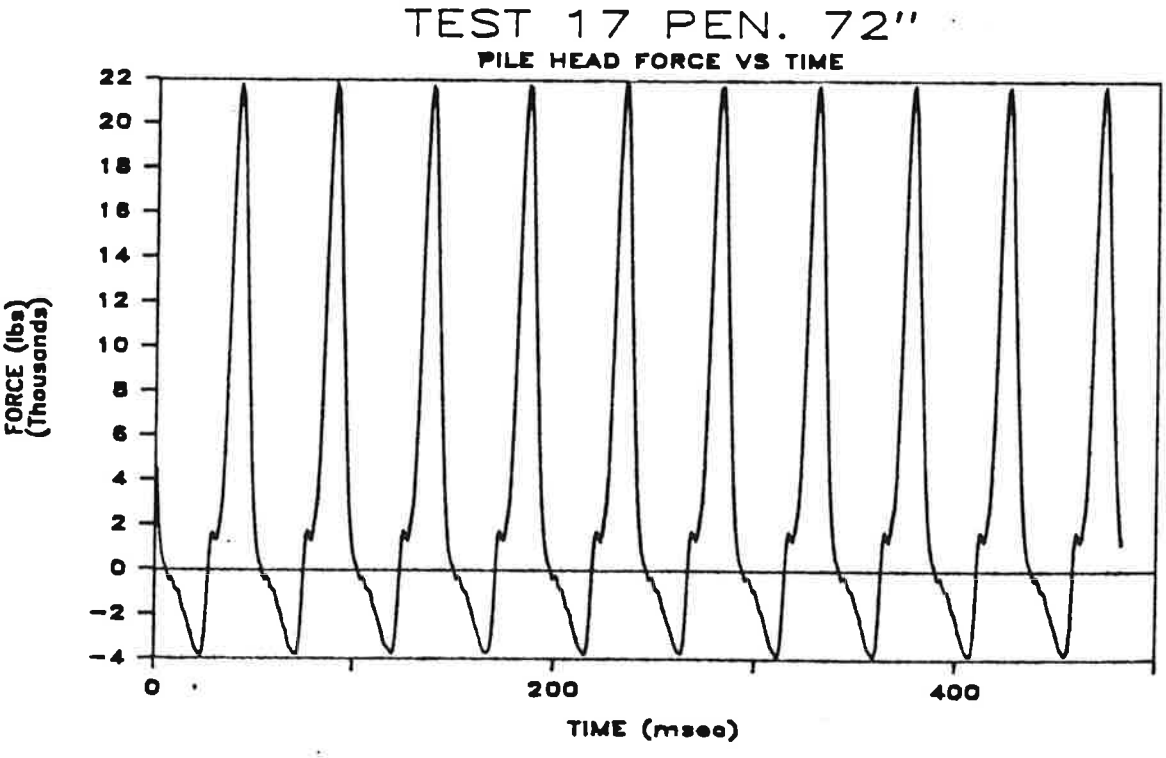

Fig. 17. Pile-Head Velocity and Force Vs. Time; Test 17
(Relative Density = 90%; Chamber Pressure = 20 psi)

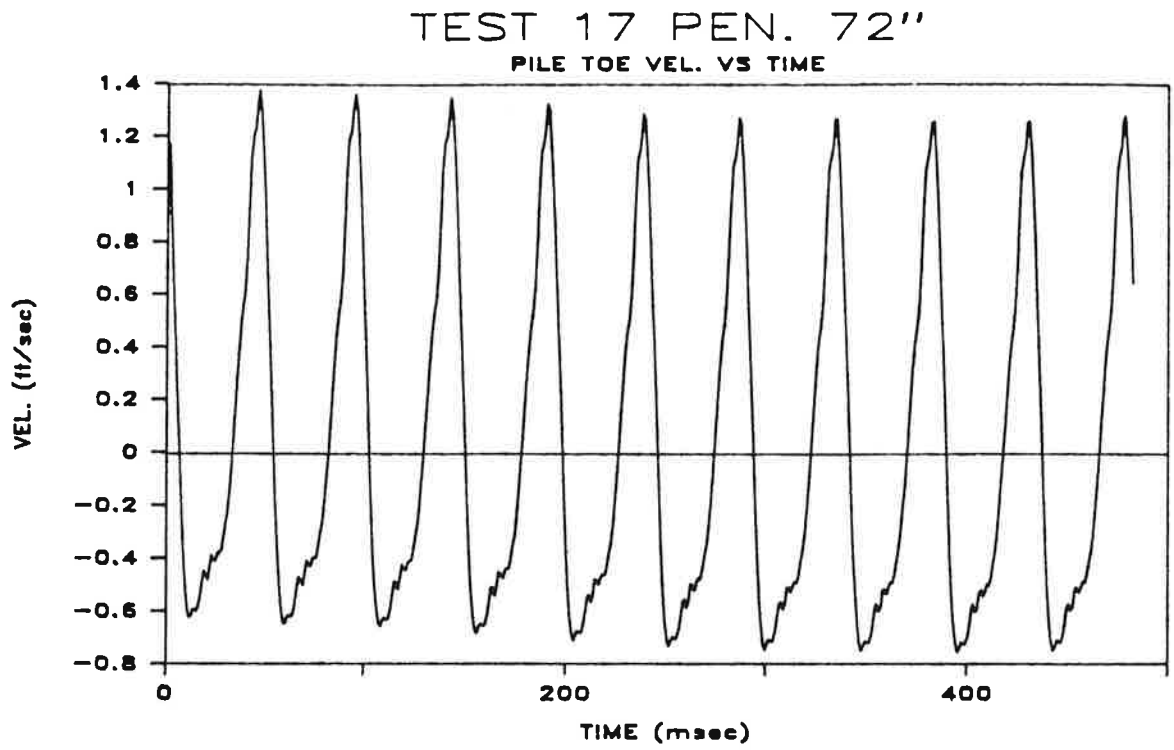

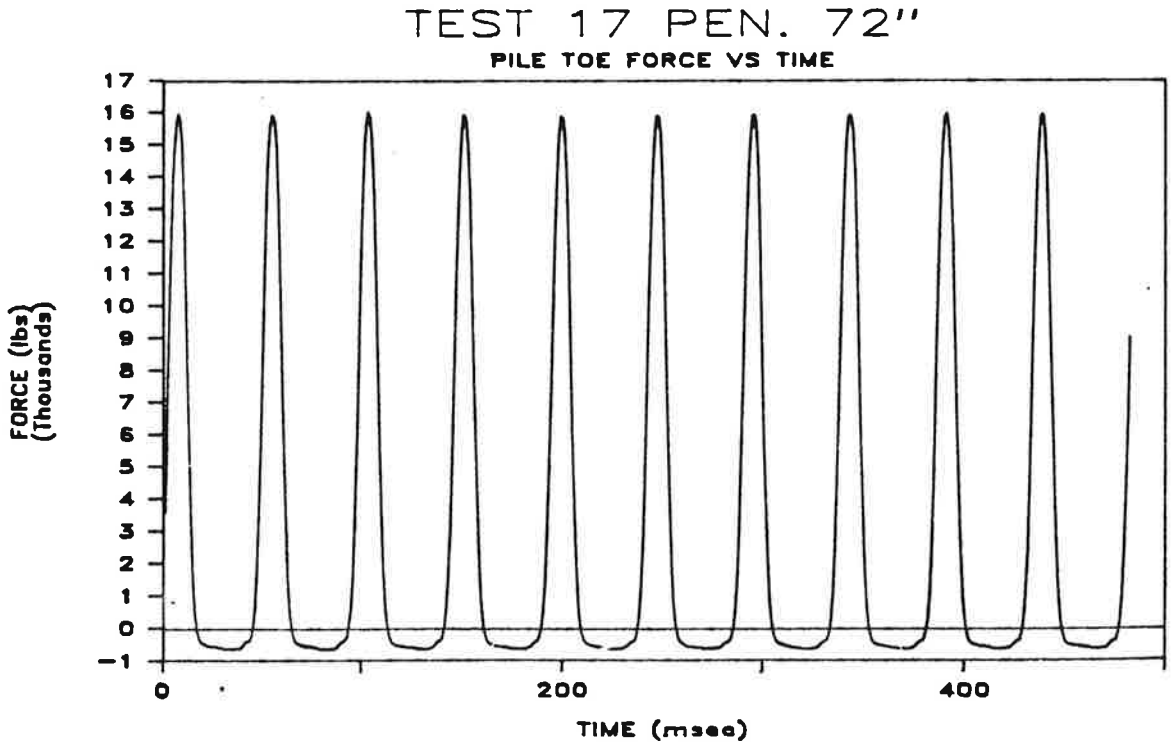

Fig. 18. Pile-Toe Velocity and Force Vs. Time; Test 17
(Relative Density = 90%; Chamber Pressure = 20 psi)

represents the "hard driving" end of the spectrum. The time history of toe force is quite different in this test than in Test 11a/13a. First, while the ratio of toe force amplitude to head force amplitude remained at about 0.65 - 0.70 in Test 17, the magnitudes of the respective peaks are about 4 times those observed in Test 11a/13a. Second, while very minor negative toe forces were observed in Test 17 (Fig. 18), near-constant negative values persisted for over one-half of each cycle, which, along with the sharp positive (compression) peaks and general non-sinusoidal nature of the toe force time history, suggests that, unlike the behavior in Test 11a/13a, the pile toe was being lifted off the underlying soil on the upstroke of the driver and thrust back against it on the downstroke. Driving thus simulated rapid impact driving in terms of toe penetration. Comparison of the pile-head force time histories for the medium-density/low pressure conditions in Figs. 15 and 16 with the head and toe force time histories for the high density/high pressure conditions in Figs. 17 and 18 indicates that greater negative shaft resistance developed on the upstroke in the dense sand under high pressure, as suggested by the presence of approximately 4 kips of negative force amplitude at the head in the absence of a similar amplitude at the toe, compared to a trivially small value in the medium dense/low pressure conditions, as evidenced by nearly equal amplitudes of negative toe and head force. This negative shaft resistance appears to have limited the negative velocity achieved on the upstroke to about one-half of that achieved on the downstroke at both the head and toe (Figs. 17 and 18), which would have limited the amplitude of displacement of the pile and thus the effectiveness of the driver. (Soon after the data reported in Figs. 17 and 18 were recovered, the pile reached refusal.)

This behavior is also viewed from the perspective of soil resistance against the shaft and toe of the in-motion pile in the final major section of this chapter.

A review of the data from Appendix M indicates that the amplitudes of pile-head and toe velocities were both of the same order of magnitude under equivalent test

conditions. Values of both parameters tended to increase with increasing relative density and chamber pressure.

Interaction of Vibro-Driver and Pile

It is observed in Figs. 15 and 17 that the peak compressive (positive) pile-head forces are considerably greater than the maximum value of unbalanced force generated by the vibrator (4.1 k at 20 Hz). This effect is addressed in Appendix E; however, from simple mechanics the bias mass weight and the product of the mass of the body of the vibrator times its maximum acceleration at the bottom of the downstroke (actually, deceleration) add to the unbalanced force to produce the measured force. The acceleration and mass of the vibrator body is thus seen to be a potentially important driver parameter. In Test 11a/13a the maximum decleration measured at the pile head on the downstroke (Fig. M13a) was approximately 3.5 g. The driver body weighed 0.78 k. Assuming that the pile head and driver body had identical acceleration time histories, the maximum force at the head of the pile on the downstroke, based on considerations of dynamic eqilibrium along the axis of the pile (Fig. E.15) would have been

4.1 k (unbalanced force) + 2.0 k (bias mass weight) + 0.78 k X 3.5 g

(inertial force of the driver body) = 8.8 kips.

Figure 15 indicates that the peak value was about 8 kips. The small discrepancy may be due to friction losses in the vibrator unit as it slid down the tracks in the service frame and to the characteristics of the connection between the pile and driver, which may have restricted to some extent in-phase motion between the driver and the head of the pile. Nonetheless, the magnitudes of the various components of this expression serve to indicate the contribution of the various components of the driver system.

On the other hand, Fig. 17 (hard driving, Test 17) indicates a peak positive force value of 21.5 kips. The maximum accleration on the downstroke (deceleration) was about 9.0 g (Fig. M21a), which raises the ideal peak compressive force at the pile head to

4.1 + 2.0 + 0.78 X 9.0 = 13.1 kips,

which is considerably less than the measured peak value of 21.5 kips. It is speculated that the vibrator in this hard-driving condition was decelerating faster than the pile at the bottom of the downstroke, which may have been permitted by flexibility in the connection to the pile head.

It appears, thererfore, that the detail of the driver-pile connection is also a potentially important parameter in a vibro-driver-pile system.

Typical Lateral Pressure Time Histories for the Vibro-Driven Pile

The relative ease of driving could conceivably be viewed in terms of the buildup of baseline pore water pressure at the pile-soil interface during driving and in terms of the excursions in pore water pressure that occur with each cycle of loading. The lower graph in Fig. 19 shows pore water pressure versus time at the lower level of the lateral pressure transducers (1.4 diameters above the toe) during insertion of the pile in Test 11a/13a, in which the conditions were coarse sand at medium density and low confining pressure. The sinusoidal pattern of pore water pressure in response to excitation is evident, but the excursions about the mean are relatively small. On the other hand, the mean (baseline) value is seen to be shifting rapidly upward, indicating an increase in background pore water pressure of about 0.3 psi in only about 8 cycles. About one-third of the 0.3 psi baseline shift is accounted for by the fact that the pile penetrated about 3 in. during the 8 cycles, so that the geostatic pore water pressure increased by about 0.1 psi during this period. At the time in which these data were acquired the sensors were only about 30 inches below the top of the chamber (equivalent to the free water surface), so that the background pore water pressure had been elevated from a geostatic value of about 1.1 psi (30 in. times 0.0361 lb/cu. in.) to a value of about 2.5 psi. While this induced excess pore water pressure was undoubtedly helpful in affecting pile penetration, it should be noted that, even in the case of the looser soil at low pressure depicted by Fig. 19, the maximum, instantaneous pore water pressures did not remotely approach the value of total pressure in the chamber. It also

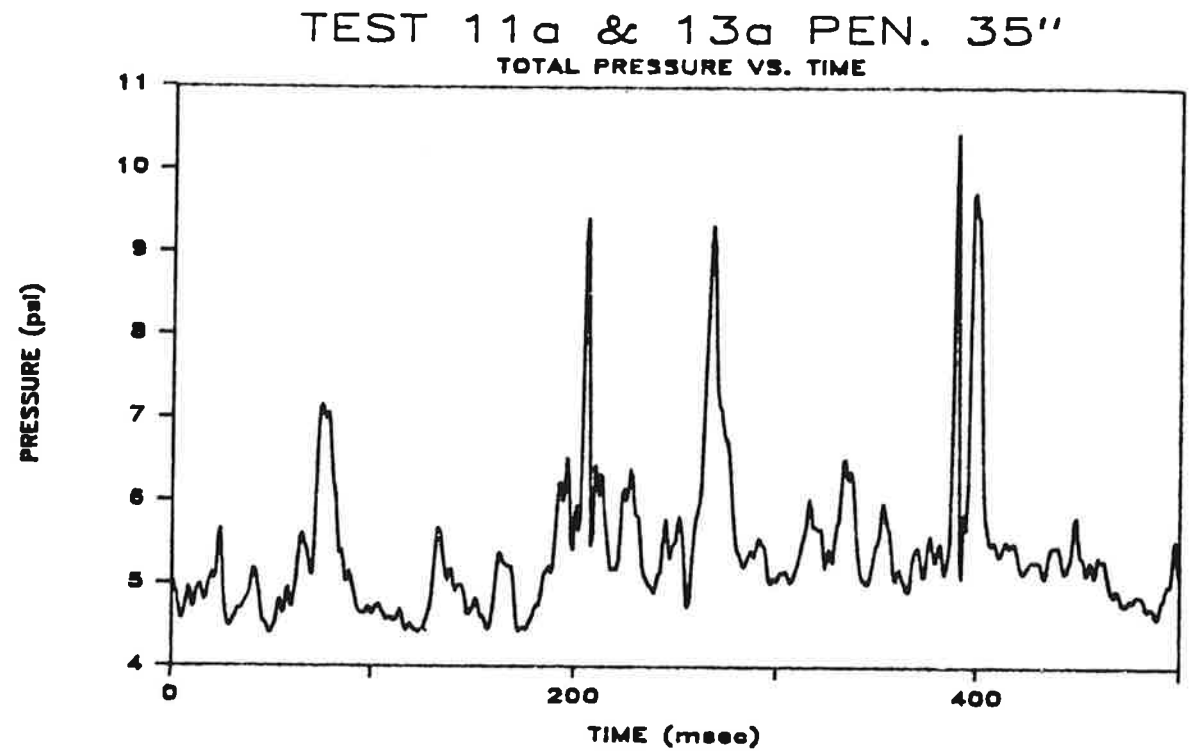

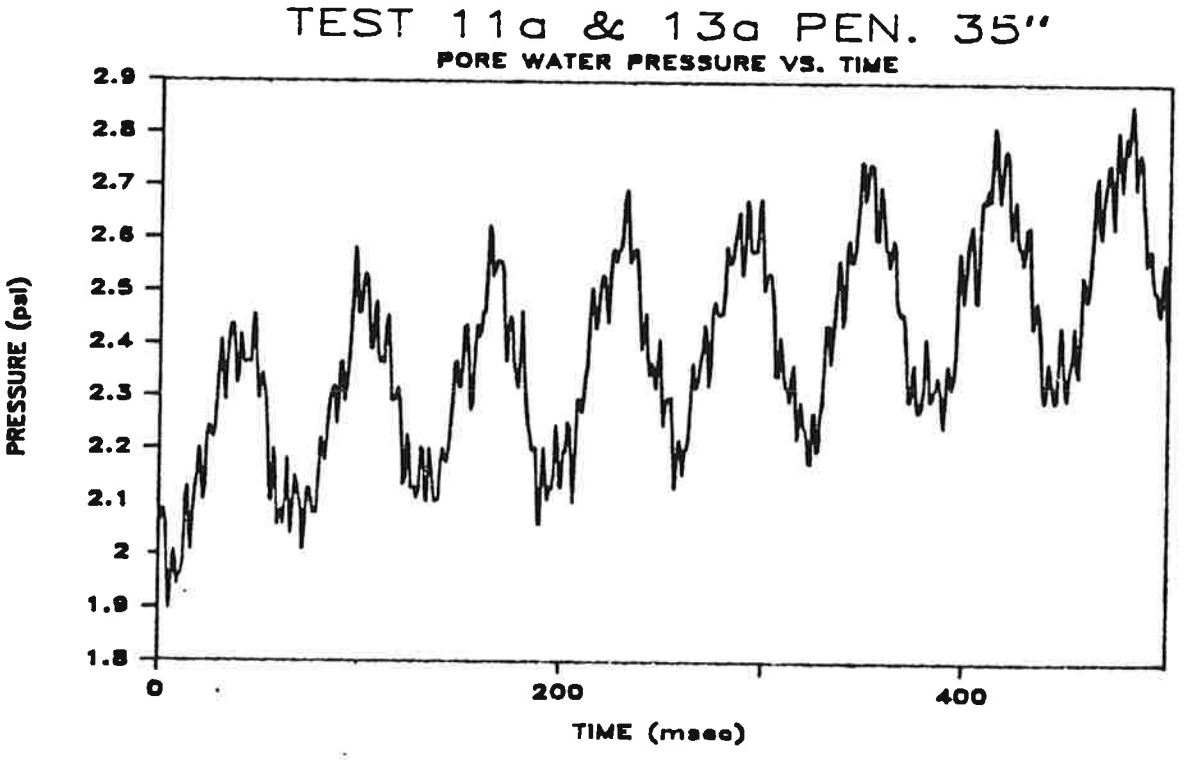

Fig. 19. Total Pressure and Pore Water Pressure Time Histories for Test 11a/13a (Relative Density = 65%; Chamber Pressure = 10 psi)

appears that they did not approach the value of total pressure at the pile-soil interface, measured at the same level as the pore water pressures, although, as indicated by the non-periodic nature of the total pressure data in the upper graph in Fig. 19, the measurements of total pressure for this test are somewhat questionable. In any event, the measured total pressures always exceeded the measured pore water pressures by a considerable amount, which suggests the maintenance of positive effective stress at the interface between the shaft and the soil and the exclusion of soil liquefaction around the pile shaft under these soil and chamber conditions.

The opposite soil and chamber conditions (high density and high pressure) are represented in Fig. 20 (Test 9). Here, it can be seen that no buildup in background pore water pressure appeared to occur but that excursions of about one-half psi occurred about the mean. The total pressure data appeared to be more reliable in this test in fine sand than in the test reported in Fig. 19 in coarse sand. The total stress data are periodic, and the excursions are much more pronounced than those in the pore water pressure data, which suggests that the soil particles may be vibrating radially against the face of the pile at the same frequency as the pile's vertical motion. Notably, however, the peak values of lateral total pressure are less than the applied effective chamber pressure plus pore water pressure, which suggests that a zone of reduced lateral stress was generated around the pile as the pile was being vibrated.

Figures 21 and 22 compare the total and pore water pressure time histories for the same test as is documented in Fig. 20. Figure 21 shows data that were recorded while the pile was still penetrating, while Fig. 22 shows data that were recorded shortly thereafter, after the pile had met refusal but continued to be vibrated. The most notable differences in the two figures are that pore water pressure excursions are reduced in the stationary pile and mean, or background, total lateral stresses are increased. The mean pore water pressure is slightly higher in the stationary pile, partly because the sensor is slightly deeper, and perhaps partly because of migration of water

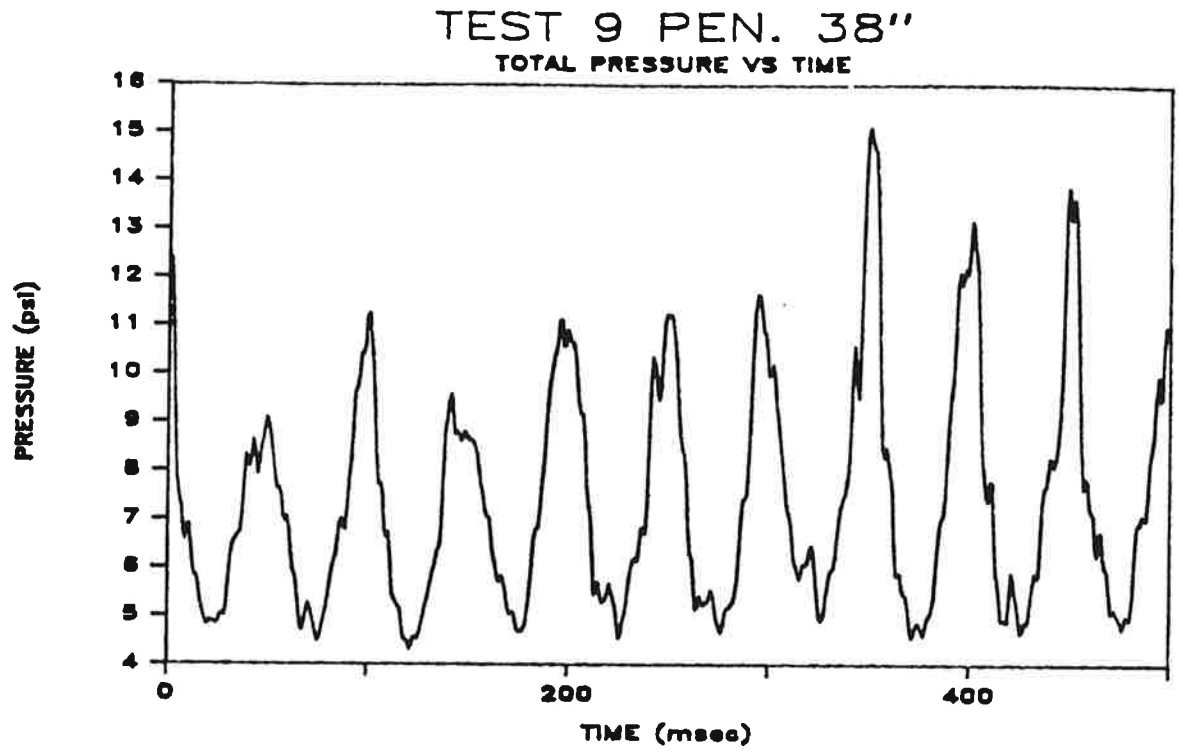

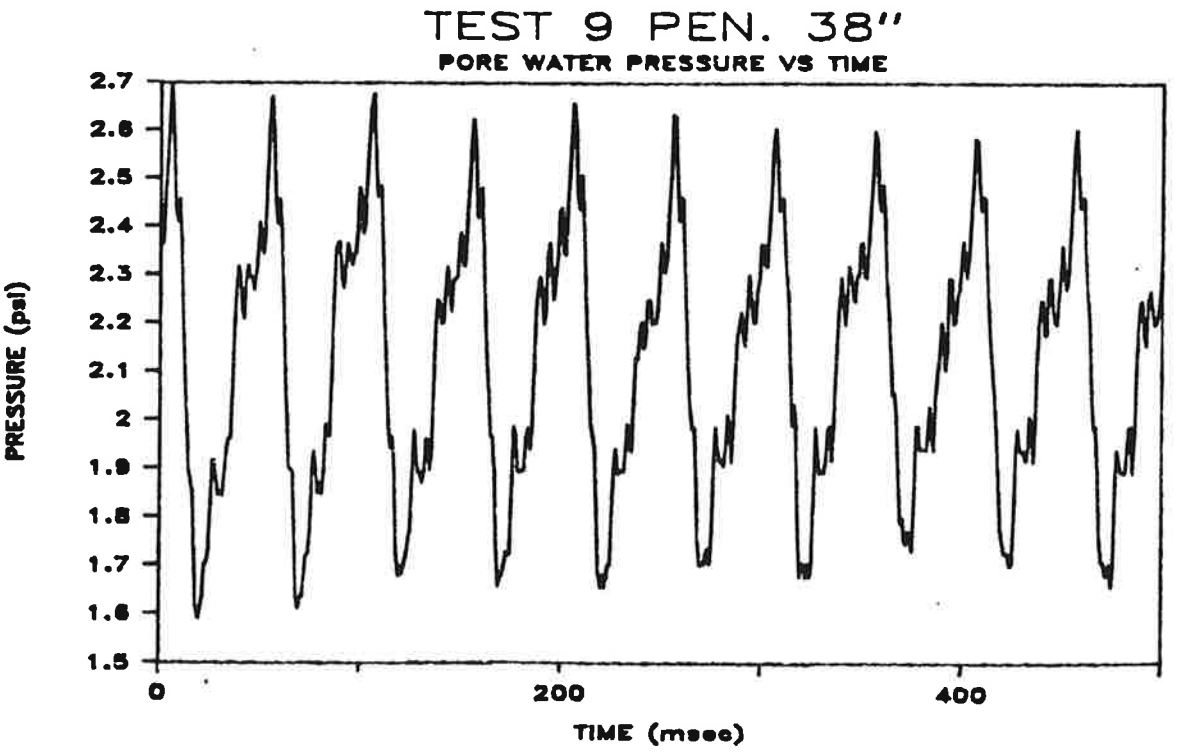

Fig. 20. Total Pressure and Pore Water Pressure Time Histories for Test 9 at Shallow Penetration (Relative Density = 90%; Chamber Pressure = 20 psi)

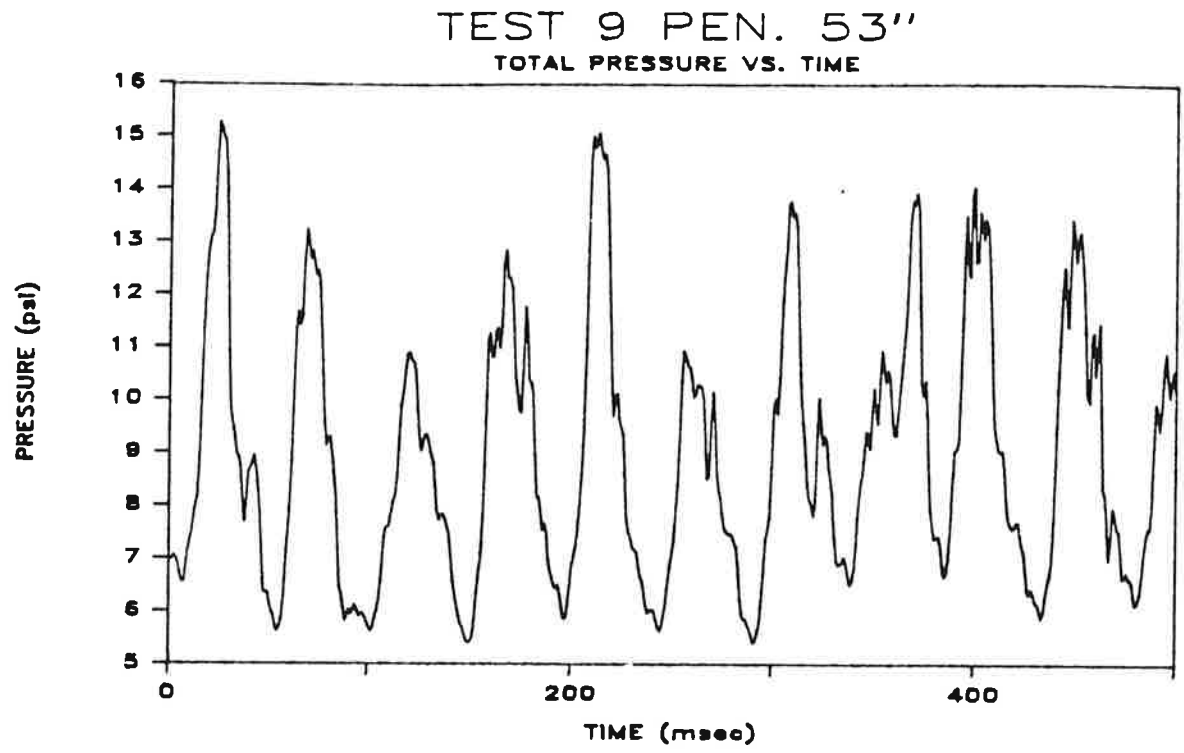

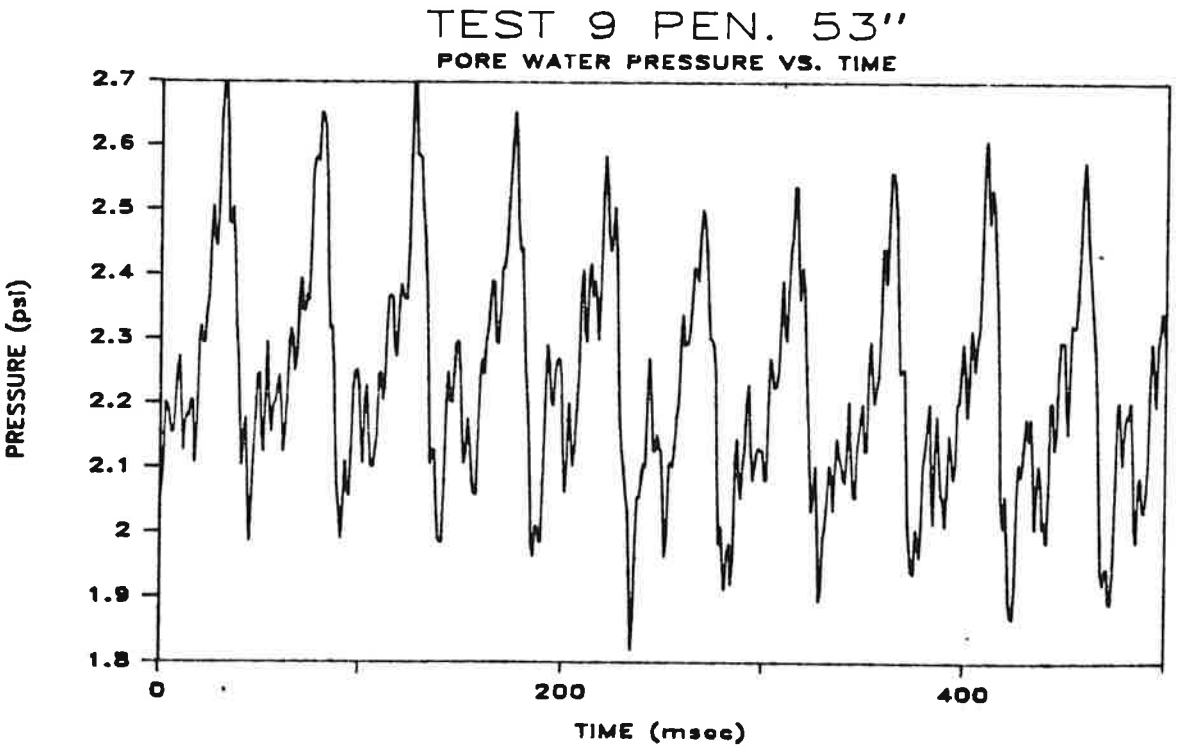

Fig. 21. Total Pressure and Pore Water Pressure Time Histories for Test 9 at Large Penetration (Relative Density = 90%; Chamber Pressure = 20 psi); Pile Penetrating

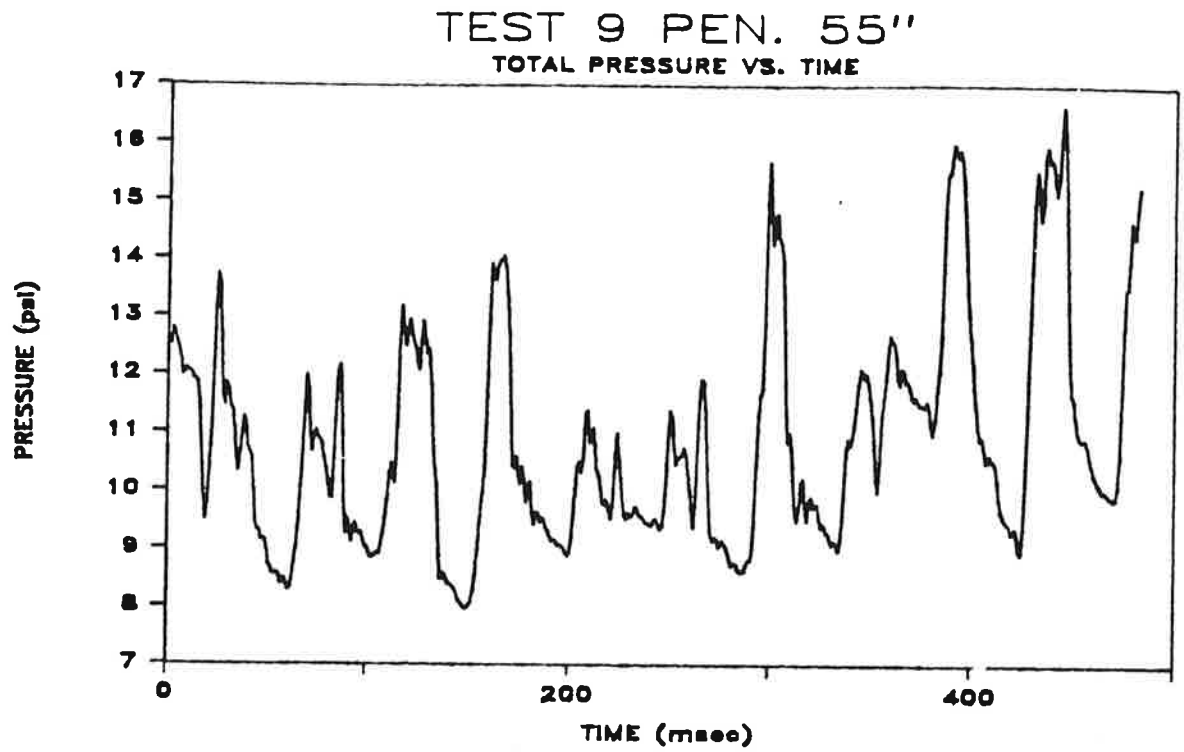

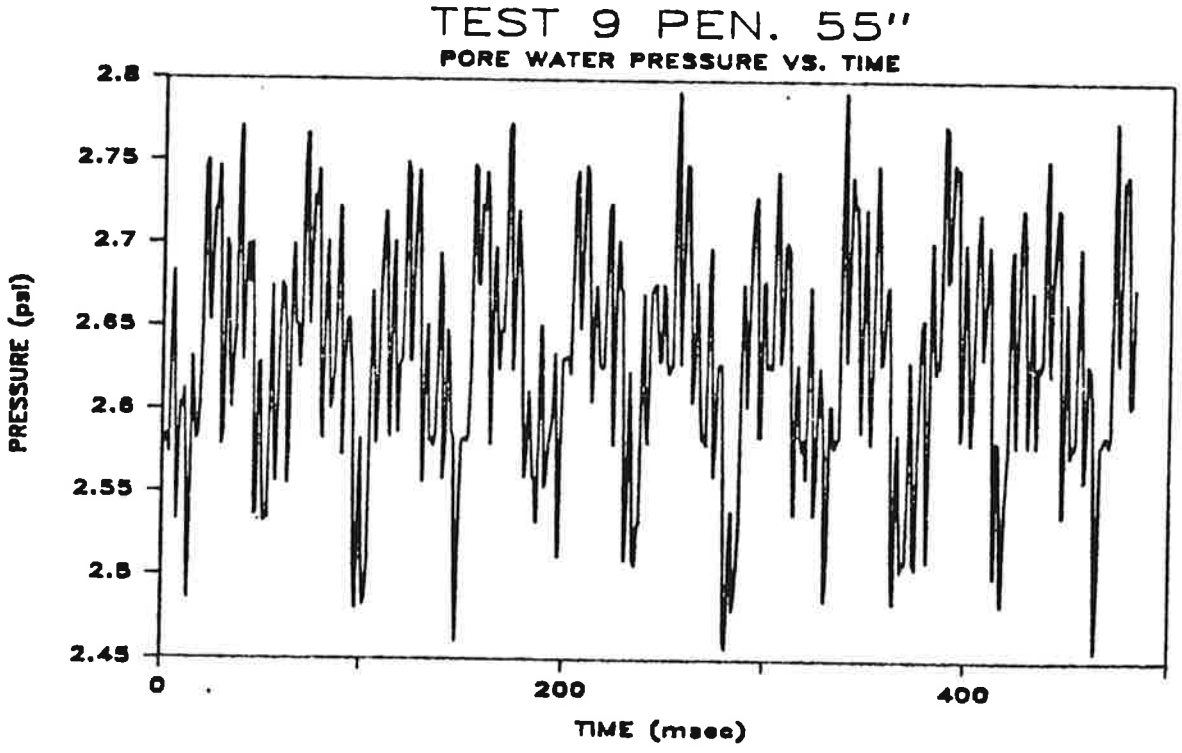

Fig. 22. Total Pressure and Pore Water Pressure Time Histories for Test 9 at Large Penetration (Relative Density = 90%; Chamber Pressure = 20 psi); Pile Stationary

toward the face of the pile from some other zone of the chamber at which the pressure was higher during penetration (perhaps beneath the toe).

It appears from analysis of these data and corresponding data from other tests documented in Appendix M that reductions in shaft resistance that occurred during vibro-driving was not primarily due to increased pore water pressure but was probably due to temporary decerases in effective stresses along the pile shaft due to the induced dynamic motion of the sand grains.

Typical Force and Velocity Time Histories for Impact and Restrike Events

Pile-head and toe force and velocity time histories for impact and restrike events are given in Appendix N. To assist in visualization, the velocity data are presented in the form of impedance (EA_{pile}/compression wave velocity of the pile material) times velocity, rather than velocity directly. At the initial force peaks the velocity-impedance generally remains constant or increases slightly as the force decreases rapidly. This behavior is opposite to that observed in impact-driven piles in the field, in which velocity-impedance decreases more quickly than force once reflected energy begins to return to the pile head. The behavior in the laboratory may be explained by the apparent fact that reflected tension waves were returning from the toe of the very short pile while the ram was still decelerating against the pile head, causing the stress to be reduced while the downward velocity of the pile head remained temporarily high.

In general, larger departures in the velocity-impedance relations from the force relations occurred at the intial peaks for the piles with low driving resistance (lower soil density and lower soil pressure conditions) than for those with high driving resistance (higher pressure and higher density), suggesting larger magnitudes of tension wave reflections, consistent with the development of lower toe resistance. The force and velocity-impedance records usually exhibited a secondary peak at a time value (4 to 5 milliseconds after the initial peak) that is consistent with the return of a reflected

compression wave from the base of the chamber. The time lapse between the initial peak and the second peak, representing the reflection of the wave from the bottom of the chamber, was generally consistent among all impact and restrike tests, except for those tests in which the pile was vibrated into position in medium-dense sand at low confining pressure, in which was the lapse period was longer. This increased lapse period is interpreted as representing lower compression wave velocities in the soil between the pile toe and the base of the chamber, which suggests that vibratory driving under those conditions may have served either to loosen that soil or to have in some way caused lower effective soil pressures, or both.

It is notable that the peak compression forces at the pile head tended to be about twice as large during impact driving as the corresponding peaks for vibro-driving (30 - 35 k versus 6.5 - 21.5 k), and the maximum tensile (negative) forces tended to be an order or magnitude greater for the impact-driven pile than for the vibro-driven pile. (Compare data from Appendix N with those from Appendix M.) It is evident that vibro-driving produced much lower axial stresses in the pile than did impact driving, which would suggest that the vibro-driver should be considered when stress conditions in the pile during installation are of concern.

Power and Energy Transmission

In order to develop a design method to predict the capacity of vibro-driven piles from installation data such as rate of penetration and driver power, it is necessary to determine how efficiently the driver is operating; specifically, how much power is effective in driving the pile compared to the theoretical power produced by the driver. It is also of interest to compare the total energy needed to drive piles with a vibrator compared with total energy needed to drive piles by impact. This section provides data relating to these two issues.

The power measured at the pile head and pile toe in the laboratory study for the vibro-driver tests is tabulated for various values of toe penetration in Table 5.

Table 5. Summary of Pile-Head and Pile-Toe Power, Acceleration, Velocity and Force for All Vibratory Tests

			Pile head				Pile toe			
Test	Pen. (In.)	Pen. Rate (ips)	power (Ft-lb/s)	a_{max} (g)	v_{max} (Ft/sec)	F_{max} (Lb)	power (Ft-lb/s)	a_{max} (g)	v_{max} (Ft/sec)	F_{max} (Lb)
5	35	0.60	2059	4.88	0.96	8390	1518	5.34	0.79	7420
	45	0.46	2711	6.20	1.11	8227	2074	7.05	1.07	6086
	60	0.28	2459	4.47	0.97	7639	1722	5.32	1.07	4679
	75	0.25	2093	3.23	0.89	7181	937	3.39	1.00	3832
6	35	1.25	2290	8.57	1.23	8113	1179	5.58	0.76	7161
	45	0.70	2392	5.42	1.04	7871	2149	5.48	1.33	5679
	60	0.50	2432	4.05	0.96	8036	1426	4.21	1.15	4624
	75	0.39	2572	4.24	0.99	9324	1390	4.21	1.15	5394
7	35	4.80	2071	3.33	1.11	5219	1258	3.69	1.17	2998
	45	3.50	2836	4.07	1.32	4678	1844	4.61	1.23	3195
	75	2.00	1870	3.16	0.85	8113	1232	4.72	1.22	3851
8	45	0.83	2590	4.50	1.13	7639	2028	5.80	1.16	4902
	60	0.71	2521	3.96	1.06	7798	1067	4.63	1.06	3198
	75	0.42	2357	3.18	0.91	7767	998	3.46	1.06	3972
9	38	0.63	4556	10.2	1.73	15400	2631	9.08	1.70	13710
	48	0.31	4260	10.0	1.64	14240	2620	7.18	1.37	11960
	53	0.10	4055	8.57	1.65	11900	2071	8.25	1.19	8609
	55	0.00	2611	5.36	0.74	14850	591	5.16	0.44	10350
11&13	35	7.50	2365	3.02	0.91	6481	2201	4.70	1.47	4693
	45	6.50	2295	4.47	0.89	7012	2067	6.48	1.31	4423
	75	3.00	2498	3.73	0.79	8343	2062	3.86	1.08	4882
14	35	1.50	2563	6.46	1.02	13150	2167	6.00	1.10	11090
	47	0.50	2856	7.90	1.22	14040	2107	7.07	1.33	11620
	55	0.45	3162	6.85	1.49	15090	2071	6.43	1.38	12150
	64	0.38	3353	6.70	1.40	15290	2060	6.13	1.34	11940
	72	0.30	3205	6.92	1.28	15960	2049	6.02	1.29	12050
15	40	1.67	3536	8.28	1.33	8173	2352	7.81	1.22	7428
	50	0.80	3387	9.03	1.36	7896	2731	8.45	1.36	7602
	60	0.70	3918	6.91	1.30	11250	2606	7.35	1.36	7823
	65	0.68	3535	6.48	1.27	10950	2603	6.74	1.35	8121
	72	0.67	3619	6.48	1.27	11870	2525	6.16	1.32	8692
16	40	10.0	3561	7.54	1.56	5768	3024	8.37	1.71	5103
	50	7.50	3200	9.36	1.55	5649	2520	9.60	1.50	4275
	77	5.00	3439	5.50	1.51	6359	2503	8.64	1.53	4529
17	35	0.40	4469	12.6	1.90	19700	2406	10.3	1.74	16460
	45	0.35	4692	11.6	1.82	19970	2421	10.2	1.68	15940
	60	0.20	4874	10.1	1.91	21880	2156	8.02	1.59	16260
	72	0.14	3971	9.24	1.66	21840	1835	7.27	1.38	16040
	74	0.00	3160	8.86	1.54	19660	1390	7.18	1.13	14220

a = Acceleration; v = Velocity; F = Force

Correspondingly, the energy measured on representative blows at various discrete penetrations is tabulated for Tests 19 - 22 (impact-hammer tests) in Tables 6 - 9. Procedures that were used to determine power and energy from the raw data are described in Appendix H. It is noted that data from Test 18 are not included because pile-head force data were not reasonable for that test, apparently due to the fact that one of the lead wires became intermittently grounded to the pile as the pile was being impacted. Table 10 summarizes the energy accepted by the pile for the various restrike events that followed installation with the vibro-driver.

By summing numerically the product of average pile-head power for an increment of time and the value of the increment of time for the entire period of driving, one can determine the total energy required to drive the pile by vibration. That energy can be compared to the total energy required to drive the pile by impact, which can be computed by summing the energy developed on each individual blow during an impact test. Data from such computations are provided in Table 11. It is observed from Table 11 that for conditions of medium dense sand (relative density = 65%) and simulated depth of 50 feet (10 psi effective chamber pressure), vibro-driving required only about 65% of the energy, on the average, required by impact driving, in terms of energy reaching the pile head (first segment of Table 11) . On the other hand, vibro-driving was found to require 3 to 8 times the total pile-head energy to install the pile for very dense sand (relative density = 90%) and/or for a simulated depth of 100 feet (20 psi effective chamber pressure), as can be determined by observing the last two segments of Table 11. It is also clear from Table 11 that more total energy was required to drive the pile either by vibration or by impact as the effective chamber pressure was increased from 10 psi to 20 psi. The total delivered energy in both methods of installation for an effective chamber pressure of 20 psi averaged approximately twice the value observed at 10 psi.

Table 6. Summary of Pile-Head and Pile-Toe Energy, Acceleration, Velocity and Force (Test 19; Blasting Sand; Relative Density 90%; Confining Pressure 10 psi)

		Pile Head					Pile Toe				
Pen. (In.)	Blow No.	E (Ft-lb)	a_{max} (g)	a_{min} (g)	v_{max} (Ft/sec)	F_{max} (Lb)	E (Ft-lb)	a_{max} (g)	a_{min} (g)	v_{max} (Ft/sec)	F_{max} (Lb)
28	43	393	188	-121	7.31	23675	98	178	-155	6.39	4544
	44	399	190	-132	7.34	24630	98	175	-179	6.30	4564
43	84	342	204	-336	7.63	27768	78	186	-206	6.42	4727
	85	371	201	-152	7.31	26969	78	188	-206	6.50	4845
44	87	373	204	-157	7.28	28245	78	193	-213	6.51	4793
	88	373	205	-156	7.32	27608	78	193	-217	6.62	4888
45	89	377	209	-153	7.36	28316	79	195	-219	6.62	4713
	90	378	209	-156	7.37	27774	79	196	-222	6.63	4906
	91	379	209	-159	7.40	28263	79	198	-223	6.67	4738
62	140	389	228	-179	7.49	32063	67	219	-260	6.85	4727
	141	386	225	-177	7.45	32209	67	219	-256	6.86	4803
76	187	335	196	-145	6.23	31688	51	229	-193	6.54	4385
	189	399	195	-144	6.43	31471	50	219	-188	6.52	4543
	190	354	205	-153	6.94	32374	50	216	-189	6.50	4561
77	191	348	203	-155	6.96	31937	50	212	-189	6.52	4442
	192	349	204	-154	6.93	31811	49	214	-189	6.47	4555
	193	347	204	-152	6.97	32515	49	211	-188	6.42	4589
	194	347	199	-153	6.86	31896	49	213	-191	6.47	4600

E = Energy; a = Acceleration; v = Velocity; F = Force

Table 7. Summary of Pile-Head and Pile-Toe Energy, Acceleration, Velocity and Force (Test 20; San Jancito River Sand; Relative Density 65%; Confining Pressure 10 psi)

		Pile Head					Pile Toe				
Pen. (In.)	Blow No.	E (Ft-lb)	a_{max} (g)	a_{min} (g)	v_{max} (Ft/sec)	F_{max} (Lb)	E (Ft-lb)	a_{max} (g)	a_{min} (g)	v_{max} (Ft/sec)	F_{max} (Lb)
20	22	438	268	-231	8.97	27753	273	396	-363	10.75	8049
	23	450	280	-257	9.37	28322	280	416	-389	11.17	8431
38	50	429	281	-257	8.28	30062	200	421	-417	11.05	9066
	51	429	280	-251	8.21	31114	200	415	-415	10.93	9002
39	52	439	285	-258	8.27	31170	200	428	-424	11.23	9149
	53	438	281	-253	8.23	30392	204	414	-424	10.83	9177
40	54	436	281	-250	8.12	31498	199	422	-419	11.19	8946
	55	437	278	-252	8.07	31415	202	420	-422	11.10	9257
41	56	431	266	-215	7.91	30423	196	400	-390	10.64	9038
	57	427	273	-236	8.01	29374	196	407	-400	10.86	9025
42	58	425	271	-239	7.96	30269	195	405	-398	10.89	9189
	59	422	268	-241	8.00	30431	194	405	-400	10.87	9049
43	60	427	271	-248	8.11	30448	191	411	-407	10.94	8856
60	94	423	269	-240	7.96	32052	174	416	-442	11.13	8565
	95	424	273	-245	8.04	31991	174	419	-446	11.14	8628
	135	419	311	-241	8.32	36363	136	488	-484	11.07	10148
76	136	416	289	-225	8.22	33944	137	441	-460	11.23	9932
	137	418	307	-233	8.14	35348	138	470	-484	11.39	10242
	138	420	283	-219	8.17	35059	142	436	-457	11.16	10328
77	139	429	309	-237	8.32	35943	141	468	-492	11.51	10529
	140	423	275	-221	8.34	33899	146	423	-457	11.45	10363
	141	431	311	-237	8.32	35337	144	483	-492	11.86	10639
78	142	432	286	-228	8.47	35705	145	437	-475	11.63	11058
	143	426	319	-246	8.54	35854	142	497	-507	12.10	11042
79	144	396	310	-240	8.29	36361	127	470	-512	11.96	11073

E = Energy; a = Acceleration; v = Velocity; F = Force

Table 8. Summary of Pile-Head and Pile-Toe Energy, Acceleration, Velocity and Force (Test 21; San Jacinto River Sand; Relative Density 90%; Confining Pressure 20 psi)

		Pile Head					Pile Toe				
Pen. (In.)	Blow No.	E (Ft-lb)	a_{max} (g)	a_{min} (g)	v_{max} (Ft/sec)	F_{max} (Lb)	E (Ft-lb)	a_{max} (g)	a_{min} (g)	v_{max} (Ft/sec)	F_{max} (Lb)
13	26	278	326	-335	8.32	27345	218	528	-407	12.26	12710
	27	277	339	-300	8.27	28979	221	537	-376	12.35	12831
32	93	342	323	-218	7.56	29745	232	482	-366	12.54	13264
	95	347	312	-233	7.44	32331	233	472	-373	12.69	12582
	120	360	308	-256	7.43	29655	204	460	-370	12.54	12064
39	121	359	309	-242	7.42	33729	204	462	-366	12.43	12111
	122	360	330	-249	7.49	33465	201	490	-373	12.38	12195
	124	363	312	-243	7.44	33782	202	446	-371	12.39	10737
	125	362	311	-227	7.48	34003	202	427	-367	12.48	11067
40	127	368	307	-250	7.56	30646	198	432	-367	12.36	12265
	128	364	305	-230	7.41	30677	193	428	-367	12.34	11211
	129	366	303	-237	7.43	34168	192	434	-371	12.34	11769
41	130	359	325	-226	7.42	32651	194	445	-361	12.40	12112
	132	350	296	-197	7.21	33040	195	418	-350	12.14	11515
48	161	370	321	-215	7.30	34344	159	457	-354	12.00	9581
	162	368	319	-221	7.33	34863	160	454	-349	11.98	11009
63	236	359	305	-233	6.82	35764	143	452	-371	11.89	10911
	237	352	293	-238	6.80	35601	141	442	-366	11.75	10448
	319	361	281	-261	6.79	38498	131	443	-392	11.52	11463
	320	372	289	-249	6.87	37776	138	444	-397	11.68	11322
	321	366	295	-255	6.86	34177	131	442	-390	11.51	10709
77	322	375	276	-244	6.88	39367	138	417	-379	11.63	11616
	323	387	299	-261	6.99	37107	133	454	-404	11.60	11220
	324	374	303	-253	6.97	36868	136	444	-400	11.69	11286
	325	380	321	-258	7.05	37482	136	447	-394	11.71	11603
	326	393	347	-258	7.09	35978	131	437	-397	11.44	11317
	327	386	293	-253	6.99	39269	128	444	-399	11.48	11921
	328	393	320	-256	7.07	36157	137	448	-398	11.66	11139
78	329	380	294	-247	6.97	35353	133	445	-397	11.51	11414
	331	380	291	-246	6.97	35139	136	443	-405	11.54	11558
	332	426	401	-260	7.51	39078	134	439	-399	11.59	12181
	333	382	385	-247	6.99	38266	132	434	-391	11.38	11935
79	334	388	317	-250	7.06	39655	135	441	-393	11.52	12169

E = Energy; a = Acceleration; v = Velocity; F = Force

Table 9. Summary of Pile-Head and Pile-Toe Energy, Acceleration, Velocity and Force
(Test 22; San Jancito River Sand; Relative Density 90%;
Confining Pressure: 20 psi vertical; 10 psi horizontal)

		Pile Head					Pile Toe				
Pen. (In.)	Blow No.	E (Ft-lb)	a_{max} (g)	a_{min} (g)	v_{max} (Ft/sec)	F_{max} (Lb)	E (Ft-lb)	a_{max} (g)	a_{min} (g)	v_{max} (Ft/sec)	F_{max} (Lb)
22	24	508	289	-229	8.56	29793	311	404	-426	10.67	9978
23	25	512	291	-233	8.58	30056	317	397	-440	10.05	10140
40	63	404	272	-190	7.68	30126	189	484	-434	10.49	10006
	64	403	272	-181	7.71	30878	195	372	-424	10.21	9979
41	65	405	271	-176	7.66	29718	193	374	-423	10.32	10232
	67	398	270	-183	7.63	29607	194	381	-423	10.42	9865
42	68	397	277	-189	7.77	30852	186	383	-437	10.31	10081
	69	399	272	-168	7.70	30431	189	380	-420	10.33	9791
43	70	407	277	-182	7.71	30182	192	388	-432	10.53	10343
	71	405	273	-191	7.71	30564	182	389	-432	10.47	9884
44	72	411	279	-197	7.87	31645	182	392	-435	10.64	9913
	73	406	279	-183	7.79	31120	185	391	-434	10.42	10282
60	116	384	283	-204	7.87	34270	146	398	-472	10.80	9723
	117	378	274	-202	7.80	33167	146	391	-459	10.71	9967
	118	391	285	-209	7.90	34836	149	405	-478	10.92	10346
76	168	364	289	-233	7.94	37941	105	413	-499	10.75	9698
	169	348	281	-230	7.75	37433	114	406	-489	10.74	9832
	170	356	283	-230	7.85	37923	108	410	-498	10.72	9638
77	171	368	290	-233	8.01	37109	114	414	-506	10.88	10101
	172	365	295	-234	7.97	37983	106	416	-512	10.87	10271
	173	363	285	-234	7.88	37225	117	421	-505	11.07	9754
78	174	361	290	-235	7.90	37018	107	417	-511	10.95	10140
	175	356	285	-235	7.85	37516	111	408	-501	10.89	9643
	176	351	285	-231	7.92	36807	103	404	-499	10.71	10096

E = Energy; a = Acceleration; v = Velocity; F = Force

Table 10. Summary of Pile-Head and Pile-Toe Energy, Acceleration, Velocity and Force for Tests with Restrike

		Pile Head					Pile Toe				
Test No.	Blow No.	E (Ft-lb)	a_{max} (g)	a_{min} (g)	v_{max} (Ft/sec)	F_{max} (Lb)	E (Ft-lb)	a_{max} (g)	a_{min} (g)	v_{max} (Ft/sec)	F_{max} (Lb)
6	5	371	269	-235	7.66	34921	157	264	-339	7.30	14712
	6	370	274	-238	7.72	34867	140	267	-345	7.29	14647
	7	380	270	-240	7.73	35603	150	267	-345	7.39	14715
7	2	414	264	-205	7.84	32611	132	297	-308	7.99	7309
	3	419	277	-241	7.86	34128	138	316	-337	8.38	7763
	4	416	275	-233	7.94	32628	141	311	-332	8.29	8052
8	5	393	329	-229	8.01	32193	197	374	-228	8.11	14194
	8	396	339	-228	8.11	34257	198	373	-281	10.32	13671
	10	396	332	-215	8.12	33376	194	366	-277	9.92	13775
9	5	339	528	-203	7.54	29836	164	473	-286	8.83	15979
	9	349	486	-229	7.65	29423	171	437	-298	9.46	15519
	13	354	452	-240	7.67	33266	172	421	-305	9.83	14746
15	4	383	337	-193	7.81	31041	211	362	-269	9.98	12563
	6	380	336	-196	7.78	31143	210	371	-272	10.02	12542
	8	393	349	-192	7.87	32041	207	371	-279	10.16	12618
16	1	353	446	-335	10.9	30379	138	562	-347	9.23	7189
	2	347	433	-303	11.2	30814	137	514	-460	9.38	6794
	3	356	371	-272	10.9	29567	138	482	-283	9.42	6503
17	5	345	330	-203	7.66	30342	101	331	-276	8.51	16392
	11	357	341	-209	7.78	32301	94	336	-309	8.83	13875
	19	373	365	-200	7.93	34137	87	336	-319	8.71	13795

E = Energy; a = Acceleration; v = Velocity; F = Force

Table 11. Summary of Total Energy Delivered to the Pile Head.

Test/Condition	Energy Delivered to Pile Head (ft-lbs)	Penetration Range (in.)	Time of Vibration (sec)
7/(S/65/10)*	29,558	25-75	15
20/(S/65/10)	47,615	25-79	Impact
11a&13a/(B/65/10)	51,864	25-78	24
16/(B/65/10)	13,600	25-77	4
5/(S/90/10)	381,341	25-75	162
6/(S/90/10)	168,263	25-75	69
18/(S/90/10)	59,968**	25-79	Impact
8/(S/90/K_O)	166,974	25-75	68
22/(S/90/K_O)	58,120	25-79	Impact
14/(B/90/10)	333,387	25-77	112
15/(B/90/10)	318,389	25-76	69
19/(B/90/10)	39,858	25-79	Impact
9/(S/90/20)	390,632	25-54	92
21/(S/90/20)	97,511	25-79	Impact
17/(B/90/20)	787,089	25-74	182

* S = SJR ; B = BLS / Relative density (%) / Effective chamber pressure (psi) ; K_O = 10 psi horiz. and 20 psi vert.

**Estimated from dynamic data of Test 22.

It is pointed out that power or energy delivered to the pile head is not equivalent to energy or power being produced by the vibro-driver or impact hammer. The theoretical power P_t of a counterrotating-mass vibrator, the type of vibrator that was used in this study to represent the most common type of vibro-driver that is used in the field, can be computed based upon principles of mechanics, as described in detail in Appendix L. Such power is a function of the operating frequency, ω (radians per second), eccentric mass, m, eccentricity of the eccentric mass, e, vibrator body mass, M, weight of the bias mass, W, and value of the constant of the isolation springs, k, located between the bias mass and the body of the vibrator, as summarized in Eqs. (1) and (2).

$$P_t = [4W + 2(me\omega^2 + MZ\omega^2)] Z (\omega/2\pi), \quad (1)$$

where,

$$Z = (me\omega^2) / M [(k/M) - \omega^2]. \quad (2)$$

It was found that the power delivered to the pile head was always less than the theoretical power developed by the driver, partially because of energy expended in moving the bias mass and apparently partially because of mechanical energy losses in the driver and/or the driver-pile connector, energy losses in sliding friction between the vibrator and the guide frame, coupling of vibrator energy into flexural energy in the pile and other factors. For the laboratory study a reasonably consistent relationship was observed between the ratio of delivered pile-head power and theoretical power (P_h/P_t) and peak pile-head acceleration at the bottom of the downstroke (positive value of acceleration in the grahps in Appendix M) (a_h), as shown in Fig. 23. P_h/P_t, which can be viewed as an efficiency factor, is seen to have increased as maximum pile-head acceleration increased. For conditions of easy driving (the condition most favorable for the vibro-driver in terms of pile-head energy required to install the pile), the average value of P_h/P_t was approximately 0.45 (four data points in Fig. 23 for the lowest accelerations). For conditions of hard driving (remaining points in Fig. 23), the average ratio was 0.75. While Fig. 23 shows a linear, least-squares, fitted relationship

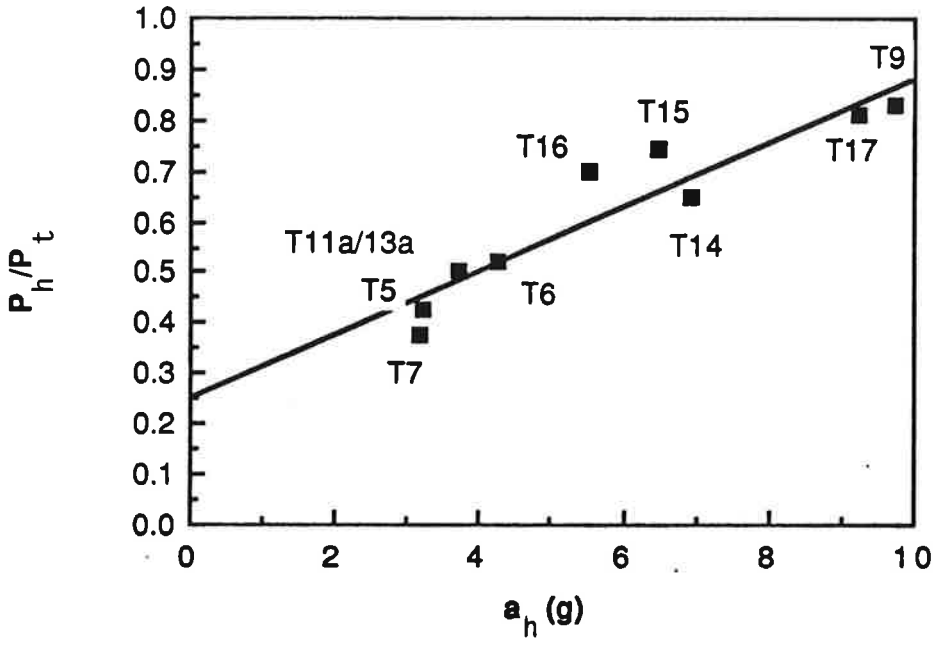

Note: Validity of This Relation Not Verified for Conditions Other Than Those Modelled in the Laboratory Tests

Fig. 23. Ratio of Pile-Head Power to Theoretical Vibrator Power Vs. Peak Pile-Head Acceleration for Vibro-Driven Piles (Capacity Tests)

(solid line) between power ratio and pile-head acceleration, the slope and intercept should be, in theory, dependent on the characteristics of the bias mass, isolation springs, connector and vibrator; hence, other slopes and intercepts may exist for various field conditions. However, further use will be made of the equation for the least-squares fit to the data presented in Fig. 23 in Chapter 3 in the development of a candidate design procedure for field verification and modification.

The theoretical energy for the impact hammer (ram weight times drop height), as operated during the laboratory study, was 810 ft-lb. The average ratio of pile-head energy (Tables 6 - 10) to this theoretical energy was consistently approximately 0.46, regardless of the conditions of the soil or the nature of the impact (continuous driving or restrike). Since both the vibratory driver and impact driver were operating at almost identical efficiencies for the conditions of easy driving, one can conclude that the ratio of mechanical driver energy required to operate the vibro-driver to that required to operate the impact hammer was approximately equal to the ratio of pile-head energies for that condition. That is, the total energy required to operate the vibro-driver was 65% of that required for the impact hammer for the case of medium dense sand at a simulated penetration of 50 feet. However, since the vibro-driver was performing more efficiently than the impact hammer for the higher soil density and for the simulated penetration of 100 feet (0.75 versus 0.46), the actual ratio of vibro-driver energy to impact hammer energy required to drive the pile was in the order or 2 to 5, compared to the ratio of 3 to 8 for energies actually delivered to the pile head.

PARAMETRIC RELATIONSHIPS FOR PENETRATION RATE AND POWER TRANSMISSION RATIO

Pile Penetration Rate

In order to lay the groundwork for the development of a candidate design method, it is desirable first to develop relationships between penetration rate (v_p) and peak pile-head acceleration (a_h). Such relationships, derived from the relationships for penetration rate previously presented in Figs. 8 - 11 and the peak pile-head acceleration data presented in Appendix M, are shown for medium dense sand (65% relative density) at 10 psi, dense sand (90% relative density) at 10 psi and dense sand at 20 psi in Figs. 24 - 26, respectively. It is seen that the v_p- a_h relationships, which were obtained from the data for a pile penetration of 12 diameters or greater, depend primarily upon soil grain size (SJR Sand was fine and Blasting Sand was coarse), relative density and effective horizontal soil pressure, all of which are factors that can be measured or estimated from a reasonably detailed site investigation program. These relationships can be expressed in one simple parametric equation, as follows.

$$v_p = \left(\frac{a_h}{\alpha_1 \alpha_2}\right)\alpha_3^{-1} \qquad (3)$$

in which

v_p = velocity of pile penetration in inches per second,

a_h = peak (single-amplitude) pile-head acceleration in g's,

α_1 = relative density parameter,

α_2 = grain-size parameter, and

α_3^{-1} = effective stress parameter.

The parameters were evaluated from linear regression analysis of the test data as follows :

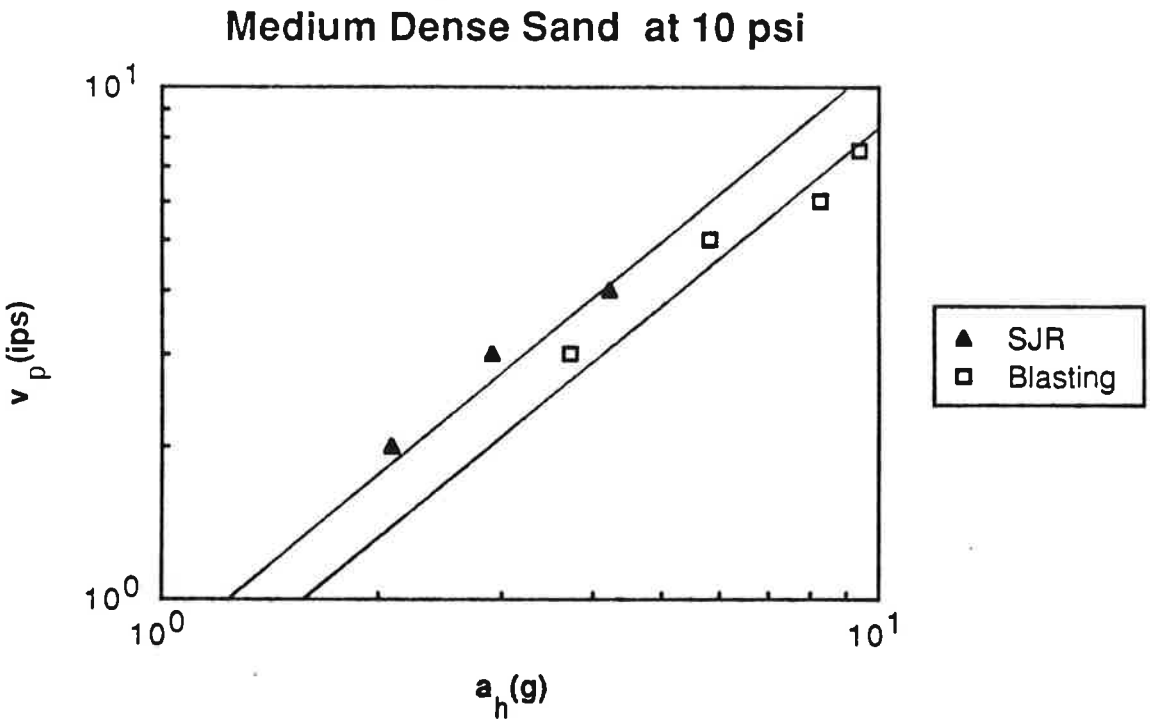

Fig. 24. Pile Penetration Velocity (v_p) Vs. Peak Pile-Head Acceleration (a_h), Sand Relative Density = 65%, Effective Chamber Pressure = 10 psi

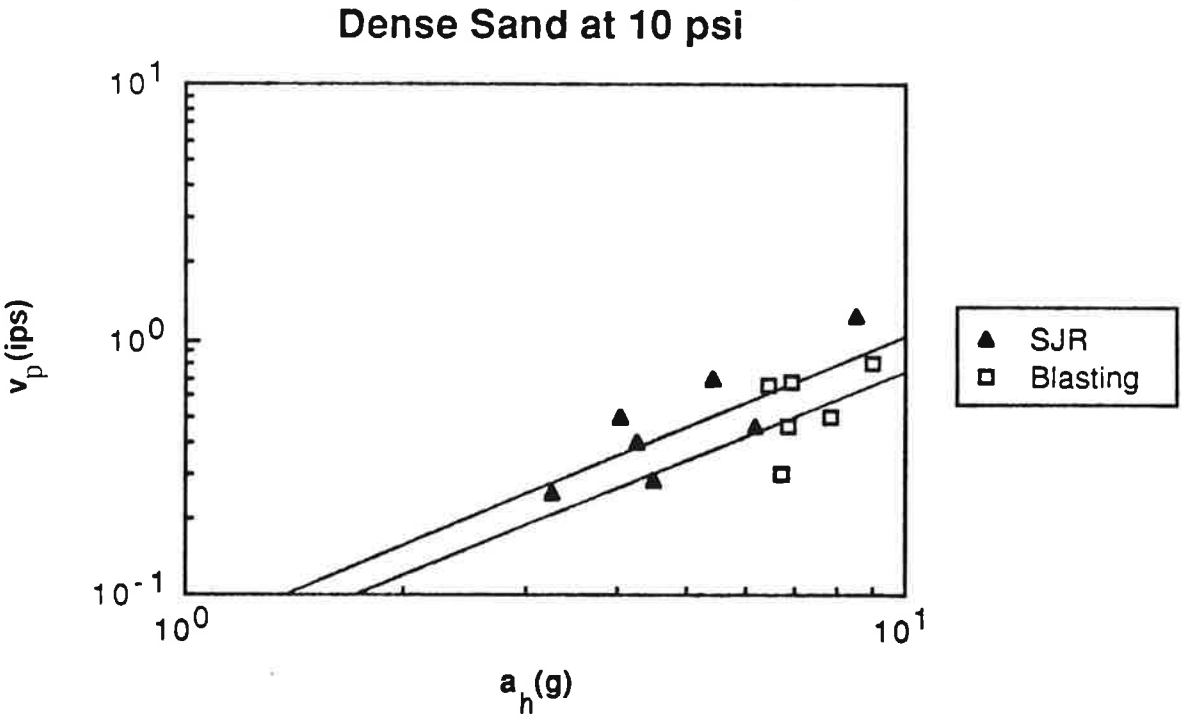

Fig. 25. Pile Penetration Velocity (v_p) Vs. Peak Pile-Head Acceleration (a_h), Sand Relative Density = 90%, Effective Chamber Pressure = 10 psi

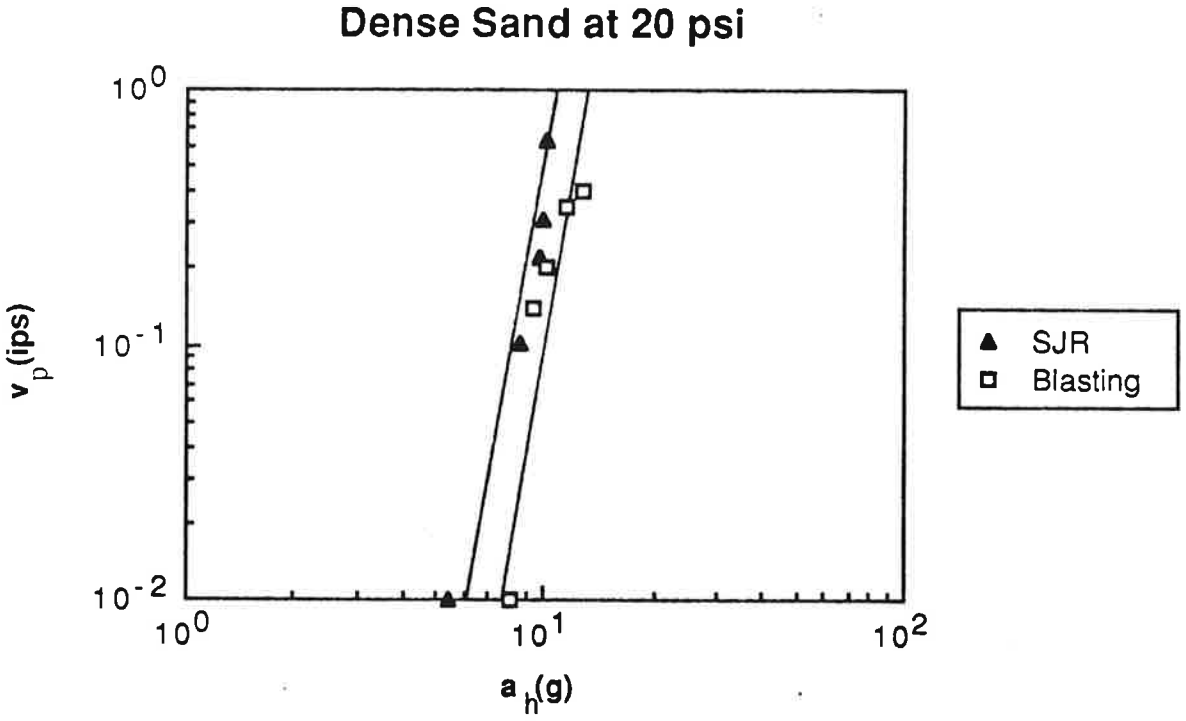

Fig. 26. Pile Penetration Velocity (v_p) Vs. Peak Pile-Head Acceleration (a_h), Sand Relative Density = 90%, Effective Chamber Pressure = 20 psi

$$\alpha_1 = -2.186 + 3.54\, D_r(\text{decimal}), \qquad 0.65 < D_r < 0.90; \tag{4}$$

$$\alpha_2 = 8.99 + 2.76\, d_{10}(\text{mm}), \qquad 0.2\ \text{mm} < d_{10} < 1.2\ \text{mm}; \tag{5}$$

$$\alpha_3^{-1} = (1.71 - 0.081\, \sigma'_h(\text{psi}))^{-1} \qquad 10\ \text{psi} < \sigma'_h < 20\ \text{psi}, \tag{6}$$

where σ'_h = lateral effective soil pressure (effective pressure applied to the boundary of the chamber).

Power Transmission Ratio

It was observed in Fig. 23 that pile-head acceleration (a_h) could be related to the ratio of power measured at the pile head (P_h) to theoretical driver power (P_t). It is convenient to develop an algebraic expression for that relationship for purposes of the later derivation of a design relationship. A linear regression analysis of the laboratory test data given in Fig. 23 (shown by the solid line in that figure) leads to the following equation:

$$\frac{P_h}{P_t} = a' + b'\, a_h(g)\ , \tag{7}$$

where $a' = 0.25$ and $b' = 0.063\ g^{-1}$ in the laboratory study.

While Eq. (7) will be used explicitly in the candidate design method that is proposed in Chapter 3, it is important to note that the constants that appear in this relationship are most probably vibrator-specific, and quite possibly pile-specific, so that Eq. (7) should be reevaluated for a variety of vibro-drivers and piles before any design method developed from this laboratory study can be applied successfully in the field.

WATER EXPULSION

The test chamber, which is described in detail in Appendix C, permitted the measurement of the volume of water expelled from the pores of the saturated soil during installation of the pile. While the pores of the soil were saturated, water volume

expelled during a test does not necessarily represent precisely the volume change in the soil produced by installing the pile, since the vertical and lateral boundaries of the chamber could expand or contract in order to maintain a constant total pressure on those surfaces. However, the volume of water expelled is believed to be an approximate measure of the volume change produced by installation and should serve as a means of assessing the relative volume change produced by vibro-driving and by impact driving. The results of the water expulsion measurements are given in Table 12.

The vibro-driver and impact driver produced about equal amounts of water expulsion for the soil at 65% relative density. Vibro-driving produced much more water expulsion than impact driving when the soil was at 90% relative denisty and more than for vibro-driving at a relative density of 65%. This result, which is contrary to intuition, appears to indicate that volume change in the vibro-driven pile is strongly associated with the time required to vibrate the pile into position, which increases with increasing relative density, as indicated in Table 12.

WAVE-EQUATION PARAMETERS FOR RESTRIKE OF VIBRO-DRIVEN PILE AND FOR IMPACT-DRIVEN PILE

Parametric studies were conducted with the impact driving data for Tests 21 and 22 (continuous driving) and the restrike data for Tests 9 and 17 using program TOPDRIVE, a one-dimensional wave equation program, which is described in Appendix O. The wave equation program was used to attempt to reproduce measured pile-head velocity time histories and pile-toe force and velocity time histories using the pile-head force time history as input, by assuming the validity of the Smith wave equation parameters and by optimizing those parameters. The primary objective of this exercise was to ascertain whether Smith-type wave equation parameters that have been shown to be acceptable for modelling the behavior of impact-driven piles can also be used to

Table 12. Summary of Total Amount of Water Expelled from Chamber

Test/Condition	Amount of Water Expelled (in^3)	(% of Pile Volume*)	Total Time of Vibration (sec) or Number of Blows	Final Penetration (in.)
7/(S/65/10)**	1548	156%	26 sec	75
20/(S/65/10)	1101	111%	144	79
11a&13a(B/65/10)	921	93%	53 sec	78
16/(B/65/10)	1032	104%	17 sec	77
5/(S/90/10)	1106	111%	217 sec	75
6/(S/90/10)	1570	158%	72 sec	75
18/(S/90/10)	NA	NA	196	79
8/(S/90/K_o)	1529	154%	105 sec	75
22/(S/90/K_o)	560***	56%	176	79
14/(B/90/10)	1055	106%	177 sec	77
15/(B/90/10)	1000	101%	118 sec	76
19/(B/90/10)	NA	NA	199	79
9/(S/90/20)	2138	215%	351 sec	55
21/(S/90/20)	627***	63%	334	79
17/(B/90/20)	866***	87%	391 sec	74

* Volume of pile at 79-inch penetration = 993 in^3

** S = SJR ; B = BLS / Relative density (%) / Effective chamber pressure (psi) ; K_o = 10 psi horiz. and 20 psi vert.

*** No water expelled was recorded after penetration of 25 inches.

NA: No valid data acquired.

Table 13. Summary of Optimum Parameters from TOPDRIVE Analyses

Test/Condition	Q(shaft) (in.)	Q(toe) (in.)	J(shaft) (sec/ft)	J(toe) (sec/ft)	R(toe)/ R(total)
9 / SJR Sand $D_r = 90\%$ $K_o = 1$ Ch. Press. = 20 psi (Restrike)	0.03	0.03	0.06	0.06	0.44
17 / BLS Sand $D_r = 90\%$ $K_o = 1$ Ch. Press. = 20 psi (Restrike)	0.08	0.10	0.09	0.07	0.48
21 / SJR Sand $D_r = 90\%$ $K_o = 1$ Ch. Press. = 20 psi (Continuous Impact)	0.04	0.04	0.07	0.08	0.24
22 / SJR Sand $D_r = 90\%$ $K_o = 0.5$ Ch. Press. = 20 psi (vertical) (Continuous Impact)	0.02	0.02	0.10	0.06	0.31

Note: Q = Smith quake; J = Smith damping; R = static capacity; D_r = relative density; K_o = earth pressure coefficient in chamber.

model piles that are vibrated into place and then restruck. A summary of the optimum values for all back-computed Smith parameters from the TOPDRIVE analyses is given in Table 13. Further details, including comparisons of computed time histories with measured time histories, are given in Appendix O.

The parametric study summarized in Table 13 considers a relatively small portion of the data acquired during this study. Specifically, it focuses on the conditions of 90% relative density and 20 psi effective chamber pressure (100 foot simulated toe penetration). Except for Test 17, which was conducted in coarse Blasting Sand, the table summarizes analyses of tests in fine San Jacinto River Sand. For those tests, values of quake and damping are not strikingly different when the pile was driven by

vibration and by continuous impact. Among the tests conducted in San Jacinto River Sand, the ratio of static toe force to total force is highest for Test 9, a restrike test, but it can be argued that that ratio is high due to the fact that in Test 9 a penetration of only 57 inches (14.25 pile diameters) was achieved. It is estimated from simple proportions that had the pile been vibro-driven to a penetration of 77 inches, which is comparable to the penetration achieved for the impact driven piles under the same conditions, that ratio would have been about 0.35, which is generally consistent with the ratios from the continuous driving tests in the San Jacinto River Sand.

It is also observed, in comparing Tests 21 and 22 in Table 13, that the effect of K_o on the Smith parameters for impact-driven piles was relatively minor, although some differences, particularly in the ratio of shaft damping to toe damping and in the value of shaft and toe quake, are evident. These differences are thought to be due primarily to the fact that the horizontal effective pressure applied to the lateral boundaries of the chamber in Test 22 was only 10 psi, so that in terms of horizontal effective stress, Test 22 simulated a pile driven only to a penetration of 50 feet, while Test 21 simulated a pile driven to a penetration of 100 feet, in isotropically stressed soil.

In the test in coarse Blasting Sand that was back-analyzed (Test 17), differences with respect to the other tests in fine sand are evident. The ratio of static toe resistance to total resistance was relatively higher than in either the vibration/restrike or continuous driving tests in San Jacinto River Sand when the corrected resistance ratio of 0.35, described above, was assumed for Test 9. The quake values are also noticeably higher than for the tests in San Jacinto River Sand. This effect indicates that the Blasting Sand behaved more nearly quasi-elastically at small displacements than did the San Jacinto River Sand. Whether this effect is due to mineralogical differences in the two sands or to effects of drainage at the toe during a hammer blow is not known.

The values of quake that appear in Table 13 are consistently lower than the values that are ordinarily recommended for analysis of pile-driving in the field, and

therefore their direct use is not recommended. The shaft damping values are generally consistent with values that are recommended for analysis of full-scale piles, while the average toe damping is about one-half of the value recommended for field use. The low quake values are most probably associated with the effects of geometric scale (pile diameter of 4 inches versus full-scale pile diameters of at least 2.5 times that value), despite the modelling of soil effective stresses in this study. The presence of reflected energy from the base of the chamber could account for the low toe damping, but no analysis of this effect was conducted, although some discussion of the effect is provided in Appendix N.

Analyses using program WEAP86, an FHWA standard wave equation program developed for the microcomputer, were also conducted for Tests 21 and 22 with the optimum parameters developed from TOPDRIVE to assess the effect of different computational algorithms. Results from WEAP86 are compared with those from TOPDRIVE in Appendix O, along with the results of a sensitivity study of cushion stiffness using WEAP 86. The comparisons were such that it appears that the parameters obtained from TOPDRIVE can also be used in WEAP86 for modelling the driving performance of the test pile.

RELATIVE STATIC BEHAVIOR OF PILE INSTALLED BY VARIOUS METHODS

Static Capacity

One of the principal objectives of the study was to determine the relationship between static capacity achieved by impact driving and by vibro-driving, with and without restrike. Detailed quasi-static load-movement curves for all of the capacity tests conducted on piles installed by various methods and descriptions of procedures for conducting the static load tests are provided in Appendix P. Since plunging failure (or the equivalent thereof for uplift loading) was rarely achieved, it was necessary to define

failure load by some consistent method involving the pattern of deflection of the pile. Five methods were investigated in this effort, and the results are presented in Tables 14 (compression loading) and 15 (uplift loading). The methods of interpretation indicated on those tables are defined in Appendix P. Upon examination of all of the load-movement curves and the summary data contained in Tables 14 and 15, it was decided that failure load would be interpreted consistently among the various tests for purposes of comparison as the value of load corresponding to a movement of the pile head of 10% of the pile diameter (0.4 inches for the model pile used in this study).

It is immediately obvious in Tables 14 and 15 that the uplift capacity of the pile was always considerably less than the compression capacity. One would be tempted to speculate that this difference is the result of the existence of toe resistance in the compression tests but not in the uplift tests, which was true but which only partially explains the difference. Reduction and analysis of the load transfer data, which are addressed in the following subsection, indicate that average unit side shear that was developed in uplift was consistently less than that developed in compression for all methods of installation.

In order to illustrate the effects of soil parameters, effective soil stress and installation method on the compression capacity of the pile, Table 16 is presented. In that table the results of all compression tests are presented three times, in each of the three segments. In the first segment the average compression capacities from each installation and loading test are grouped according to method of installation and the value of relative density of the soil in the test chamber. Average capacity is reported in terms of normalized capacity, in which a normalized capacity of unity (1.0) corresponds to the average capacity of the vibro-driven pile without restrike for the conditions reported in the middle column. The first segment of Table 16 indicates the effect of relative density (D_r), isolated from other effects, on the average capacities of the pile installed by vibro-driving (only), by vibro-driving with restrike and by

Table 14 . Comparison of Failure Loads in Kips for Compression Load Tests

Test	Condition*	Nordlund (Slope)	Davisson (Offset)	Mazur-kiewicz	Mvmt. of 0.1B	Mvmt. of 1 in.
7	S/65/10/VR	11.0	12.5	12.5	13.5	15.0
20	S/65/10/I	12.5	14.5	14.0	16.0	17.5
11&13	B/65/10/V	10.0	11.5	12.0	12.0	13.0
16	B/65/10/VR	11.0	12.0	12.5	12.5	13.0
5	S/90/10/V	16.0	18.0	20.0	21.0	22.0
6	S/90/10/VR	22.0	22.0	25.0	25.0	26.0
18	S/90/10/I	13.0	15.5	16.0	17.0	18.5
14	B/90/10/V	23.0	23.0	27.0	27.0	28.5
15	B/90/10/VR	21.0	21.5	23.0	24.0	27.5
19	B/90/10/I	19.0	20.5	20.5	21.0	22.5
8	S/90/K_o/VR	14.0	16.0	15.0	17.5	19.5
22	S/90/K_o/I	15.0	16.0	15.0	17.5	20.0
9**	S/90/20/VR	25.0	25.0	27.5	28.0	32.0
21	S/90/20/I	25.0	25.0	27.5	28.0	30.0
17	B/90/20/VR	35.0	31.0	36.0	38.5	44.0

* S=SJR ; B=BLS/ Relative Density (%) / Confining Pressure (psi) ; K_o = 10 psi horiz. and 20 psi vert. / V = Vibro-driven ; R = Restrike ; I = Impact-driven

** Load-Movement curve determined by APILE program. See Appendix P.

Table 15. Comparison of Failure Loads in Kips for Uplift Load Tests

Test	Condition*	Nordlund (Slope)	Davisson (Offset)	Mazur-kiewicz	Mvmt. of 0.1B	Mvmt. of 1 in.
7	S/65/10/VR	5.0	2.5	5.5	5.0	5.0
20	S/65/10/I	6.5	4.5	8.0	8.0	8.0
11&13	B/65/10/V	2.0	3.5	3.5	4.0	4.0
16	B/65/10/VR	2.0	3.5	3.5	4.0	4.0
5	S/90/10/V	5.0	8.0	8.5	8.5	9.0
6	S/90/10/VR	5.0	7.5	8.0	8.0	8.5
18	S/90/10/I	5.0	7.0	8.0	8.0	8.0
14	B/90/10/V	7.0	8.5	9.5	10.0	12.0
15	B/90/10/VR	6.0	8.0	9.5	9.0	10.0
19	B/90/10/I	7.0	9.0	10.0	10.5	11.0
8	S/90/K_o/VR	5.0	7.0	7.5	7.5	8.0
22	S/90/K_o/I	6.0	8.5	9.0	9.5	10.0
9**	S/90/20/VR	12.5	13.5	14.5	15.5	16.0
21	S/90/20/I	13.0	14.5	16.0	17.0	18.0
17	B/90/20/VR	13.0	14.5	19.0	19.0	24.0

* S=SJR ; B=BLS/ Relative Density (%) / Confining Pressure (psi) ; K_o = 10 psi horiz. and 20 psi vert. / V = Vibro-driven ; R = Restrike ; I = Impact-driven

** Load-Movement curve determined by APILE program. See Appendix P.

Table 16. Summary of Mean Normalized Capacity (Average of All Capacity Tests) in Terms of Relative Density, D_r, Effective Chamber Pressure, σ'_h, and Grain Size, d_{10}, Relative to Method of Installation

Method of Installation	$D_r = 65\%$	$D_r = 90\%$
Impact	1.3	1.7
Vibro Only	1.0	2.0
Vibro/Restrike	1.1	1.7

Method of Installation	$\sigma'_h = 10$ psi	$\sigma'_h = 20$ psi
Impact	0.9	1.4
Vibro Only	1.0	-
Vibro/Restrike	0.9	1.7

Method of Installation	$d_{10} = 0.2$ mm	$d_{10} = 1.2$ mm
Impact	0.9	1.0
Vibro Only	1.0	0.9
Vibro/Restrike	1.0	1.2

continuous impact driving. In this simple form of presentation it can be observed that for all tests conducted in both sands at 65% relative density, the capacity produced by impact driving exceeded that for vibro-driving without restriking by a factor of 1.3. Vibration with restrike produced a capacity 1.1 times that for vibro-driving only. It follows that vibro-driving with restrike produced, on the average, a capacity of 85% (1.1 / 1.3) of that of the pile installed with continuous impact driving. For all tests conducted at a relative density of 90%, installation by vibration (only) produced a capacity that was 118% (2.0 / 1.7) of that which was observed for either continuous impact driving or vibro-driving with restrike. These data indicate that the relative density of the sand has a major influence on whether vibro-installation will produce a pile with a capacity equivalent to or better than that of an impact-driven pile. While restriking improved the capacity of the pile in medium-dense sand (D_r = 65%), restriking was somewhat counterproductive in the dense sand (D_r = 90%).

Even under the conditions in which the capacity of a vibro-driven (only) pile was inferior to that of the impact driven pile (relative density of 65%), the vibro-driven (only) pile developed, on the average, 77% of the capacity of the impact-driven pile (1.0 / 1.3). Furthermore, no significant differences can be observed in the initial slopes of the load-settlement or load-uplift curves between vibro-driving (only) and continuous impact driving (Appendix P).

It is also of interest to note that increasing the relative density of the soil from 65% to 90% resulted in an increase in average compression capacity in the vibro-driven (only) pile by a factor of 2, while it resulted in an increase in the average compression capacity of the continuously impact-driven pile by a factor of only 1.3 and of the restruck vibro-driven pile by a factor of 1.5.

In the middle segment of Table 16 all of the compression capacities for the pile installed and subjected to a loading test with an effective chamber pressure of 10 psi are compared, in normalized fashion, with those for an effective chamber pressure of 20

psi. Contrary to the effect of soil relative density, it appears that method of installation had relatively less effect with respect to chamber pressure (simulated depth) as a variable. Although no vibro-driven (only) piles were installed and load-tested with an effective chamber pressure of 20 psi, and no estimate of the effect of effective pressure on capacity can therefore be ascertained for that method of installation from Table 16, it can be observed that increasing the effective soil stress from 10 to 20 psi produced an increase in static capacity of vibro-driven and restruck pile by a factor of 1.9 (1.7 / 0.9) and of continuously impact-driven piles by a factor of 1.6 (1.4 / 0.9).

The final segment of Table 16 compares the pile capacities from all compression loading tests in terms of the effective grain size of the sand. Very little influence of effective grain size on static capacity can be observed.

An alternate method of comparing the compression capacities of the restruck vibro-driven pile with that of the continuously impact-driven pile is given in Fig. 27, in which the static compression capacity Q is plotted for the impact-driven pile (Q_{IMP}) against that for the vibro-driven pile (Q_{VIB}) for all five pairs of tests in in the laboratory study in which conditions were otherwise identical and for which direct comparisons can therefore be made. The first of the two tests in the legend is a test on a vibro-driven pile, while the second is a test on an impact-driven pile. See Appendix B or Table 14 for details of each test. All of these paired tests involved vibro-driven piles that were restruck. Viewed in this manner, it appears that the capacity of the restruck vibro-driven pile was, on the average, essentially equal to that of the continuously impact-driven pile.

Unit Load Transfer Relationships

Graphs of unit load transfer (unit shaft resistance, f, and unit toe resistance, q) versus local pile movement, w, often called unit load transfer relationships, are useful devices in describing the manner in which the soil develops resistance to pile

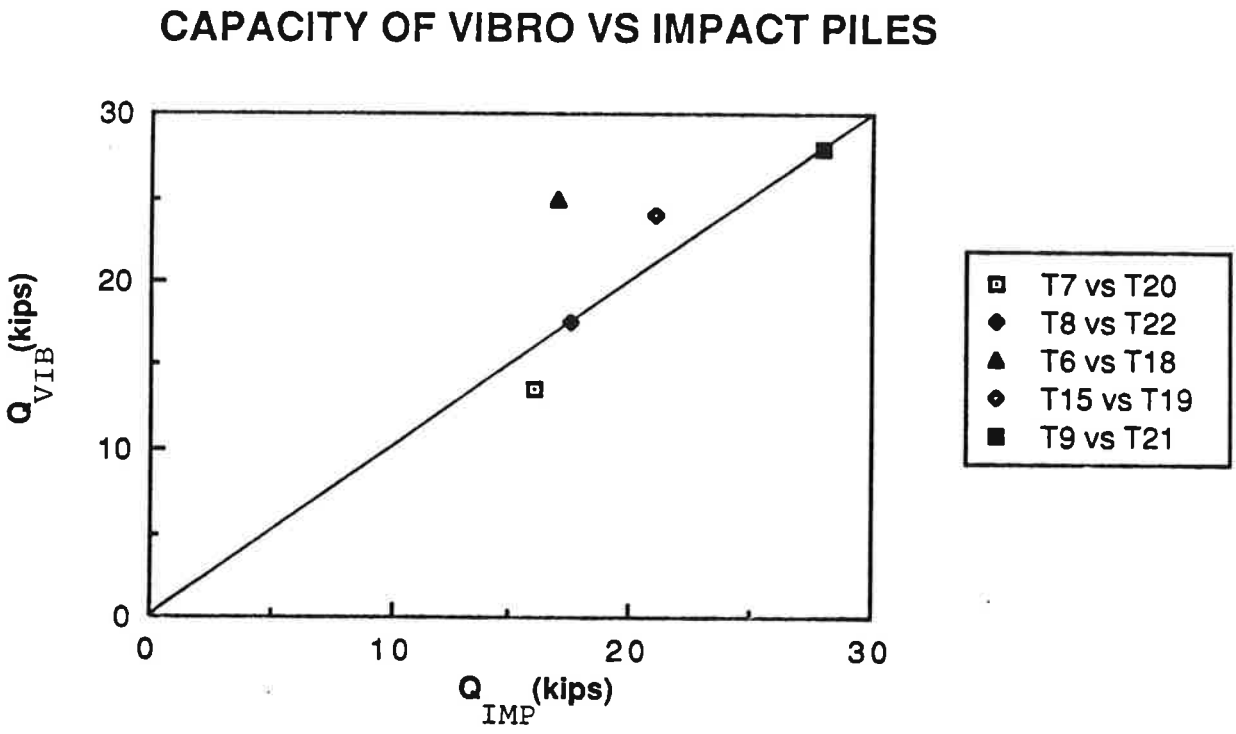

Fig. 27. Comparison of Compression Capacites of Pile Driven by Vibration and Restruck with Pile Driven Continuously by Impact Under Identical Soil Conditions

movement. Such relationships are also sometimes used to synthesize the static behavior of piles of geometries that are different from those from which the relationships were derived. For example, a brief description may be found in Appendix P of the use of unit load transfer relationships developed for the pile in Test 9 in synthesizing the pile-head behavior of the same pile installed to a deeper penetration.

Individual f-w and q-w curves derived from the strain gage data in the static loading tests are given in Appendix Q, which also describes the method used to derive these relations from the acquired data. Also presented in Appendix Q are normalized f-w and q-w relationships, in which the stress (f or q) is divided by the effective octahedral chamber pressure (average of twice the horizontal effective pressure and the vertical effective pressure applied to the chamber). In all cases except the cases where $K_o = 0.5$, the octahedral effective stress was taken to be equal to the horizontal effective stress at the boundary of the sand column, σ'_h, although the vertical effective stress exceeded slightly the horizontal effective stress by an amount equal to the pressure produced by the buoyant body weight of the soil. The notation σ'_h has been retained to represent octahedral effective stress in graphical presentations, even in the cases where $K_o = 0.5$.

The normalized relationships of Appendix Q are summarized in this section by further normalizing the displacement w by dividing by the pile diameter, B, and producing average relationships for several groupings of tests. Those groupings are, in order, (a) all tests conducted in SJR Sand at 65% relative density; (b) all tests on impact-driven pile in SJR Sand at 90% relative density; (c) all tests on vibro-driven pile in SJR Sand at 90% relative density; (d) all tests on vibro-driven pile in BLS Sand at 65% relative density (no impact test performed for this condition); (e) all tests on impact-driven pile at 90% relative density; and (f) all tests on vibro-driven pile at 90% relative density. Figures 28 - 33 present the f-w relations in this order, and Figs. 34 - 39 present

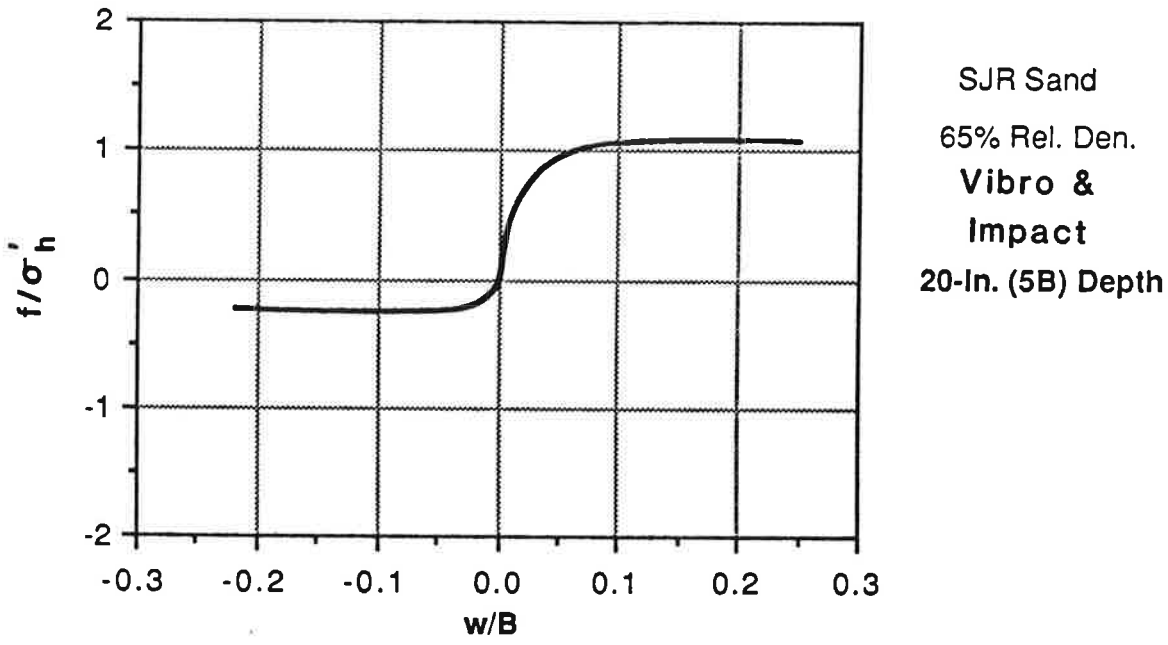

Fig. 28a. Summary Normalized f-w Relation for Pile Driven by Impact or Vibrated into SJR Sand at 65% Relative Density; Top Half of Pile

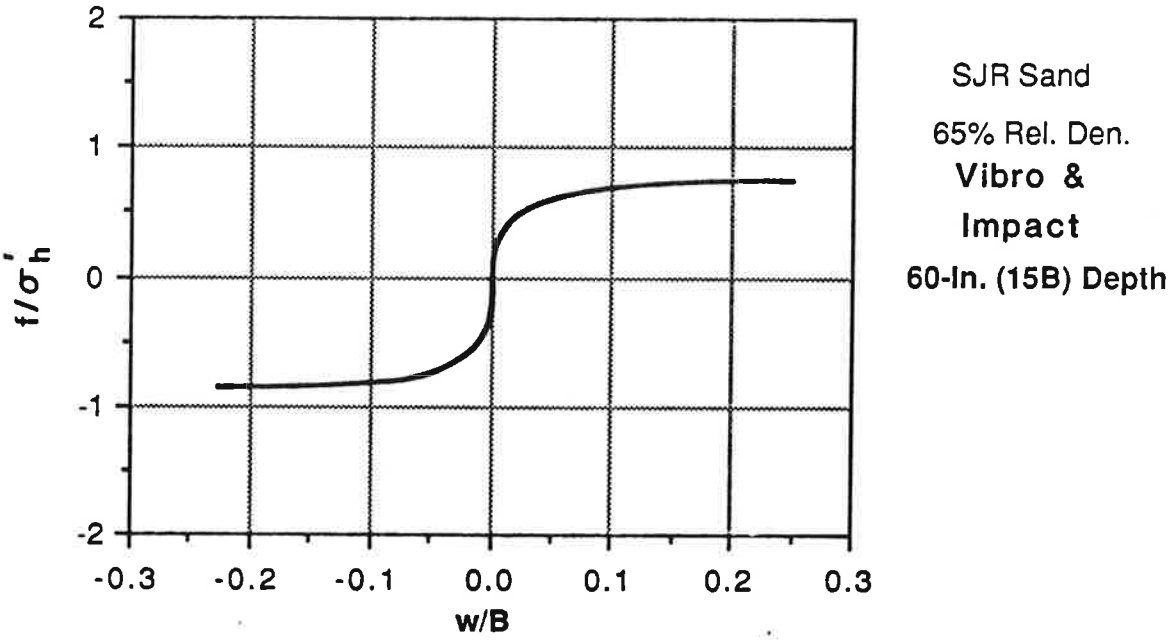

Fig. 28b. Summary Normalized f-w Relation for Pile Driven by Impact or Vibrated into SJR Sand at 65% Relative Density; Bottom Half of Pile

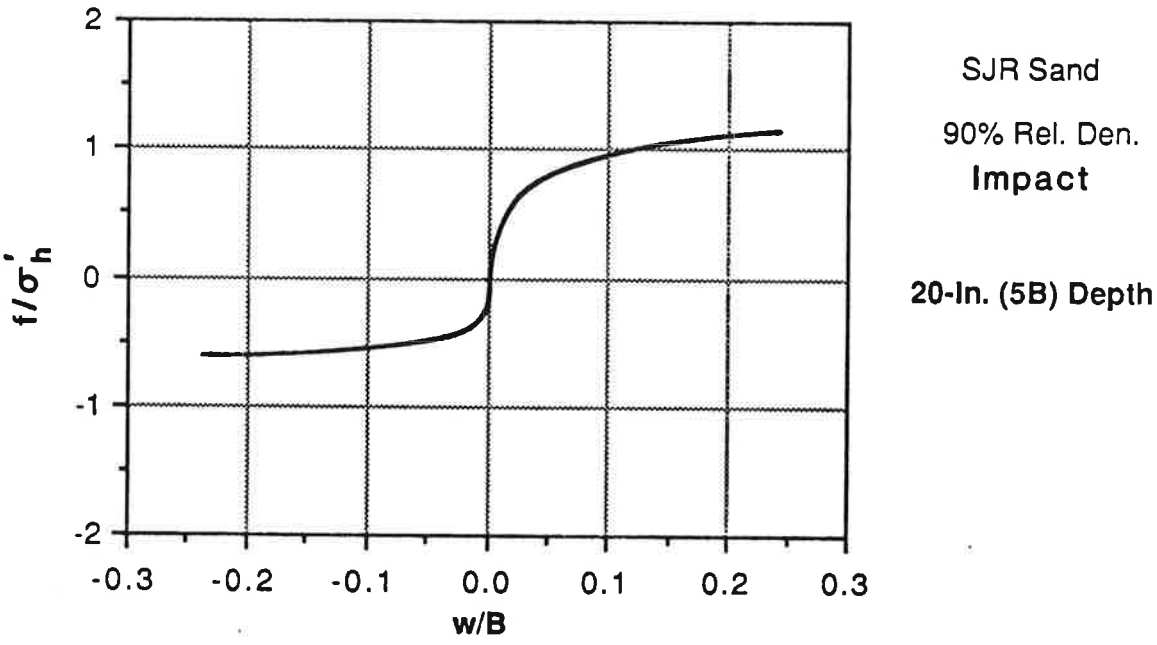

Fig. 29a. Summary Normalized f-w Relation for Pile Driven by Impact into SJR Sand at 90% Relative Density; Top Half of Pile

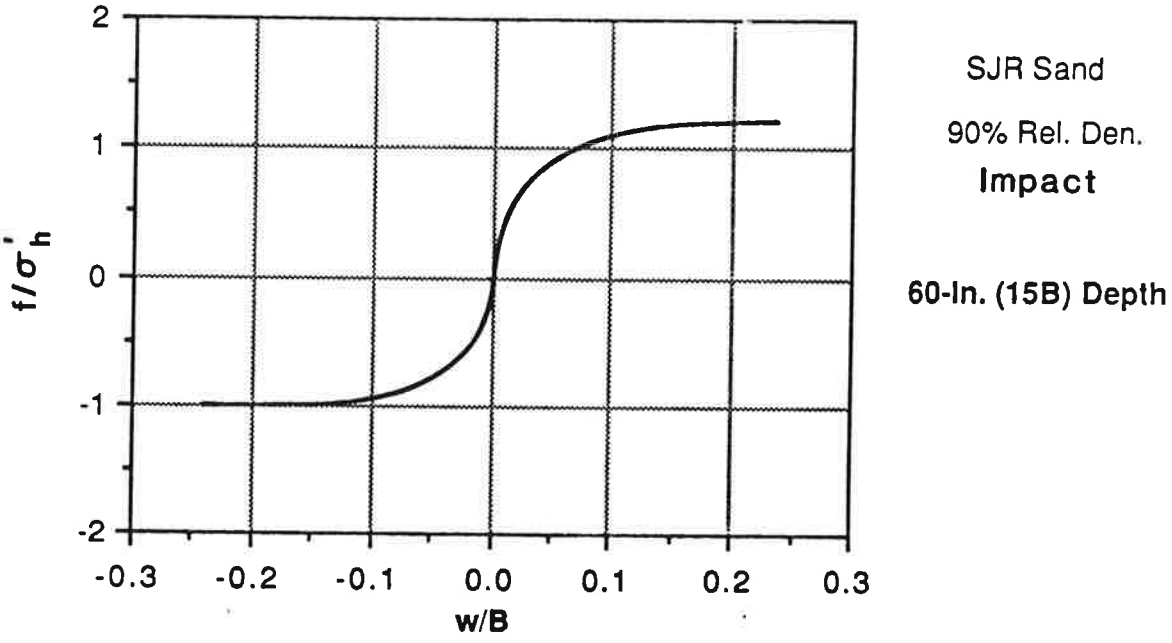

Fig. 29b. Summary Normalized f-w Relation for Pile Driven by Impact into SJR Sand at 90% Relative Density; Bottom Half of Pile

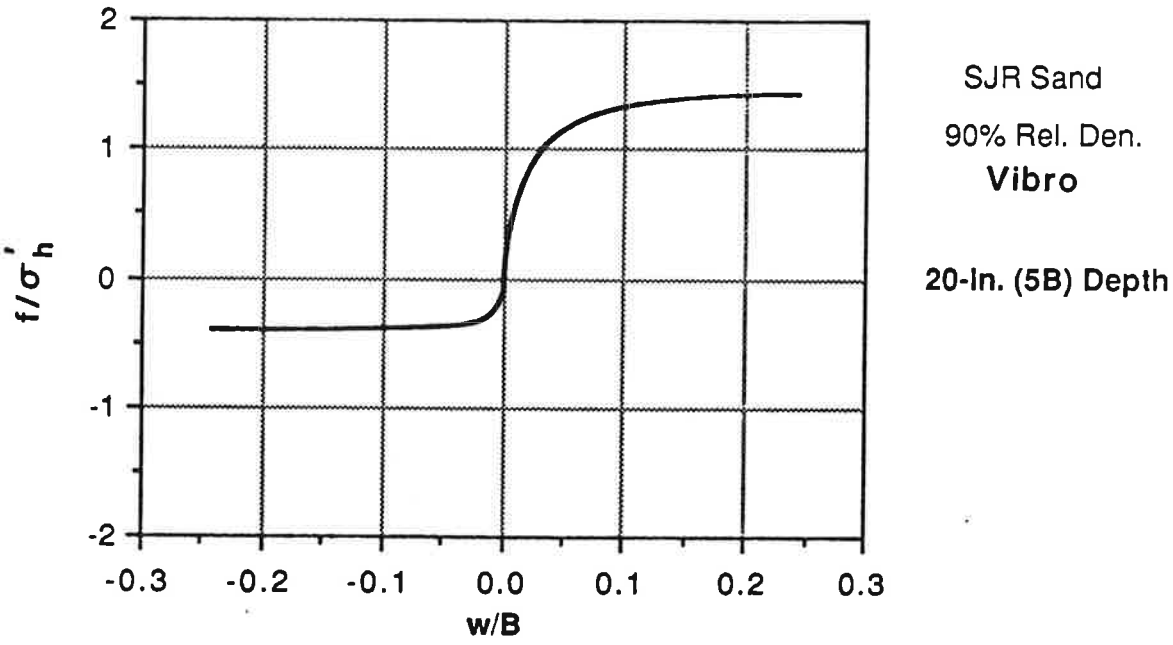

Fig. 30a. Summary Normalized f-w Relation for Pile Vibrated into SJR Sand at 90% Relative Density; Top Half of Pile

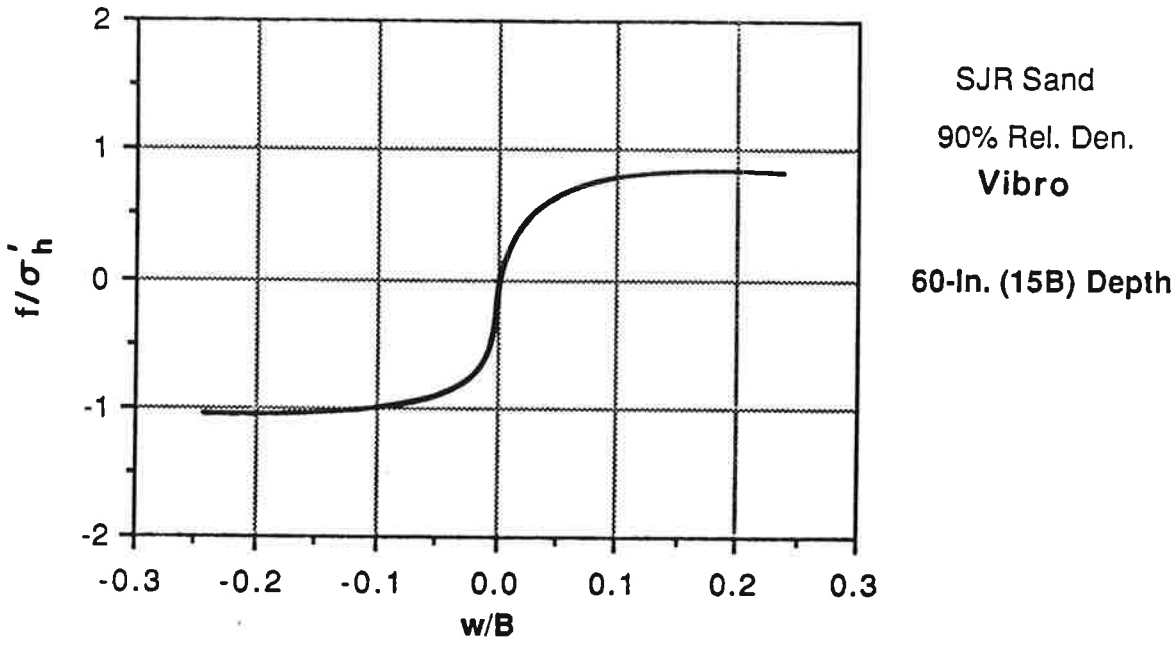

Fig. 30b. Summary Normalized f-w Relation for Pile Vibrated into SJR Sand at 90% Relative Density; Bottom Half of Pile

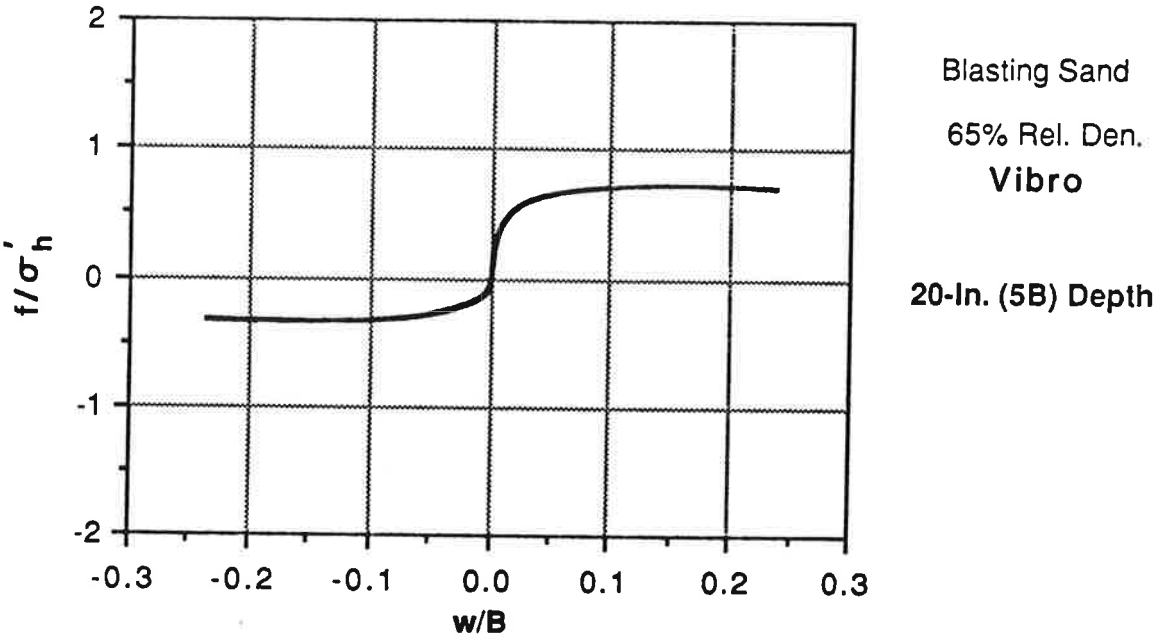

Fig. 31a. Summary Normalized f-w Relation for Pile Vibrated into BLS Sand at 65% Relative Density; Top Half of Pile

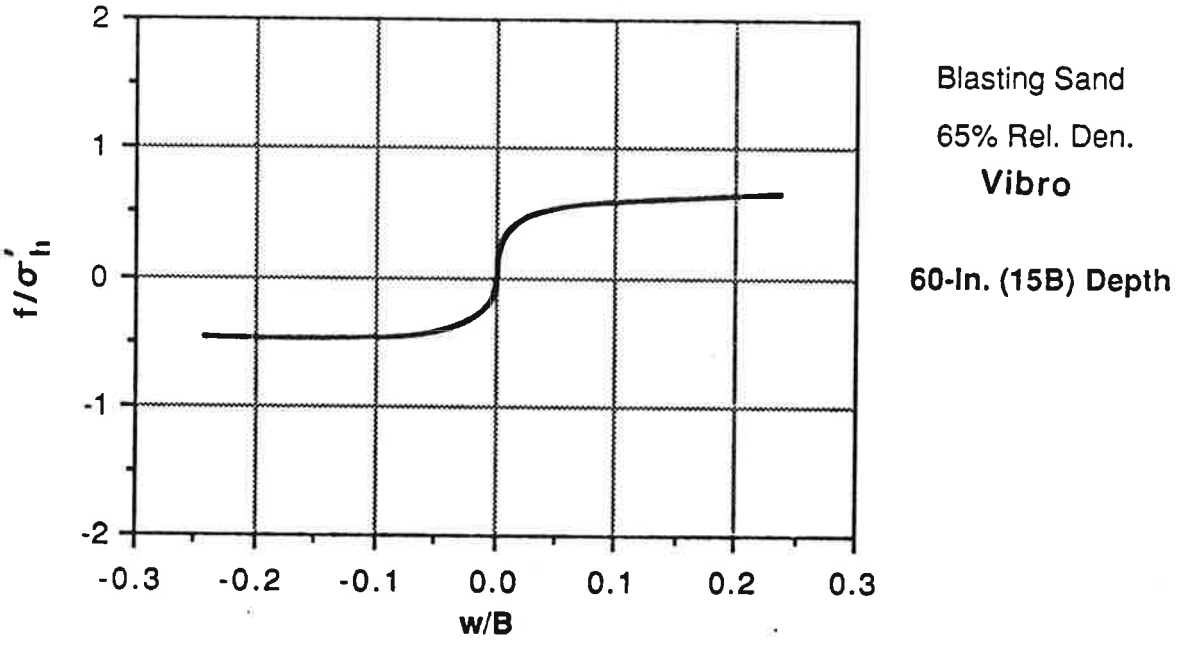

Fig. 31b. Summary Normalized f-w Relation for Pile Vibrated into BLS Sand at 65% Relative Density; Bottom Half of Pile

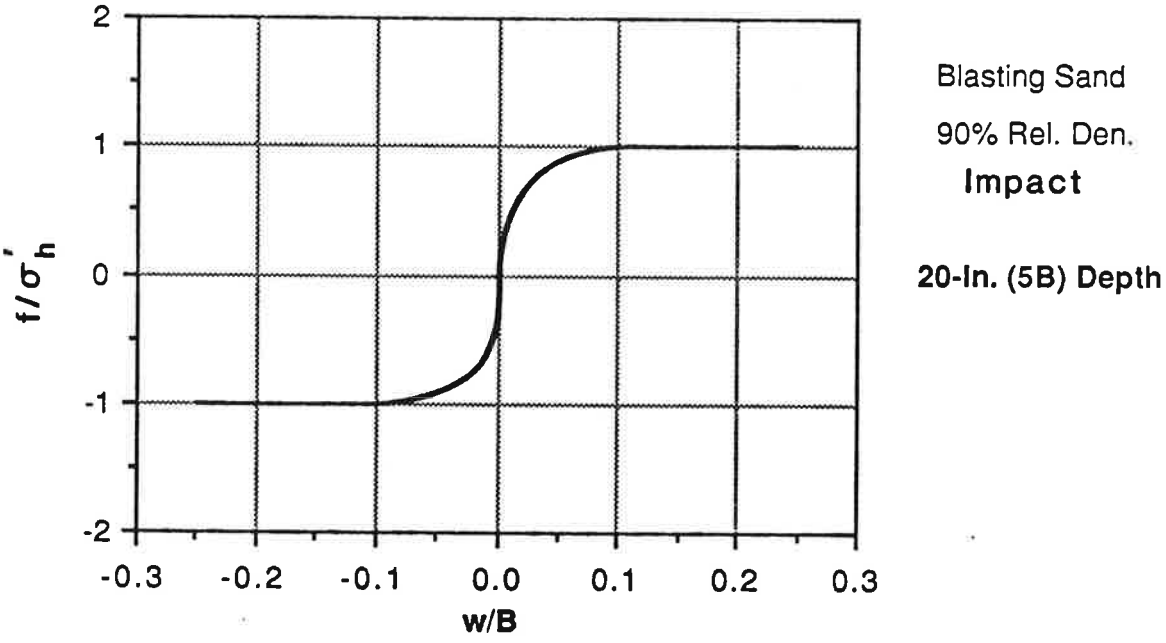

Fig. 32a. Summary Normalized f-w Relation for Pile Driven by Impact into BLS Sand at 90% Relative Density; Top Half of Pile

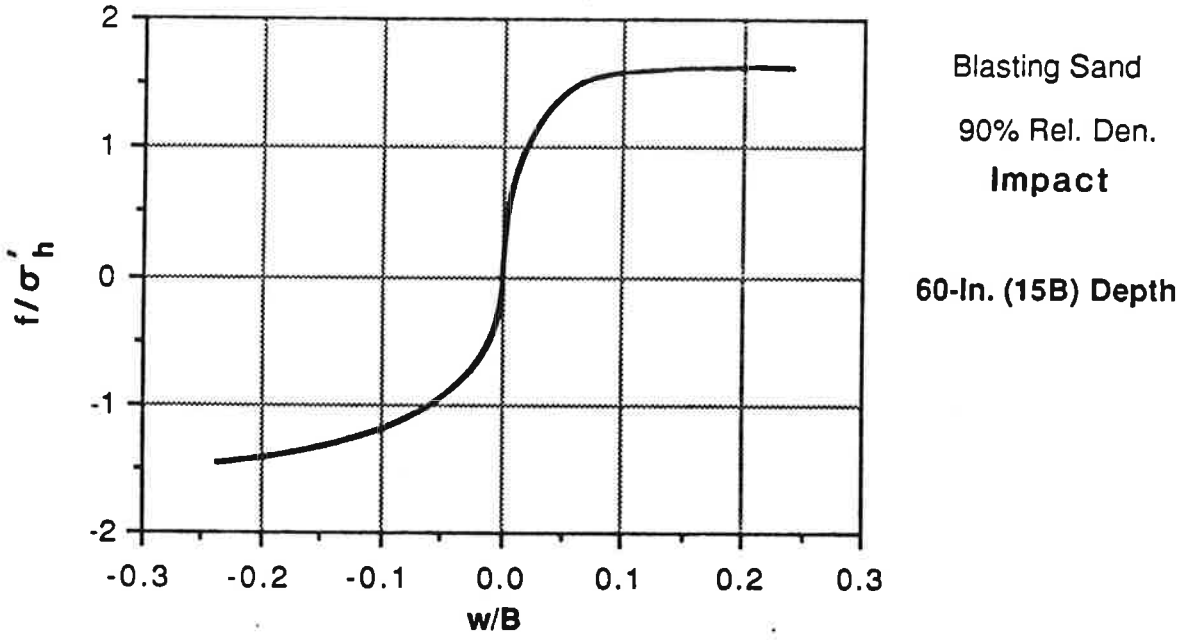

Fig. 32b. Summary Normalized f-w Relation for Pile Driven by Impact into BLS Sand at 90% Relative Density; Bottom Half of Pile

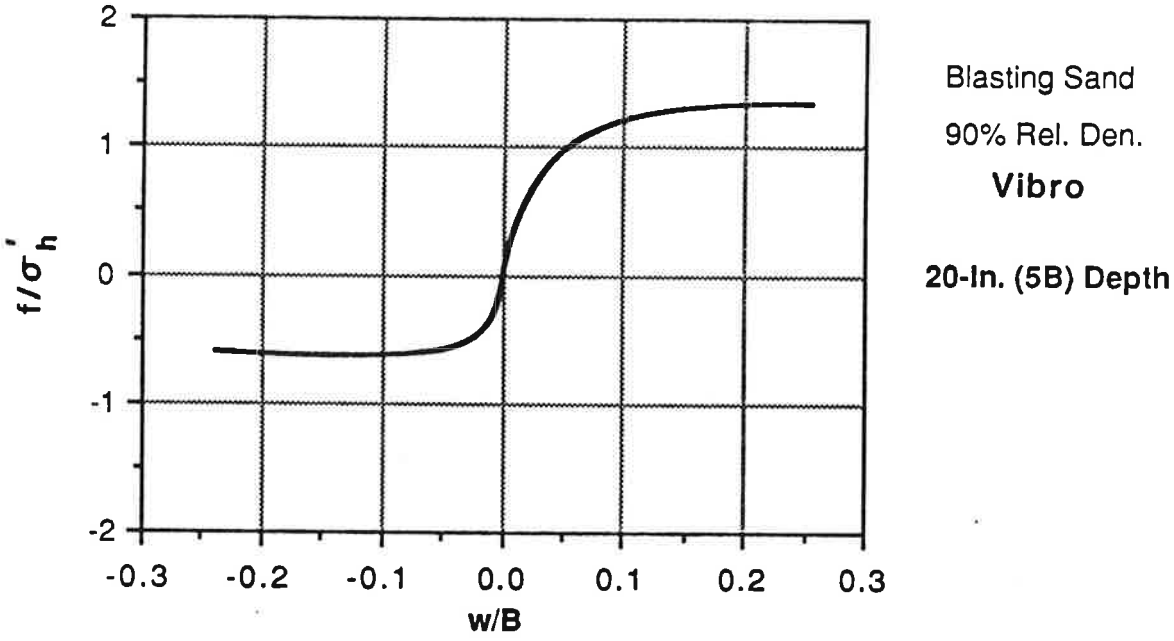

Fig. 33a. Summary Normalized f-w Relation for Pile Vibrated into BLS Sand at 90% Relative Density; Top Half of Pile

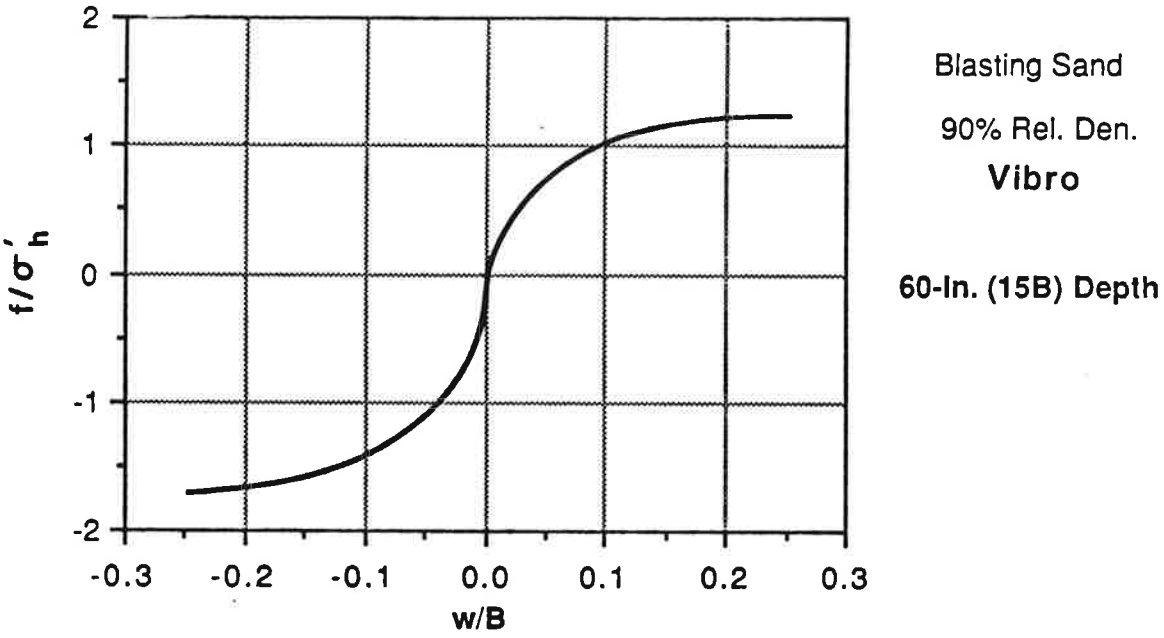

Fig. 33b. Summary Normalized f-w Relation for Pile Vibrated into BLS Sand at 90% Relative Density; Bottom Half of Pile

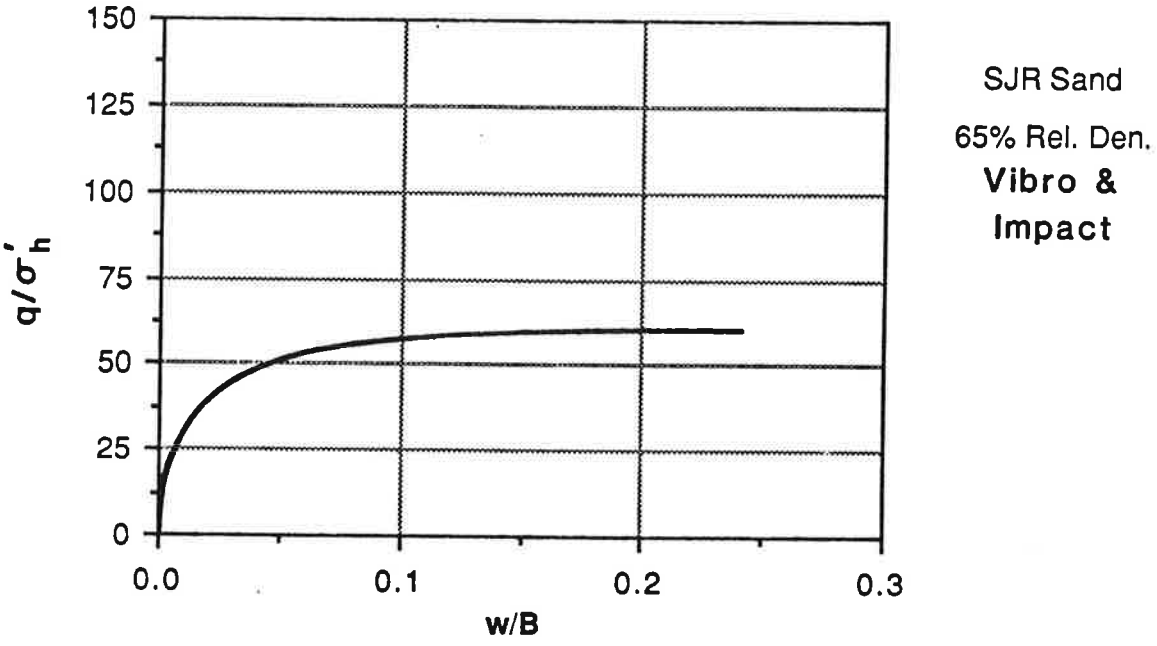

Fig. 34. Summary Normalized q-w Relation for Pile Driven by Impact and Vibrated into SJR Sand at 65% Relative Density

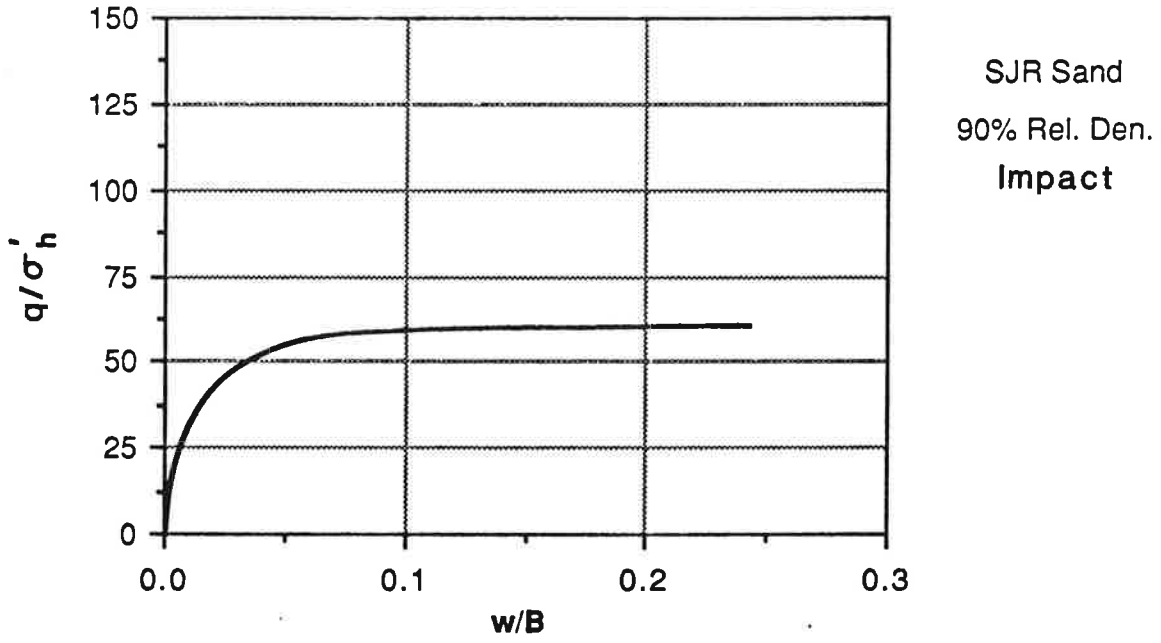

Fig. 35. Summary Normalized q-w Relation for Pile Driven by Impact into SJR Sand at 90% Relative Density

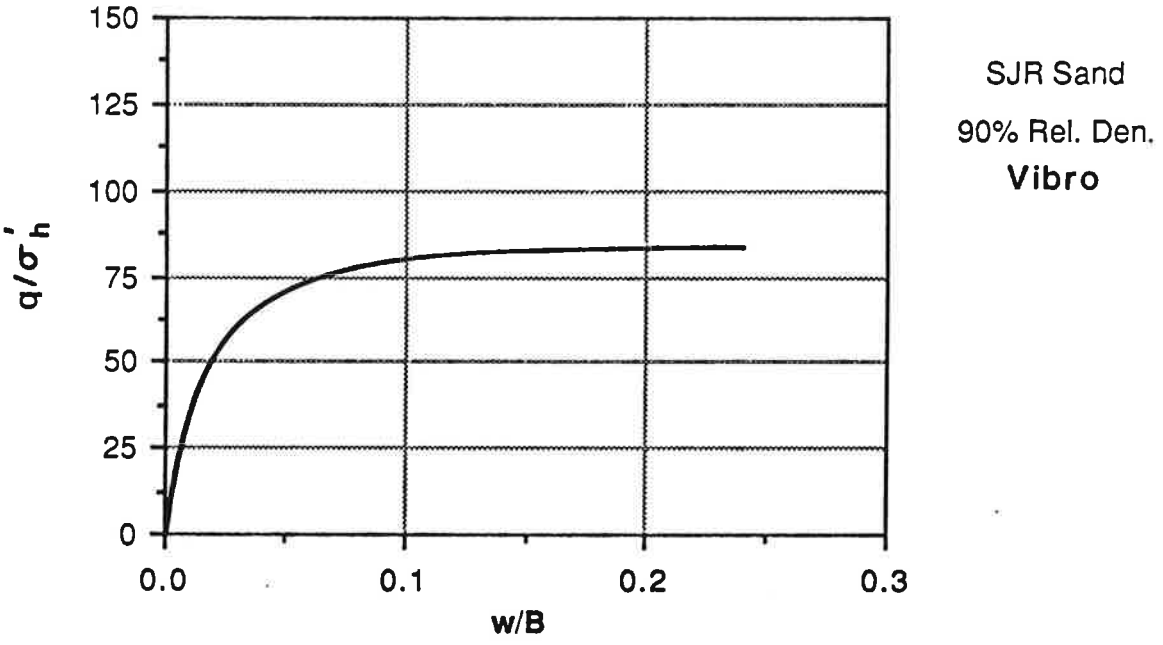

Fig. 36. Summary Normalized q-w Relation for Pile Vibrated into SJR Sand at 90% Relative Density

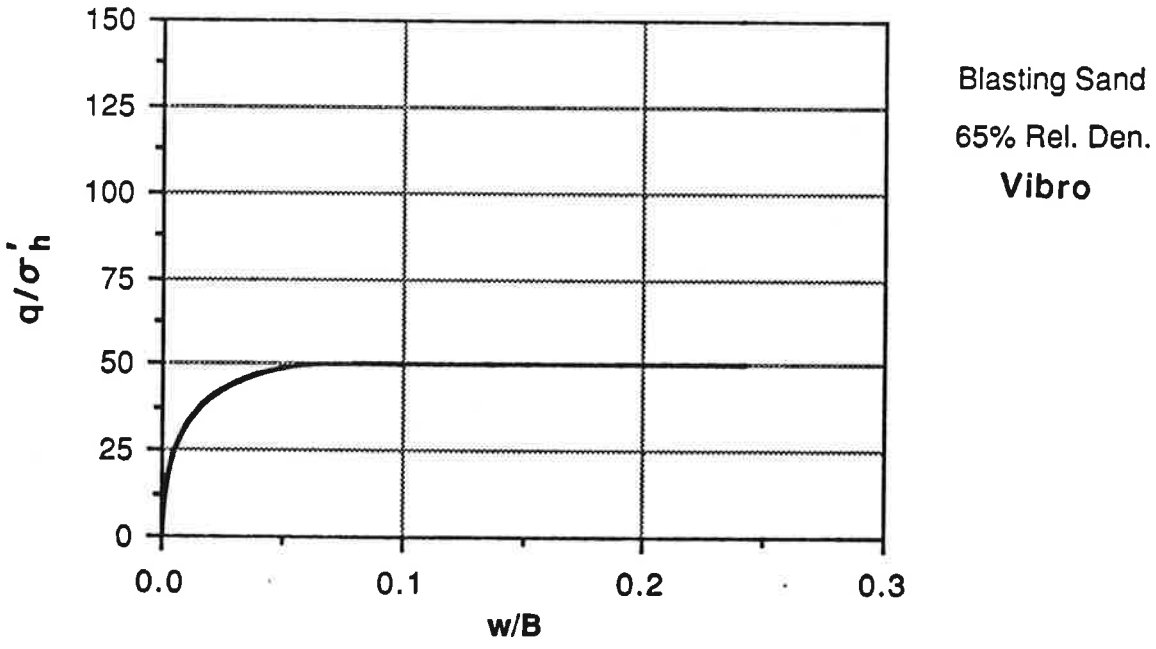

Fig. 37. Summary Normalized q-w Relation for Pile Vibrated into BLS Sand at 65% Relative Density

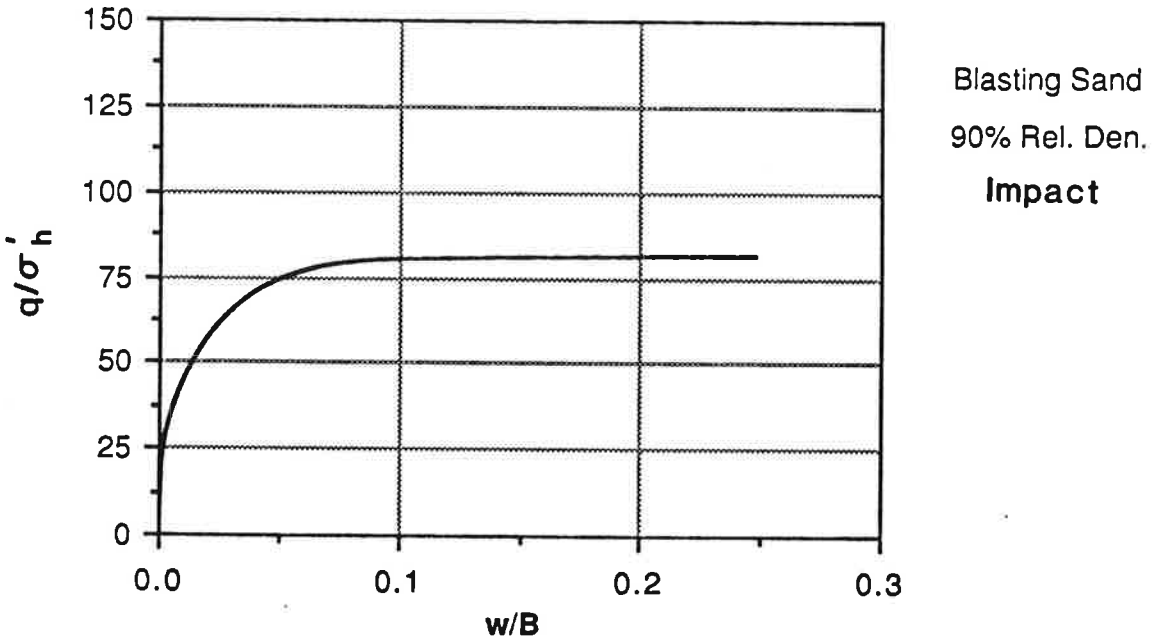

Fig. 38. Summary Normalized q-w Relation for Pile Driven by Impact into BLS Sand at 90% Relative Density

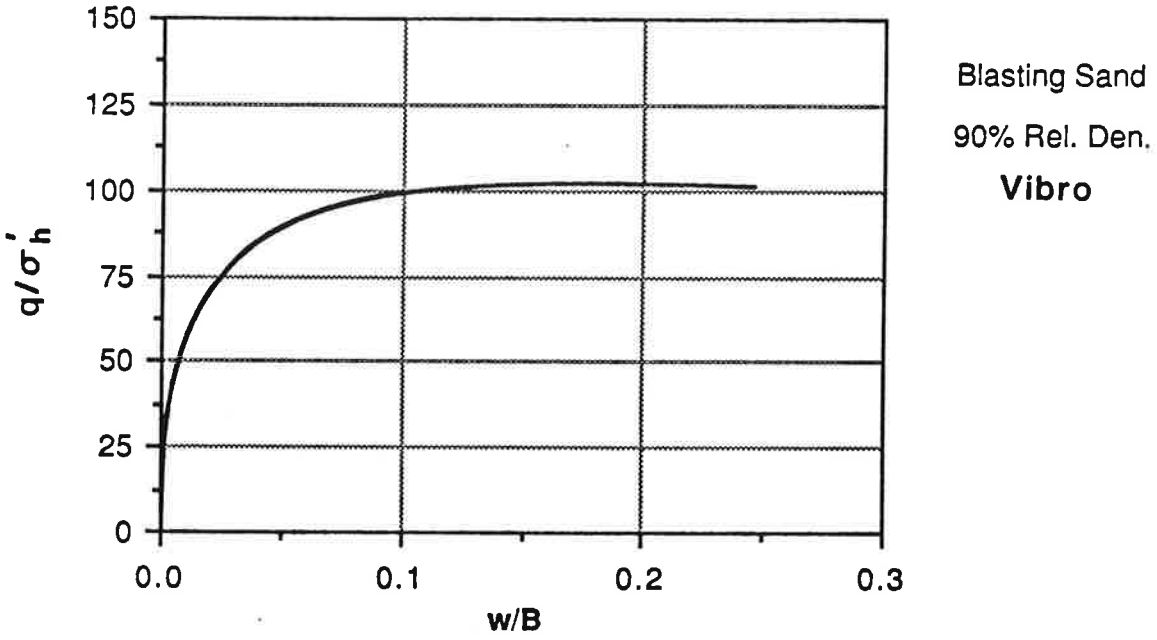

Fig. 39. Summary Normalized q-w Relation for Pile Vibrated into BLS Sand at 90% Relative Density

the corresponding q-w relations. Residual stress effects are included in these graphs; however, the residual stresses at the end of installation were generally small. Values are explicitly noted on the individual figures in Appendix Q and are summarized in Table 17.

Several observations from Figs. 28 - 39 and from the individual relations in Appendix Q can be made.

a. Ultimate unit shaft resistance in compression (positive w/B) was higher in the impact-driven pile than in the vibro-driven pile in medium-dense SJR Sand. (The results for vibro-driving and impact-driving for 65% relative density are combined in Fig. 28, so Appendix Q, Fig. Q.54, must be consulted to confirm this statement.)

b. Ultimate unit toe resistance was higher for the vibro-driven pile, with and without restriking, for both sands at 90% relative density than for the impact-driven pile (Figs. 35 and 36; Figs. 38 and 39).

c. Maximum ultimate values of unit shaft resistance occurred in the upper half of the pile (depth of 20 inches or 5B in Figs. 28 - 33) when the pile was installed by vibration or by vibration with restriking. However, the continuously impact-driven pile produced the maximum ultimate values of unit shaft resistance in the lower half of the pile (depth of 60 inches or 15B in Figs. 28 - 33). This suggests that the effect of the penetration of the toe past a given elevation may have degraded the shaft resistance in the vibro-driven pile and that as the pile penetrated deeper the shaft resistance at that elevation was gradually restored by vibration of the soil. No such effect, or perhaps the opposite effect, occurred with the impact-driven pile.

d. The general tendency of the development of ultimate values of f was for f in compression loading to exceed f in uplift loading in the top half of the pile but not in the bottom half of the pile. No particular trend with respect to method of installation could be determined in this regard. Average ultimate f values divided by the mean effective chamber pressure for all loading tests from Figs. 28 - 33 were as follows.

Table 17. Residual Stresses Developed After Installation

Soil Type	Relative Density (%)	Method of Installation	σ'_h (psi)	Test No.	Residual Stress (ksf)		
					Shaft		Toe
					20-In. (5B) Depth	60-In. (15B) Depth	
SJR Sand	65	Impact	10	20	0.4	0.3	6.8
		Vibro/Restrike	10	7	0.2	-0.4	9.0
SJR Sand	90	Impact	10	18	0.3	-0.2	4.2
			20	21	-0.2	-0.7	38.9
			10(H)/20(V)	22	-0.1	-0.3	19.3
		Vibro	10	5	0.7	-0.4	-0.8
		Vibro/Restrike	10	6	0.3	-0.8	15.2
			10(H)/20(V)	8	0.1	-0.2	8.8
BLS Sand	65	Vibro	10	11a&13a	0.1	-0.5	14.2
		Vibro/Restrike	10	16	-0.3	-0.2	23.0
BLS Sand	90	Impact	10	19	-0.5	-0.3	31.7
		Vibro	10	14	-0.1	-0.1	9.8
		Vibro/Restrike	10	15	-0.1	-0.3	13.8
			20	17	0.1	-0.4	14.2

Notes: 1. Test 9 was not included due to shallow penetration.
2. Positive sign indicates stress directed upward on pile.

	Compression Loading	Uplift Loading
Top Half of Pile	1.12	0.52
Bottom Half of Pile	1.03	1.10.

These data suggest that a surface effect existed during loading, whereby the free, pressurized surface of the sand within the chamber permitted development of Reidel shear planes (shear planes not at or parallel to the pile soil interface, but at an angle to the interface), which possessed a lower shear strength than the interface plane and which therefore permitted failure to occur at a lower shearing stress during uplift loading than during compression loading. It is probable that this effect also exists in the field, but it is not clear how deep it penetrates relative to the diameter of the pile (i. e., whether the effect was scaled properly in the laboratory test chamber). For this reason no attempt was made to compare uplift capacities for various methods of installation in the way in which compression capacities were compared.

e. The ultimate value of f was, on the average for all tests, 80% of the lateral effective chamber pressure for D_r = 65% and 120% of the lateral effective chamber pressure for D_r = 90%. These values tended to be slightly lower for the lower relative density and slightly higher for the higher relative density in BLS Sand than in SJR Sand, which indicates that the effective grain size has some influence on this effect. Since the angle of interface shear varied from 25° to 30° (Fig. I.11), it can be demonstrated that the insertion of the pile into the chamber produced an increase in the horizontal effective stress in the chamber at the pile-soil interface. Assuming that $f_{max} = \sigma'_{hi} \tan \delta$, where σ'_{hi} = horizontal effective stress at the pile-soil interface, and δ = the angle of interface shear (average value of 27.5°), the average horizontal effective stress at the pile-soil interface can be computed to be 0.8 / tan 27.5° = 1.5 times the simulated horizontal in-situ (lateral effective chamber) pressure for D_r = 65% and 1.2 / tan 27.5° = 2.3 times the simulated horizontal in-situ pressure for D_r = 90%. The pile, whether vibrated or driven into place, therefore must have served to increase the

effective stress in the soil immediately surrounding the pile at the time of static loading. It should be possible, theoretically, to confirm this observation directly from readings that were made on the total pressure cells on the face of the pile prior to the performance of the first loading test (which was always a compression test) on each pile that was installed. Values of total lateral stress measured at the location of each of the two total pressure cells on the pile (middepth and toe, Fig. D.1) divided by applied lateral chamber pressure plus the static pore water pressure at the depth of the transducer are shown in Table 18. These values should be in the general range of 1.5 to 2.3, assuming that relatively little effective stress change occurred during static loading of the pile. Instead, however, the values varied from less than zero (probable malfunctioning instrument) to in excess of 8. The total stress data summarized in Table 18 may be correct, but it is probable that the sensing faces of the transducers were too small relative to the size of the soil grains to provide effective averaging of the stresses. Hence, the total pressure data must be interpreted very carefully. [Values of pore water pressure at the pile-soil interface divided by the theoretical hydrostatic pore water pressure in the chamber are also given in Table 18. These values were generally close to unity, as they should be since the measurements were taken after excess pore water pressures had dissipated, except for two impact tests in which hard driving had apparently caused a zero shift, and Test 9, in which the pile could not be vibro-driven to full depth and where a small absolute error in pore water pressure could therefore produce a relatively large error in the pore pressure ratio. There is nothing in these data that indicate erroneous performance of the pore water pressure transducer.]

f. The ultimate values of both f and q were generally about 80% fully developed at a local displacement of 5% of the pile diameter but continued to increase slightly at larger displacements. Deformation softening behavior was not observed in either shaft or toe resistance when the pile was installed either by vibro-driving or by impact-driving.

Table 18 . Normalized Pressure Transducer Readings Before and After Static Load Tests

Test (Condition)	Type of Test*	Normalized Total Pressure				Normalized Pore Water Pressure	
		middepth		toe			
		before	after	before	after	before	after
5	C	0.22	2.77	0.69	0.89	0.82	0.75
(S/90/10/V)**	U	2.77	0.63	0.97	2.97	0.76	0.79
6	C	0.81	1.13	0.60	0.92	0.96	0.90
(S/90/10/VR)	U	1.08	0.44	1.06	2.64	0.89	0.92
7	C	0.25	0.24	0.86	0.87	1.25	1.29
(S/65/10/VR)	U	0.33	0.30	0.81	0.82	1.32	1.33
8	C	0.91	0.92	0.53	0.53	0.85	0.86
(S/90/K_o/VR)	U	0.92	0.94	0.80	0.86	0.83	0.84
9	C	-0.02	-0.03	0.43	0.54	0.56	0.56
(S/90/20/VR)	U	0.06	0.05	0.54	0.47	0.56	0.56
11a&13a	C	0.32	0.63	0.44	1.20	0.84	0.87
(B/65/10/V)	U	0.65	0.63	1.39	1.26	0.85	0.83
14	C	0.24	6.13	0.18	1.51	0.88	0.91
(B/90/10/V)	U	4.52	3.22	1.41	1.86	0.92	0.86
15	C	0.45	8.76	-0.02	0.81	0.82	0.85
(B/90/10/VR)	U	8.82	4.39	0.74	0.65	0.81	0.83
16	C	1.39	1.39	0.59	0.59	0.90	0.90
(B/65/10/VR)	U	1.40	1.48	0.60	0.61	0.90	0.91
17	C	0.01	4.50	1.09	2.71	1.26	1.26
(B/90/20/VR)	U	5.30	2.55	2.70	2.96	1.26	1.25
18	C	0.48	1.18	0.05	1.19	0.05	0.05
(S/90/10/I)	U	1.29	1.17	1.26	1.18	0.05	0.05
19	C	1.24	2.64	1.36	1.40	0.97	0.98
(B/90/10/I)	U	3.05	4.36	2.45	4.71	0.94	0.93
20	C	-	-	1.07	1.22	0.69	0.75
(S/65/10/I)	U	-	-	1.29	1.30	0.95	0.90
21	C	0.88	1.04	0.97	1.04	-	-
(S/90/20/I)	U	1.04	1.18	1.11	2.08	-	-
22	C	0.61	0.89	1.23	1.29	0.96	1.01
(S/90/K_o/I)	U	1.06	1.09	1.32	1.34	1.02	1.02

Normalization factor = lateral effective chamber pressure

* C = Compression ; U = Uplift

** S = SJR ; B = BLS / Relative density (%) / Effective chamber pressure (psi) ; K_o = 10 psi horiz. and 20 psi vert. / V = Vibro ; R = Restrike ; I = Impact

Computation of Static Compressive Capacity

The candidate design method outlined in Chapter 3 requires the estimation of static compressive capacity when it is desired to use the method to select a driver. It is possible to compute the ultimate unit shaft resistance f_{max} and ultimate unit toe resistances q_{max} for a pile using the following expressions.

$$f_{max} = \beta' \sigma'_h \ , \quad \text{and} \tag{8}$$

$$q_{max} = N_\sigma \sigma'_o \ , \tag{9}$$

where $\beta' = N_h \tan \delta$, in which N_h is a factor that converts in-situ lateral effective stress into an equivalent effective horizontal stress at the pile-soil interface after pile installation and loading to a failure state and δ is the angle of pile-soil interface shear, σ'_h = in-situ lateral effective stress in the soil mass into which the pile is driven, N_σ = bearing capacity factor at the pile toe, and σ'_o = mean effective stress in the soil at the elevation of the toe = $(1+ 2K_o) \sigma'_v / 3$, in which σ'_v is the vertical effective stress in the soil at the elevation of the toe and K_o is the in-situ coefficient of earth pressure at rest.

In order to obtain the capacity of a pile, the above equations are applied as follows:

$$Q = \sum_{k=1}^{N} \beta_k \sigma'_{hk} A_{sk} + N_\sigma \sigma'_o A_t \tag{10}$$

in which Q is the compression capacity of the pile, N is the number of vertical increments into which the pile is divided for computational purposes, k is the increment number, A_{sk} is the peripheral area of increment k, and A_t is the area of the toe. From the results of the static tests, it appears appropriate to take N = 2 for the laboratory test pile, in which the two pile increments are, respectively, the top half and the bottom half of the penetrating portion of the pile. If a procedure such as this is applied in practice, it is clear that the lateral in-situ effective ground stresses must be established on a site through appropriate exploration.

The values of both β' and N_σ can be obtained in principle directly from the normalized unit load transfer graphs in the preceding section as the ordinate values that correspond to a value of w/B of 0.1. The values can also be obtained for the each of the individual tests by using the individual-test unit load transfer curves in Appendix Q. Values obtained for the individual tests are tabulated in Table 19. The values of these two factors are observed to be dependent primarily upon the method of installation and the relative density of the sand and less importantly upon the other factors. The values that are given in Table 19 have been averaged and summarized in Table 20. The factors presented in this table can be used with Eqs. (8) - (10) to back-compute the static compression capacity of the simulated full-scale piles that were tested in this laboratory study, and it may be possible to use these equations in practice for piles in clean sand with appropriate verification and/or modification, provided the profile of in-situ lateral effective stresses can be determined through in-situ testing or other means. Table 20 also provides a succinct summary of the significant effects of the various factors that were studied on the static capacity of the laboratory test pile.

Table 19. Summary of N_σ and β' Factors

Soil Type	Relative Density (%)	Type of Installation	Test No.	N_σ	β' 20-in. Depth (Top Half)	β' 60-in. Depth (LowerHalf)
SJR Sand	65	Impact	20	60.1	1.20	0.81
		Vibro/Restrike	7	56.8	0.97	0.56
SJR Sand	90	Impact	18	65.2	1.02	1.15
			21	51.9	0.99	0.90
			22	60.1	1.29	1.30
		Vibro	5	71.7	1.84	0.67
		Vibro/Restrike	6	93.6	2.43	0.54
			8	74.0	1.18	0.93
BLS Sand	65	Vibro	11a&13a	48.6	0.78	0.59
		Vibro/Restrike	16	48.9	0.56	0.76
BLS Sand	90	Impact	19	80.9	0.97	1.61
		Vibro	14	122.5	1.27	1.57
		Vibro/Restrike	15	114.5	1.65	0.95
			17	77.4	1.13	1.28

Note : Test 9 was not included due to shallow penetration.

Table 20. Summary of Values of β' and N_σ Obtained in Laboratory Study

Method of Installation	β' Top Half of Pile (i = 1)	β' Bottom Half of Pile (i = 2)	N_σ Rel. Density = 65%	N_σ Rel. Density = 90%
Impact	1.1 (D_r = 65%)	0.8 (D_r = 65%)	60	65
	1.1 (D_r = 90%)	1.2 (D_r = 90%)		
Vibro or Vibro/Restrike	0.8 (D_r = 65%)	0.6 (D_r = 65%)	51	92
	1.6 (D_r = 90%)	1.0 (D_r = 90%)		

LOAD TRANSFER DURING VIBRATORY DRIVING

Unit Load Transfer Relationships for Pile in Motion

Further insight into the behavior of the test pile during vibratory driving can be gained by observing unit load transfer relations (f-w and q-w curves) that developed during vibro-driving and comparing those relations with the equivalent relations developed during subsequent static load testing, as described in the preceding section. The procedure for developing the "in-motion" unit load transfer curves was based on the simultaneous measurement of time histories of force at the head and toe of the pile and the acceleration of the pile. The measurement of head and toe acceleration also permitted the computation of displacement through double integration of the acceleration signal. Additional details are given in Appendix H.

In-motion f-w and q-w curves are shown for a penetration of about one diameter less than full penetration for several tests in Figs. 40 - 45. The f-w curves are average relationships for the entire penetrating portion of the pile. Two to three cycles of vibro-driving are shown, and each relation begins with an arbitrarily assumed w value of zero, which was chosen to correspond approximately to the beginning of a downstroke of the driver. Positive values of f or q correspond to upward-directed stresses on the shaft or toe, while downward-directed stresses are represented by negative signs. Figures 40 - 45 correspond to a wide variety of soil conditions: Figs. 40 - 42 pertain to SJR (fine) Sand; Figs. 43 - 45 pertain to BLS (coarse) Sand; Figs. 41 and 43 pertain to 65% relative density; Figs. 40,42,44 and 45 pertain to 90% relative density; Figs. 40, 41, 43 and 44 pertain to 10 psi effective chamber pressure; and Figs. 42 and 45 pertain to 20 psi effective chamber pressure. Effects of instantaneous residual stresses are included in these figures, since the zeroes for the instruments were those acquired prior to insertion of the pile.

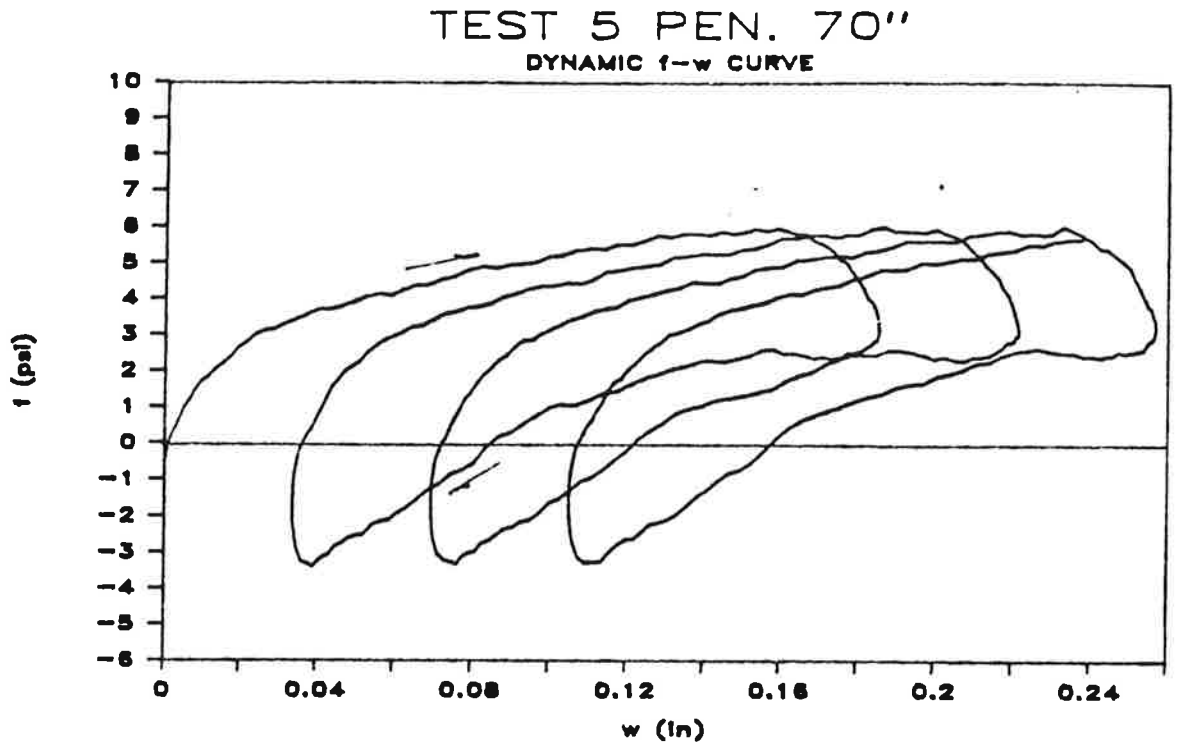

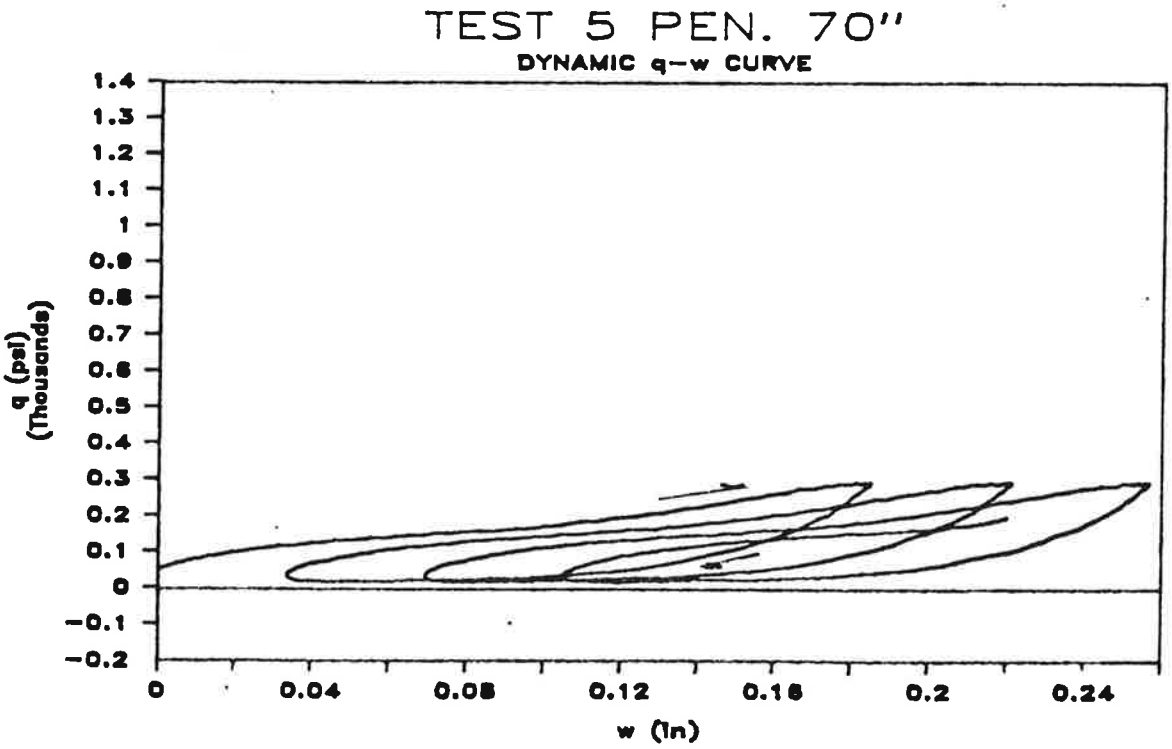

Fig. 40. Unit Load Transfer Curves for Pile in Motion; Test 5; SJR (Fine) Sand, 90% Relative Density; 10 Psi Effective Chamber Pressure; 70-Inch Penetration

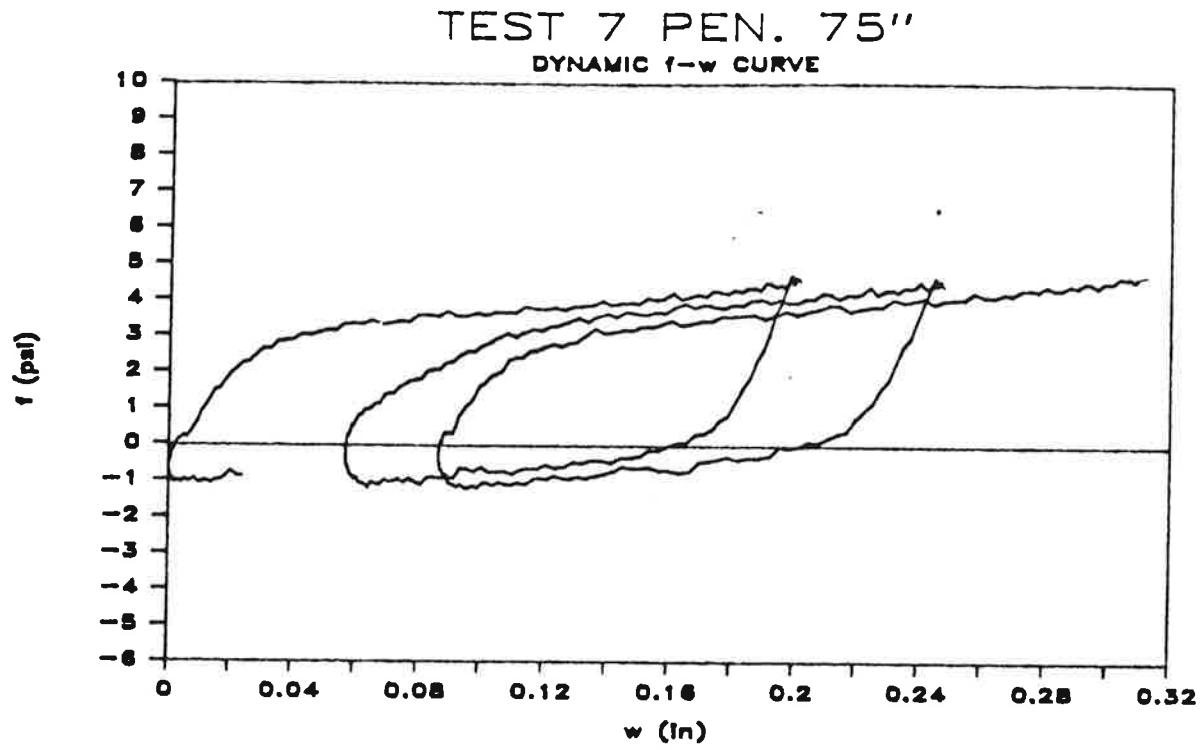

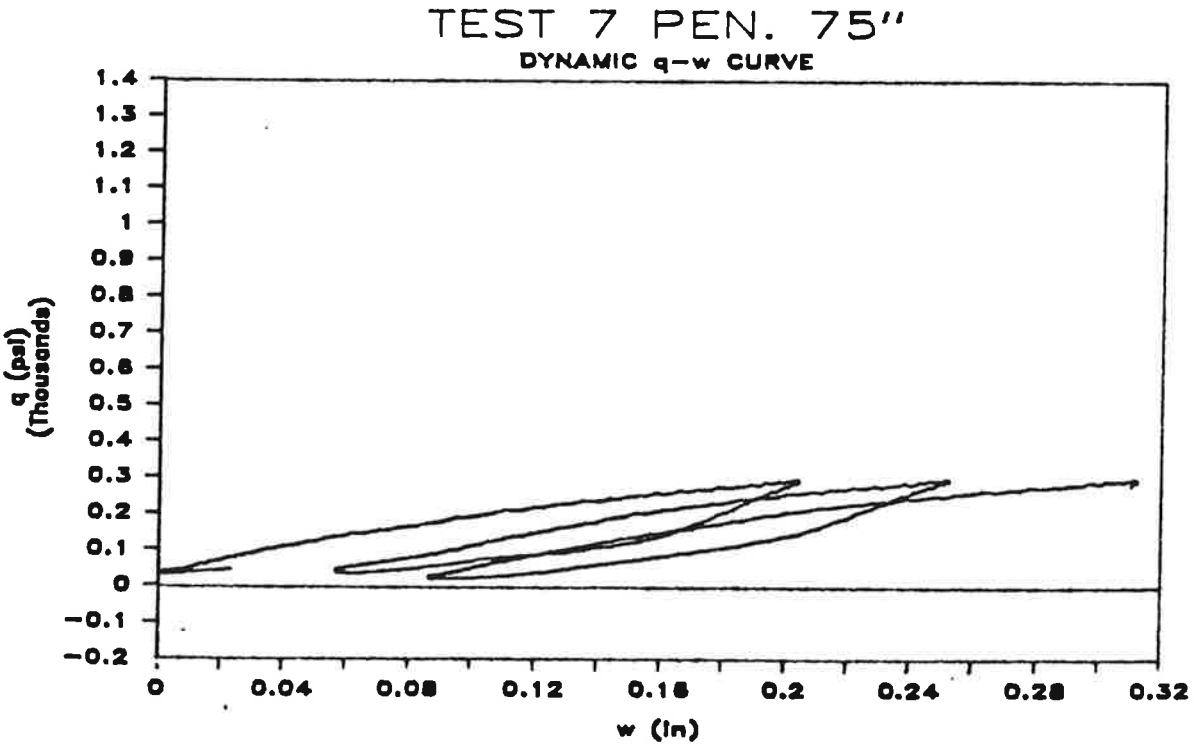

Fig. 41. Unit Load Transfer Curves for Pile in Motion; Test 7; SJR (Fine) Sand, 65% Relative Density; 10 Psi Effective Chamber Pressure; 75-Inch Penetration

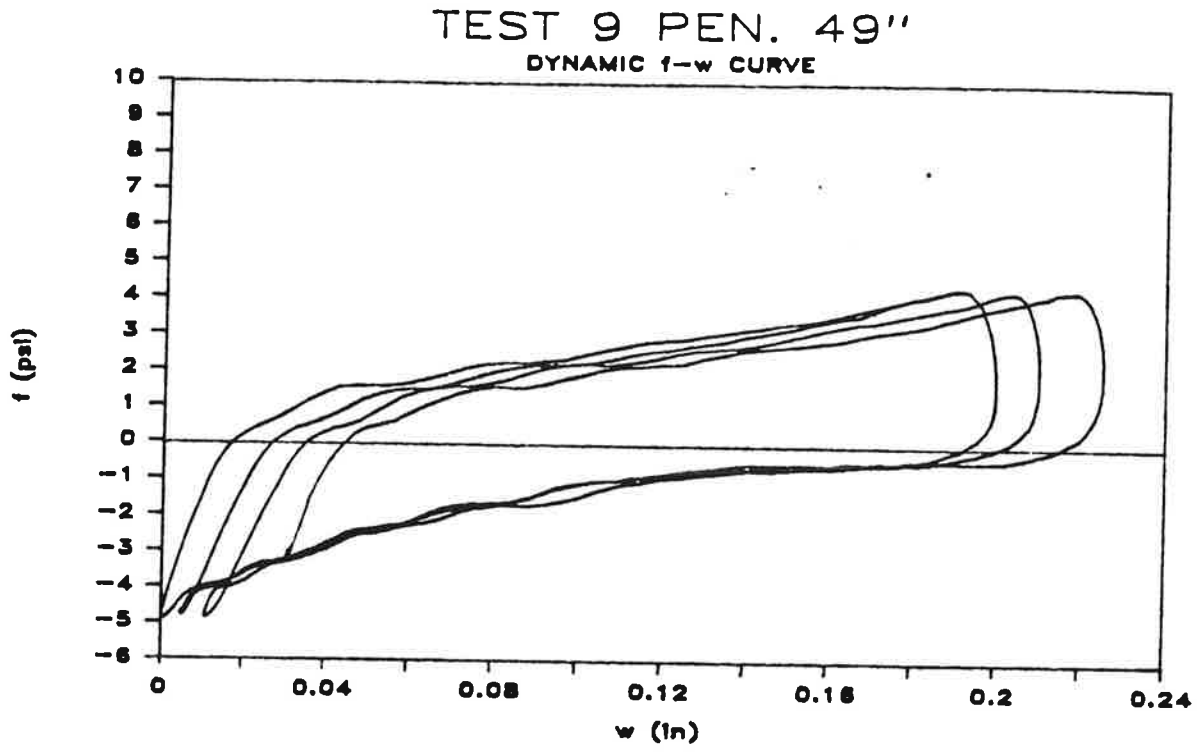

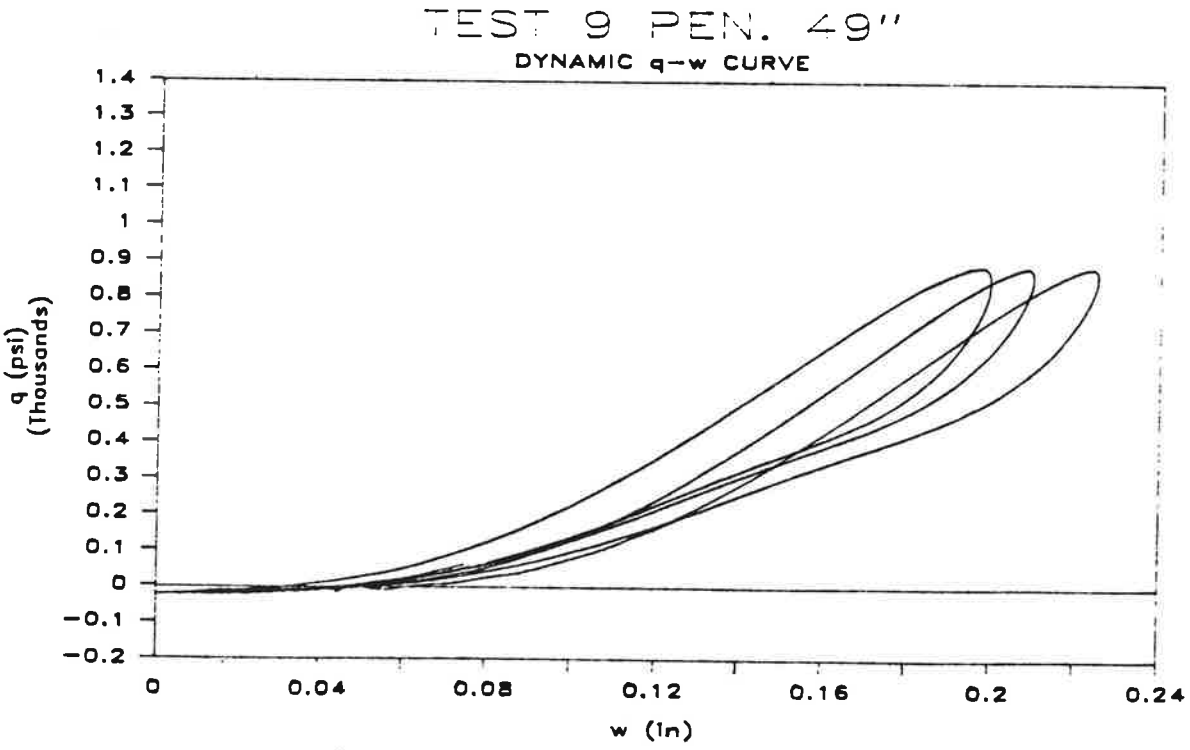

Fig. 42. Unit Load Transfer Curves for Pile in Motion; Test 9; SJR (Fine) Sand, 90% Relative Density; 20 Psi Effective Chamber Pressure; 49-Inch Penetration

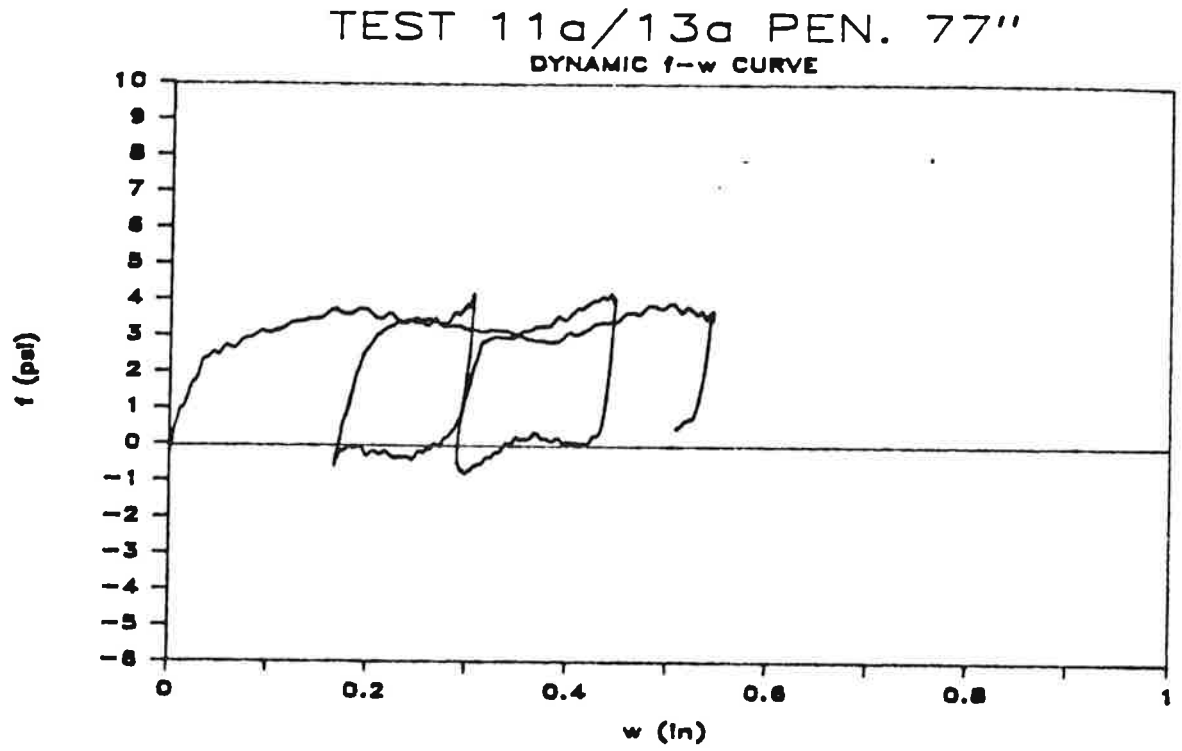

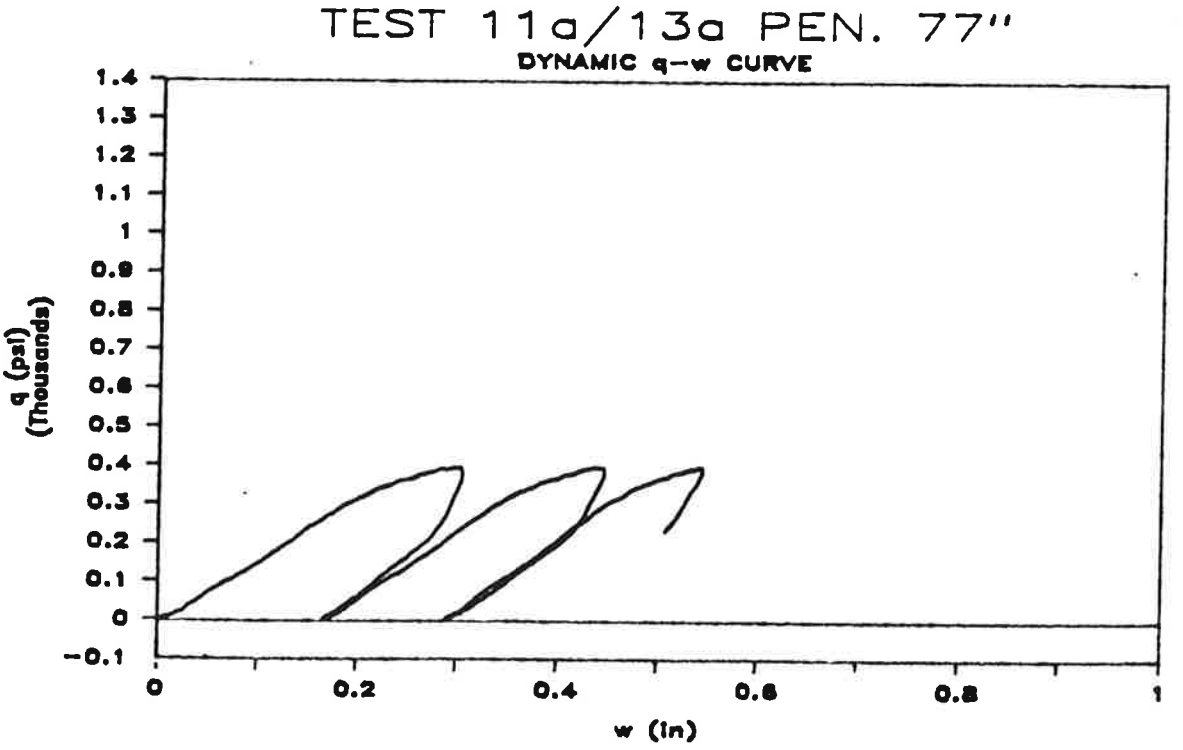

Fig. 43. Unit Load Transfer Curves for Pile in Motion; Test 11A/13A; BLS (Coarse) Sand, 65% Relative Density; 10 Psi Effective Chamber Pressure; 77-Inch Penetration

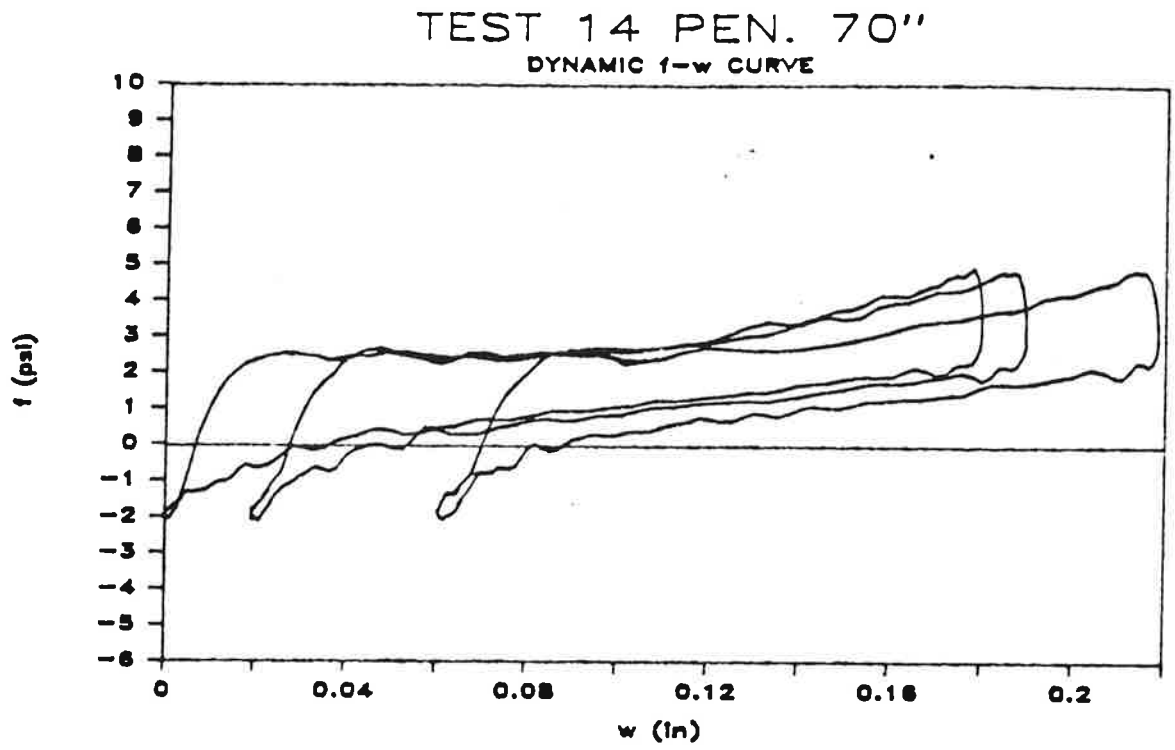

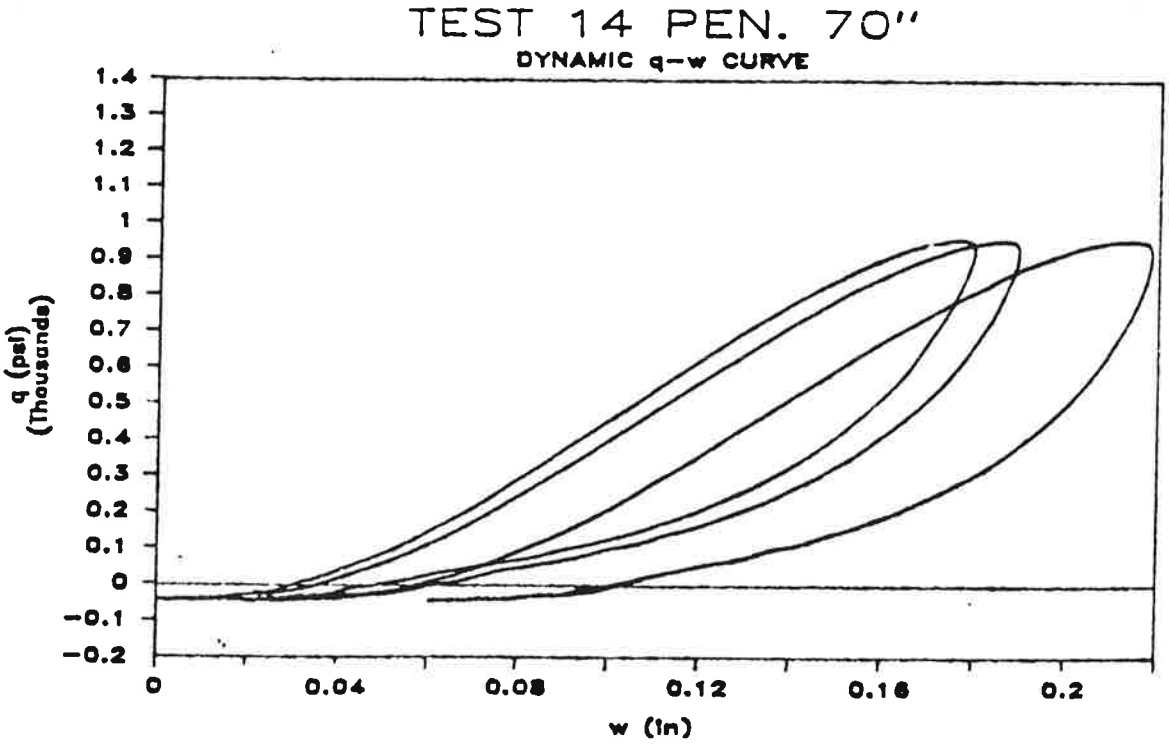

Fig. 44. Unit Load Transfer Curves for Pile in Motion; Test 14; BLS (Coarse) Sand, 90% Relative Density; 10 Psi Effective Chamber Pressure; 70-Inch Penetration

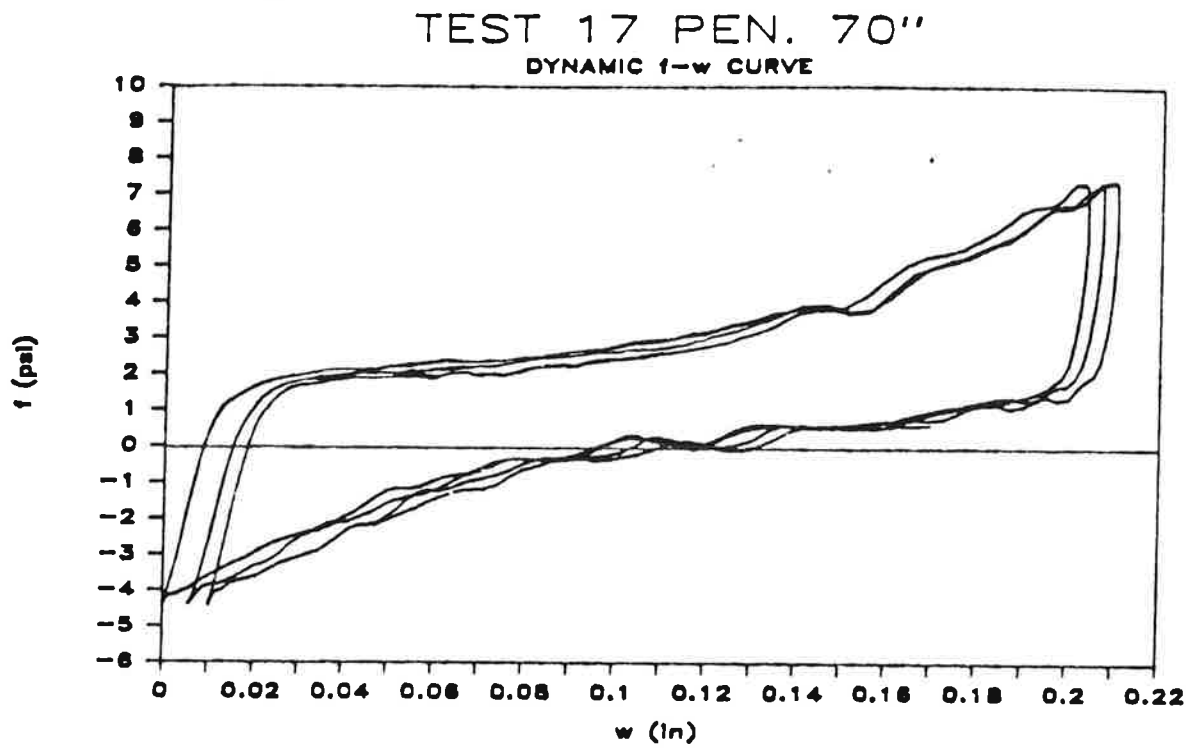

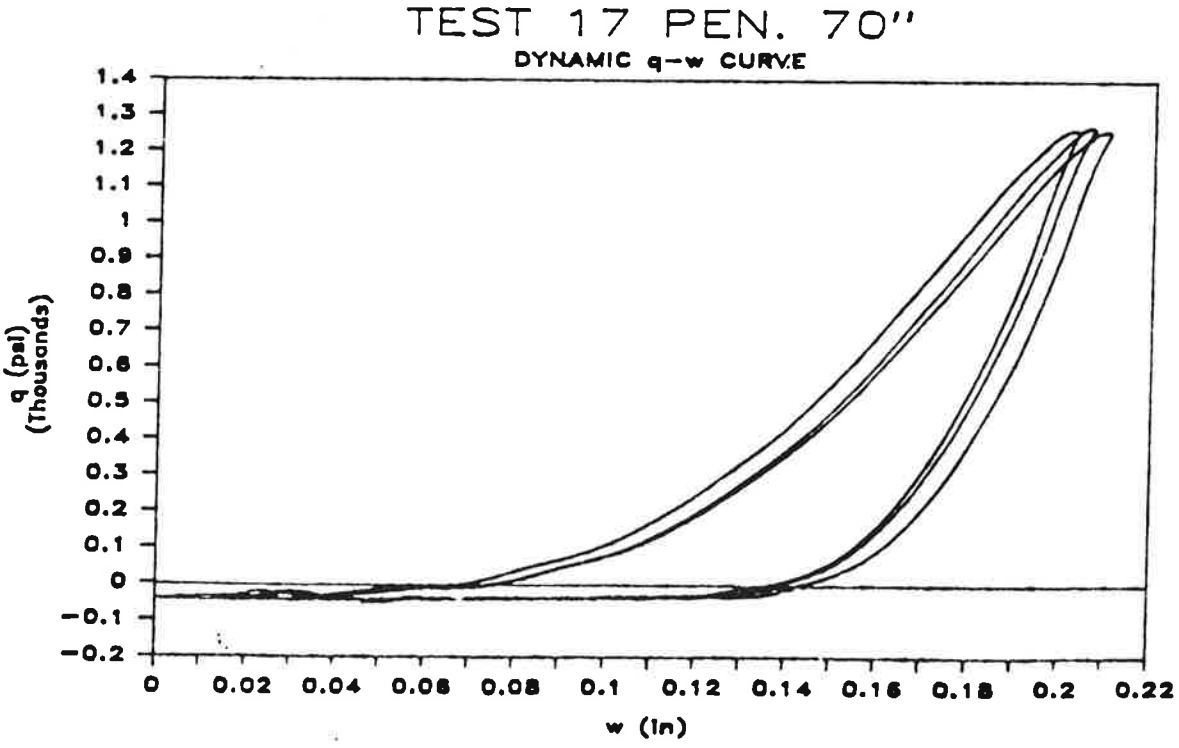

Fig. 45. Unit Load Transfer Curves for Pile in Motion; Test 17; BLS (Coarse) Sand, 90% Relative Density; 20 Psi Effective Chamber Pressure; 70-Inch Penetration

For purposes of contrast, Fig. 46 is included, in which conditions are identical to those of Fig. 45 (Test 17), except that the pile is not penetrating (has reached refusal at a penetration of one diameter greater than that represented in Fig. 45).

The following observations can be made from Figs. 40 -46.

a. In order to investigate the effect of relative density, Fig. 40 can be compared with Fig. 41 (SJR Sand), and Fig. 44 can be compared with Fig. 43 (BLS Sand). The maximum and minimum values of f were not strongly influenced by relative density in either soil, although the value of minimum f was somewhat larger (in absolute terms) for the higher relative density in both sands, which may account, at least in part, for the greater difficulty in driving at higher relative density. In the SJR Sand the peak value of q was also essentially independent of relative density, but in the BLS Sand the peak value of q appeared to be essentially proportional to the relative density. The differences in effect of relative density on toe capacity in the two soils may be due to either grain shape effects or to the development of more efficient drainage in the coarser sand.

b. The effect of effective chamber pressure (simulated depth) can be observed by comparing Figs. 40 and 42 (SJR Sand) and Figs. 44 and 45 (BLS Sand). The effective stress had relatively little effect on the maximum or minimum values of f in SJR (fine) Sand but produced approximately a 50% increase in the peak value of f in BLS (coarse) sand. The effect of effective chamber pressure is more pronounced when peak q values are compared. In SJR Sand the peak value of q was almost proportional to effective chamber pressure, while doubling the effective chamber pressure produced about a 30% increase in peak q in the BLS Sand. Apparently, therefore, the increased resistance to penetration at higher effective pressure (or greater depth) occurred in both shaft resistance and toe resistance, except that a very small effect occurred in shaft resistance in the fine sand.

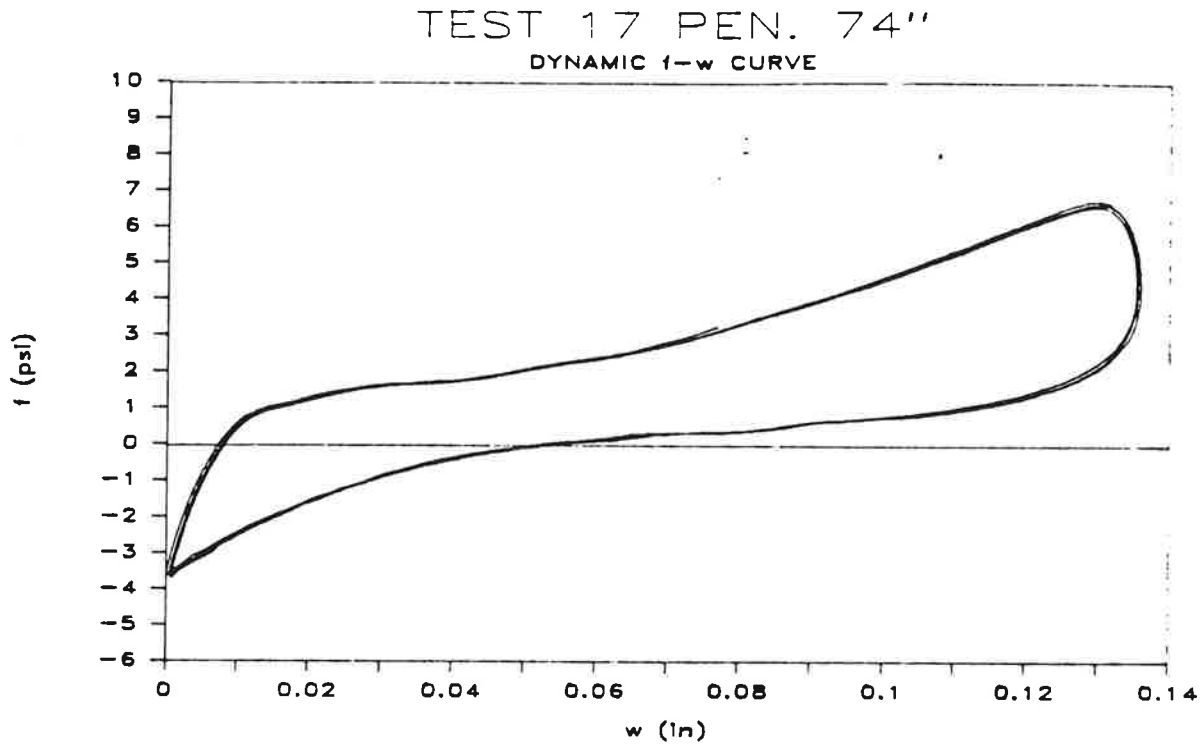

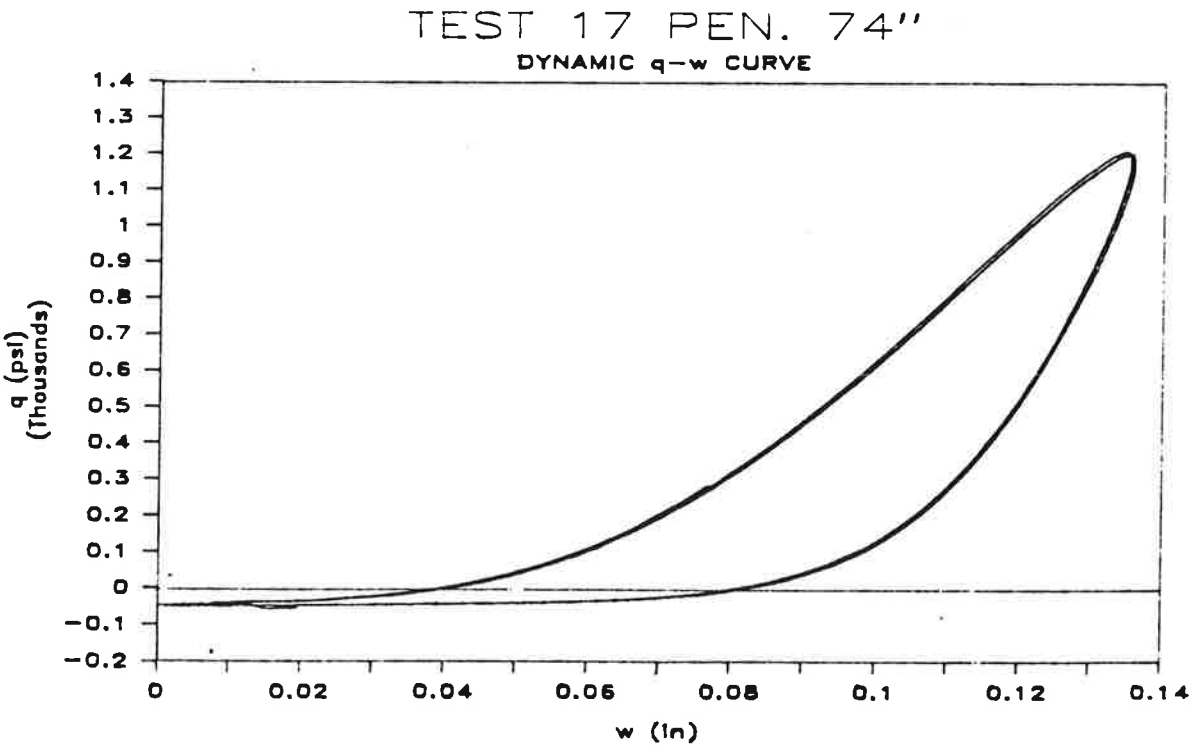

Fig. 46. Unit Load Transfer Curves for Pile at Refusal; Test 17; BLS (Coarse) Sand, 90% Relative Density; 20 Psi Effective Chamber Pressure; 74-Inch Penetration

c. A comparison of Figs. 45 and 46 (pile in motion vs. pile in a refusal state) reveals no significant changes in the shapes of the curves or the peak values for the two conditions but indicates that both the f-w and q-w curves are much stiffer for conditions of refusal. In fact, for the case of refusal (Fig. 46), the positive peaks correspond more closely to points on the static unit load transfer curves than for the case of pile-in-motion, as is discussed below.

d. The in-motion f-w curves typically steepened with the loading branch as the pile approached the bottom of the downstroke (maximum w). This behavior is contrary to common soil models used for evaluating impact driving, in which a reduced slope, or even a negative slope, exists at this point as the pile velocity approaches zero. It is believed that the reduced unit shaft resistance near the middle of the stroke was due mainly to the dynamic mobility of the sand particles near the pile-soil interface produced by the vibration of the pile. As the pile decelerated near the bottom of the downstroke, the particle mobility decreased and the unit shaft resistance increased, producing the increased slope.

e. A comparison among all figures indicates that for conditions of high relative density, the toe unit load transfer curves appear to become convex, or strain-hardening, which is not a characteristic of the curves produced from conditions of lower relative density at 10 psi effective chamber pressure. This behavior is believed to be the result of continued lifting of the toe off the underlying soil on the upstroke of the pile, followed by impact on the downstroke. The loading branch of the curve is convex, however, because in the half cycle, or portion thereof, that the toe was lifted off the soil, the soil had experienced some upward movement into the cavity formed by the upward-moving pile toe, probably due to pore water suction coupled with shear failure produced by lateral stresses greatly exceeding vertical stresses in the soil immediately beneath the toe. As the toe moved back down into the cavity, the cavity was partially filled with loose soil, requiring the toe to seat itself before developing significant toe resistance. It

is noted that once the toe reseated in the soil the loading branch of the in-motion q-w curve was essentially linear (i. e., Fig. 44) to a deflection of about 0.10 inches beyond the point of seating, whereafter some yielding began to occur, which in turn produced toe penetration. A "rapid impact" phenomenon is thus apparent in the very dense sand. In the tests in which the relative density was 65% (Figs. 41 and 44) the loading branches of the q-w curves tended to be monotonically increasing, which suggests that the pile was penetrating so fast that the toe did not lift off the underling soil on an upstroke of the hammer. It is not reasonable, therefore, to view toe penetration as a rapid impact phenomenon in medium (and, by implication, loose) sand.

f. If it is assumed that the vibrator and the pile are in phase, the peak positive values of f and q, integrated over the shaft area and the toe area, respectively, yield peak shaft resistance Q_s and peak toe resistance Q_t. These values sum to give the measured peak dynamic force at the head of the pile, as discussed in the section "Interaction of Vibro-Driver and Pile," plus the mass of the pile itself multiplied times the peak pile deceleration. The weight of the pile was small (0.080 k), and its peak inertial force was typically only about 5 g X 0.080 k = 0.4 k (about 3% of the average peak pile-head force), so that the effect of the inertial force of the laboratory test pile itself was relatively small in this laboratory study.

Other, more subtle, information is contained in Figs. 40 - 46, and a careful study of the relationships may be very useful in future development of mathematical models for simulation of the driving of piles by vibration. For example, failure did not appear to occur in the soil at the toe of the pile in the densest sand. However, penetration occurred because the stiffness of the loading branch of the q-w curve was significantly lower than that of the unloading branch.

For purposes of comparison with the static load transfer curves obtained during the static loading tests following installation, the relationships presented in Figs. 40 - 46 are replotted to a smaller scale on Figs. 47 - 53 with the static relationships. Since

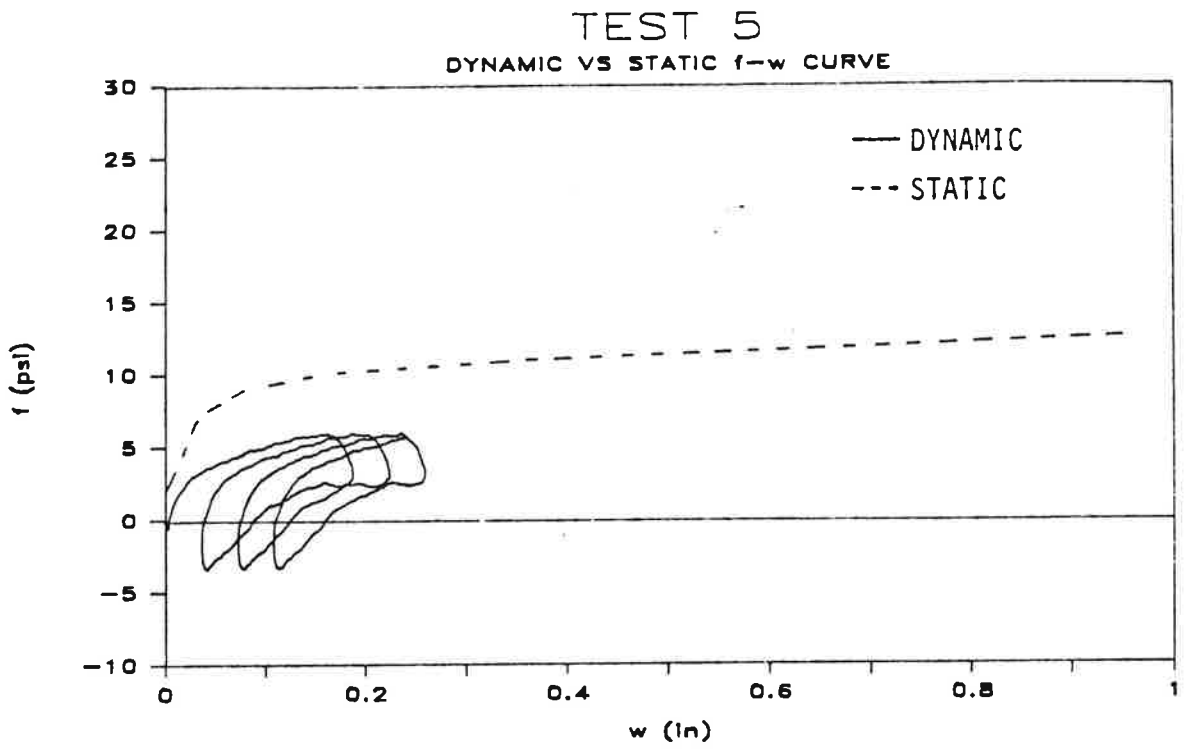

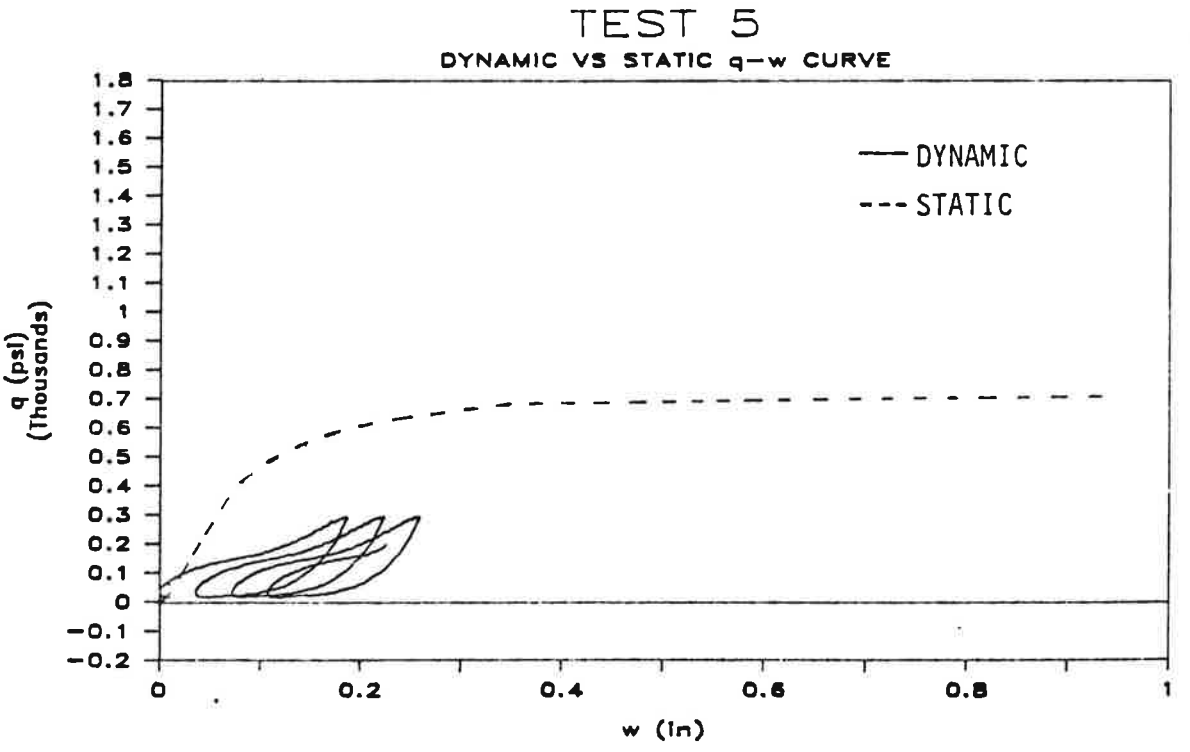

Fig. 47. Comparison of Unit Load Transfer Curves for Pile in Motion and for Static Loading; Test 5; SJR (Fine) Sand; 90% Relative Density; 10 Psi Effective Chamber Pressure; Pile-in-Motion Curves for 70-Inch Penetration

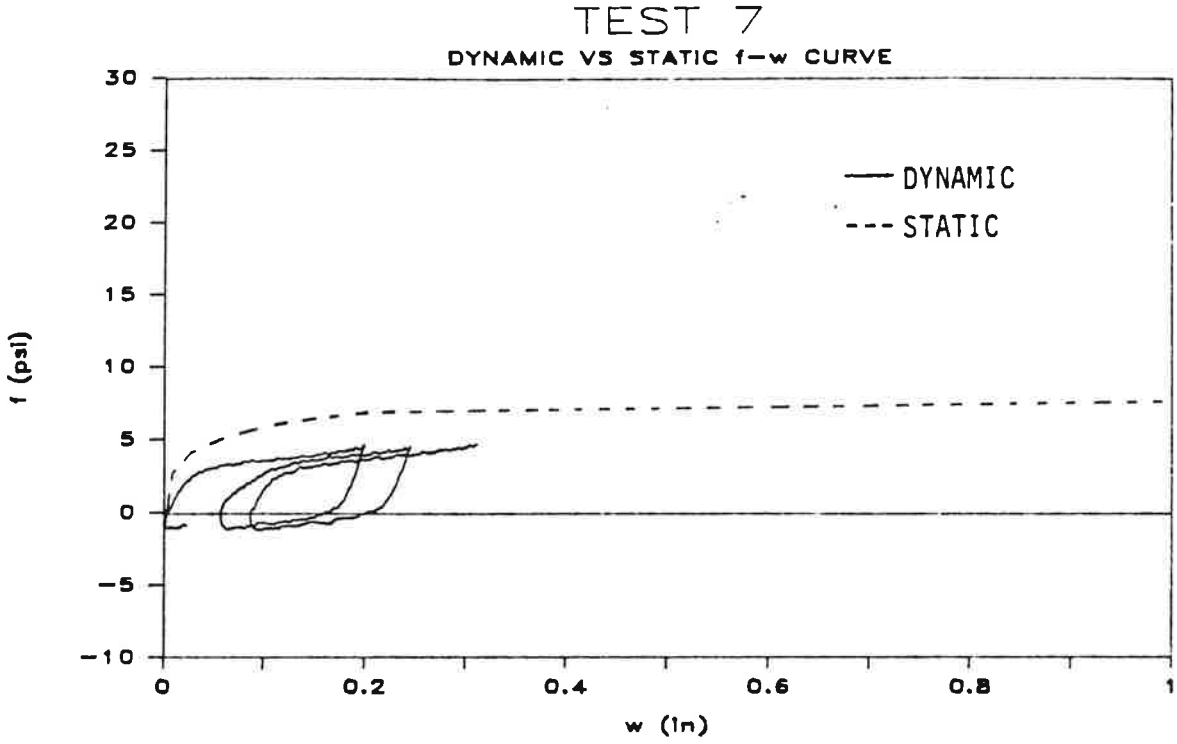

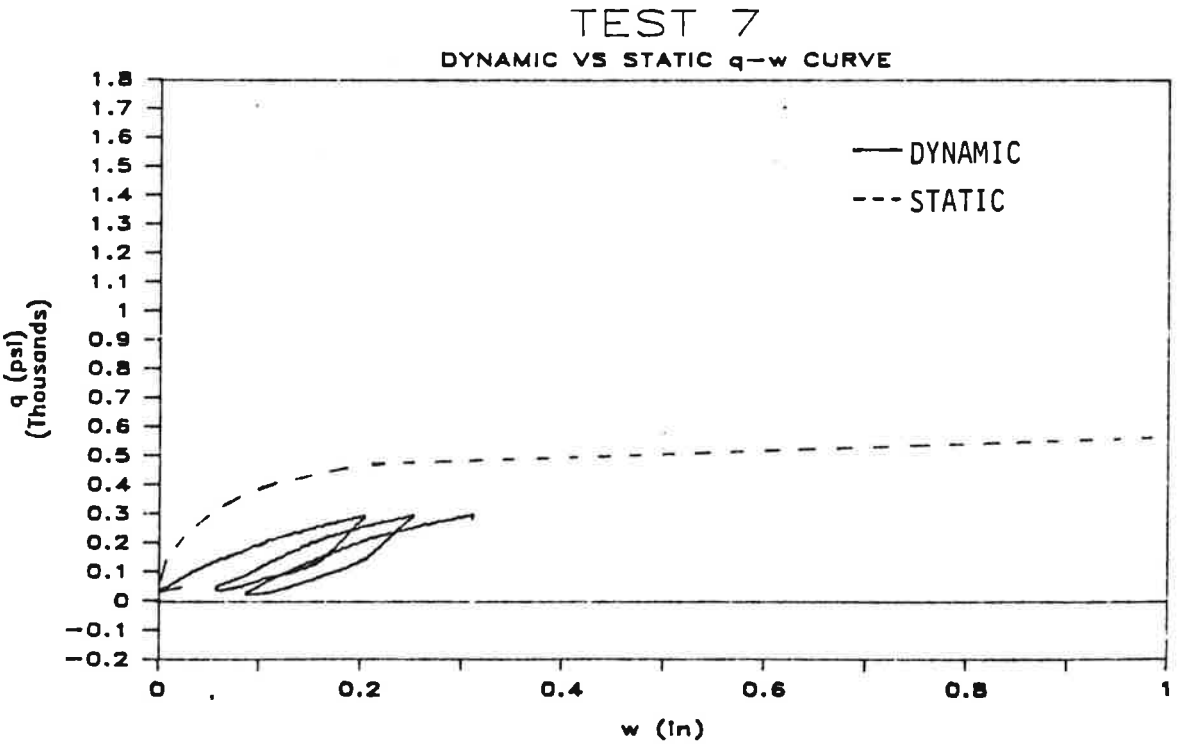

Fig. 48. Comparison of Unit Load Transfer Curves for Pile in Motion and for Static Loading; Test 7; SJR (Fine) Sand; 65% Relative Density; 10 Psi Effective Chamber Pressure; Pile-in-Motion Curves for 75-Inch Penetration

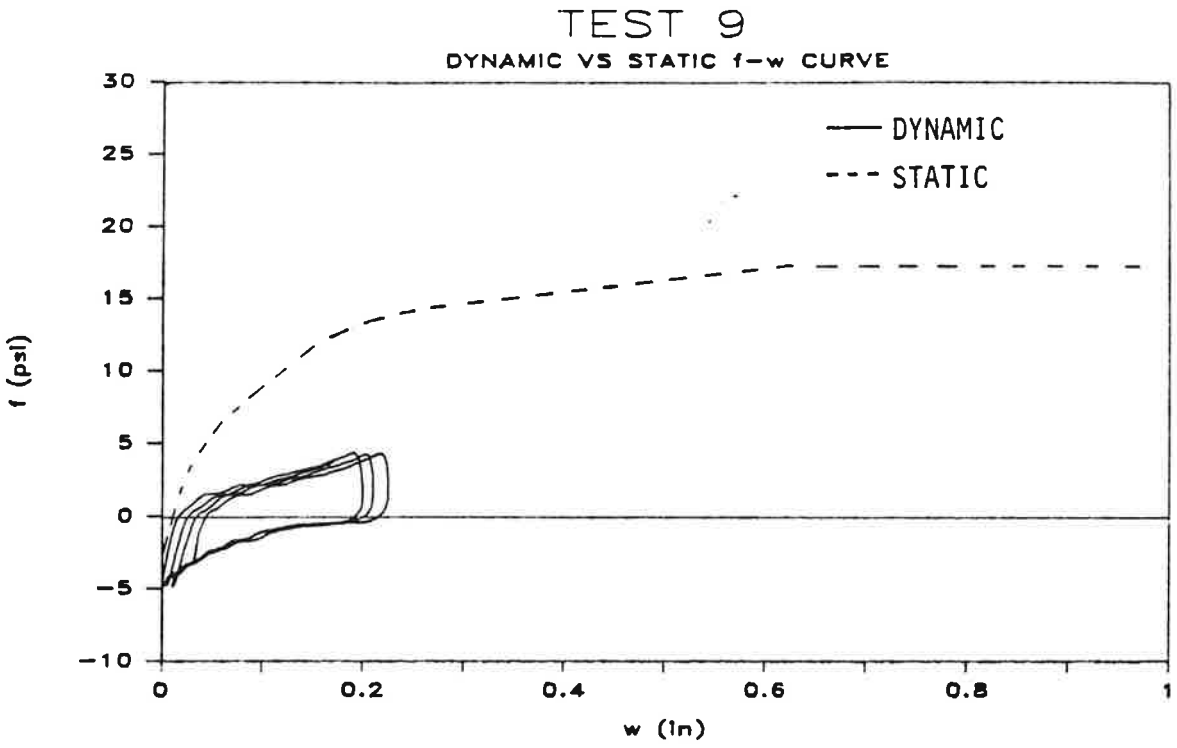

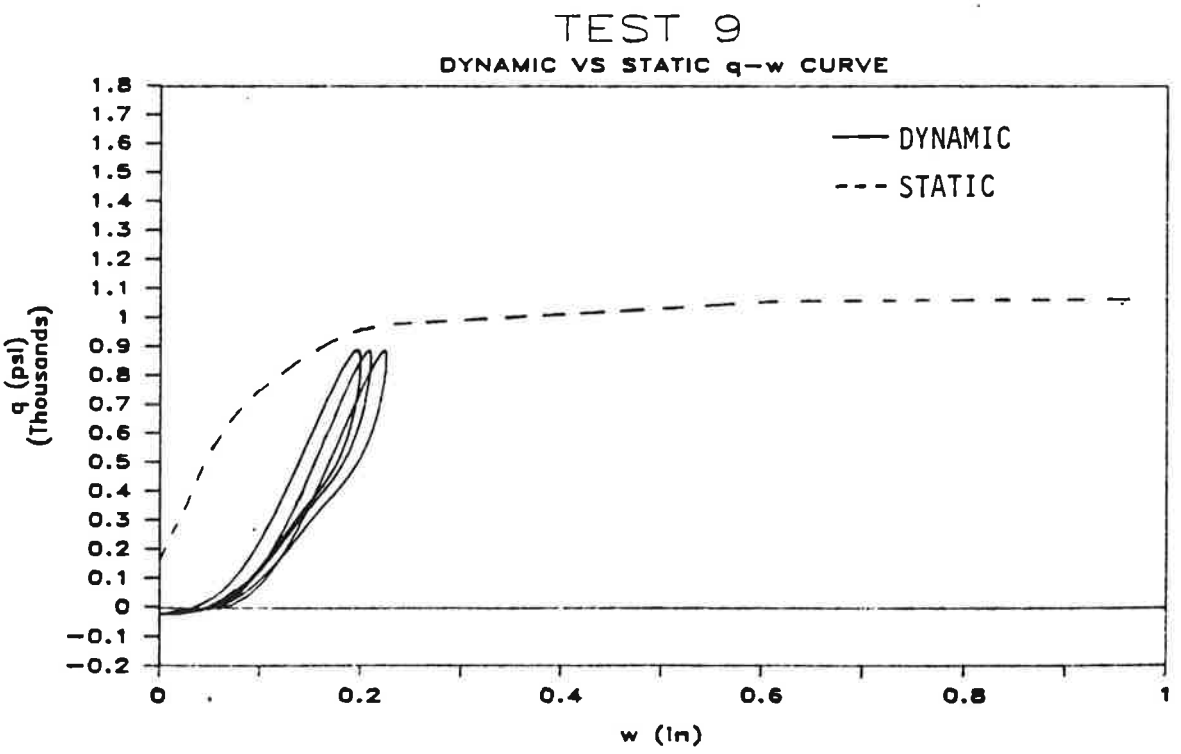

Fig. 49. Comparison of Unit Load Transfer Curves for Pile in Motion and for Static Loading; Test 9; SJR (Fine) Sand; 90% Relative Density; 20 Psi Effective Chamber Pressure; Pile-in-Motion Curves for 49-Inch Penetration

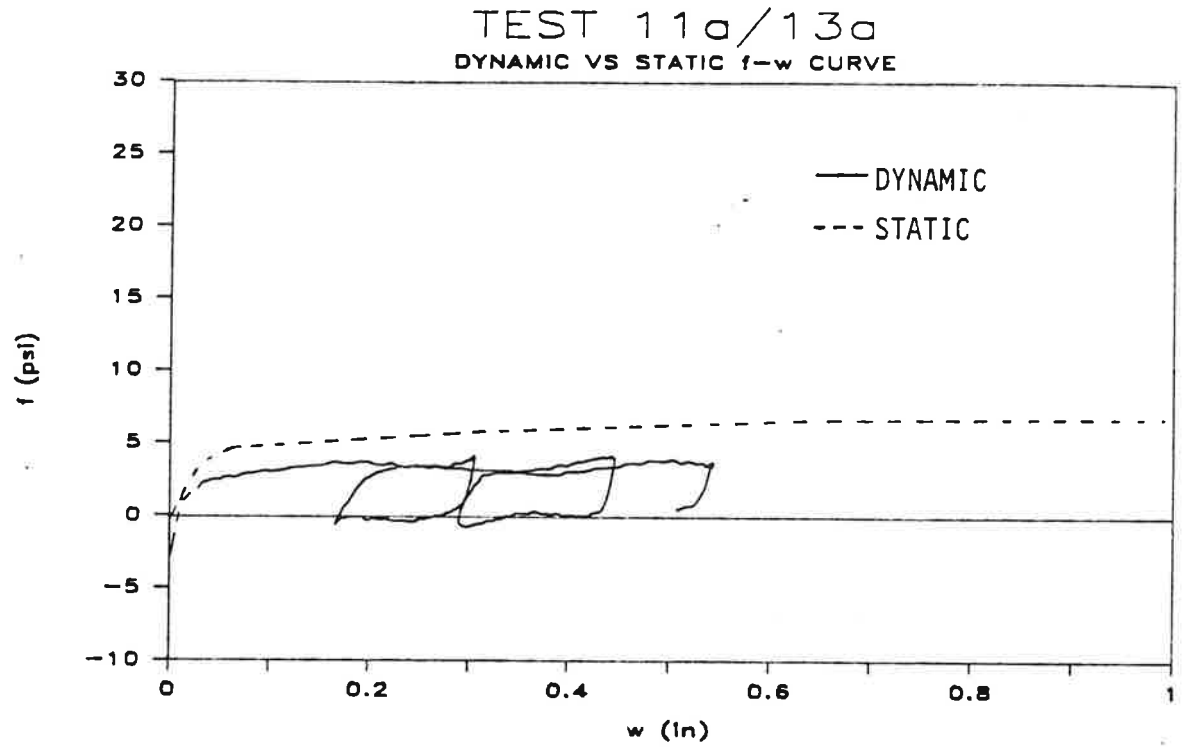

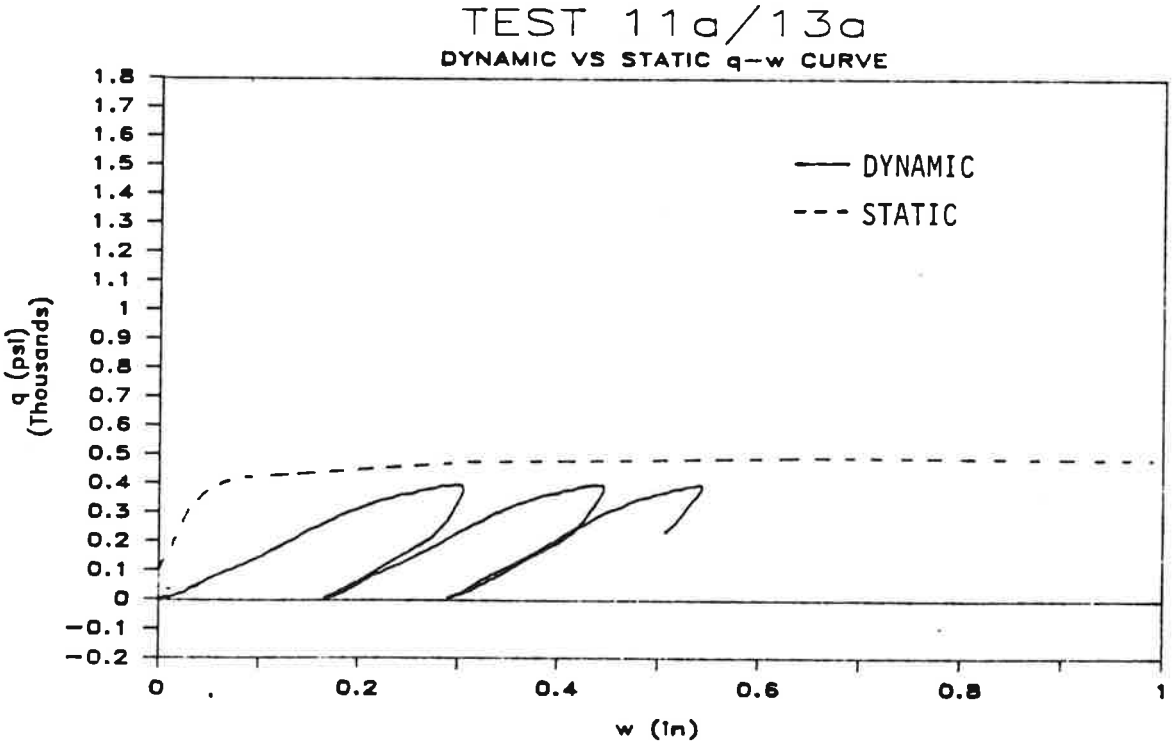

Fig. 50. Comparison of Unit Load Transfer Curves for Pile in Motion and for Static Loading; Test 11A/13A; BLS (Coarse) Sand; 65% Relative Density; 10 Psi Effective Chamber Pressure; Pile-in-Motion Curves for 77-Inch Penetration

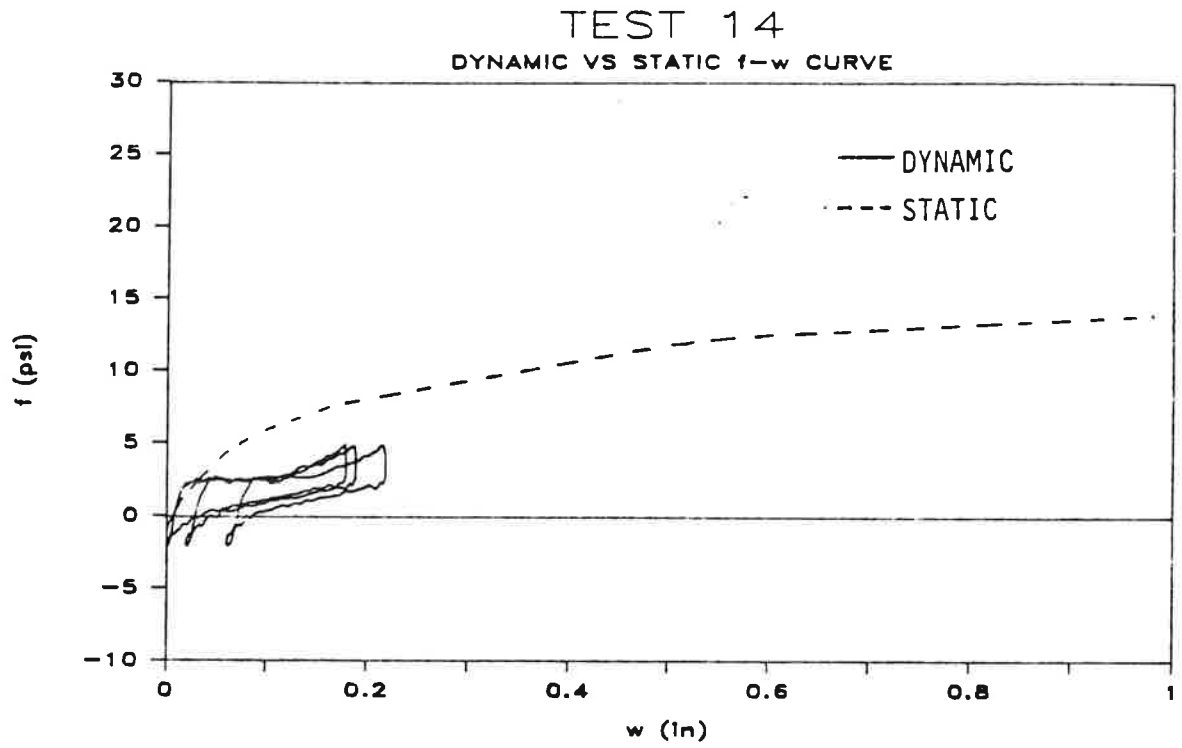

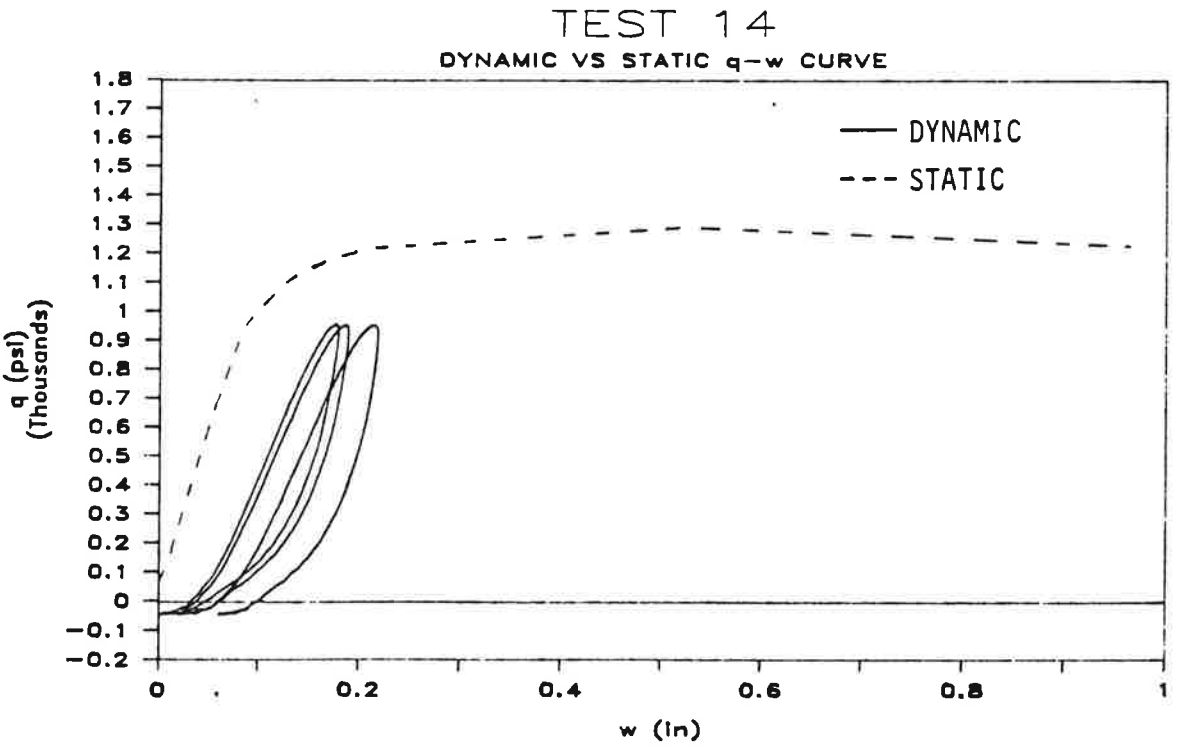

Fig. 51. Comparison of Unit Load Transfer Curves for Pile in Motion and for Static Loading; Test 14; BLS (Coarse) Sand; 90% Relative Density; 10 Psi Effective Chamber Pressure; Pile-in-Motion Curves for 70-Inch Penetration

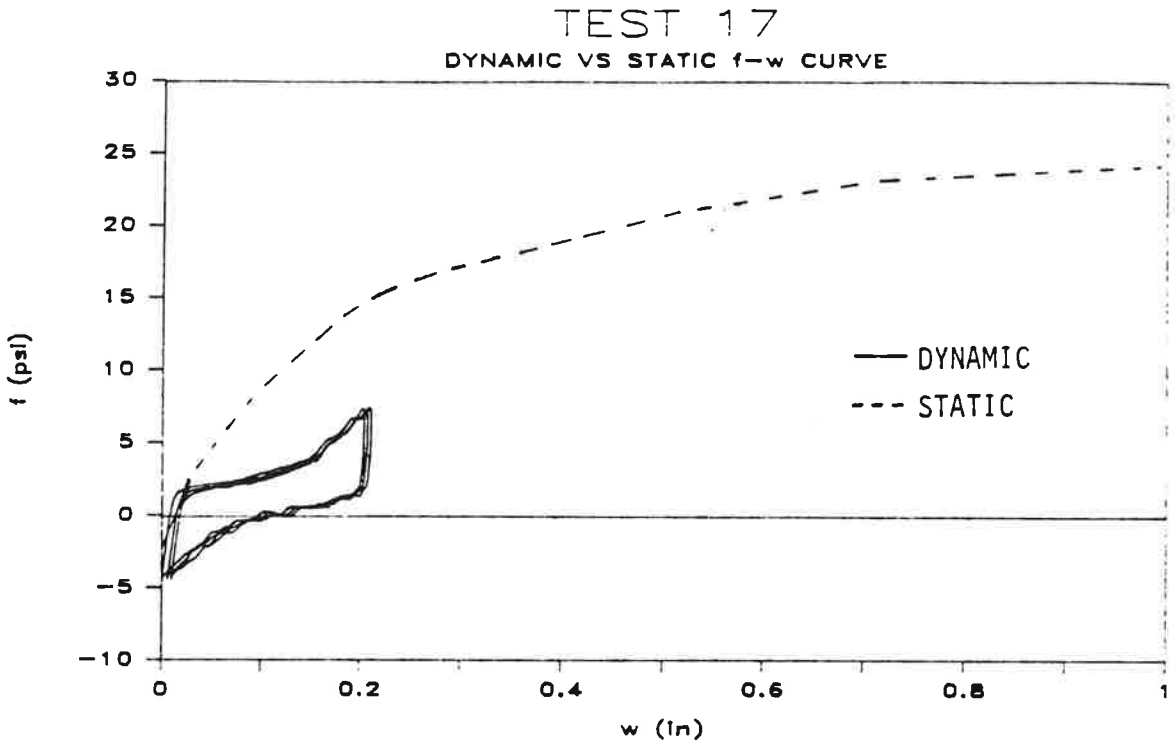

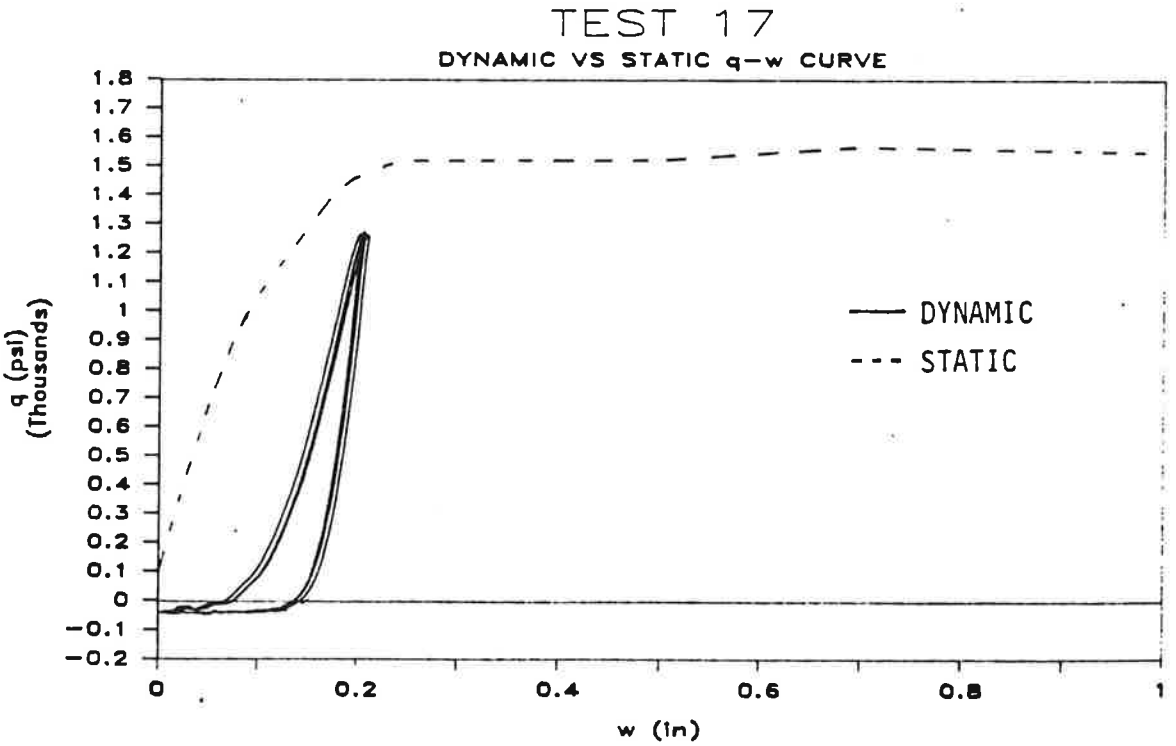

Fig. 52. Comparison of Unit Load Transfer Curves for Pile in Motion and for Static Loading; Test 17; BLS(Coarse) Sand; 90% Relative Density; 20 Psi Effective Chamber Pressure; Pile-in-Motion Curves for 70-Inch Penetration

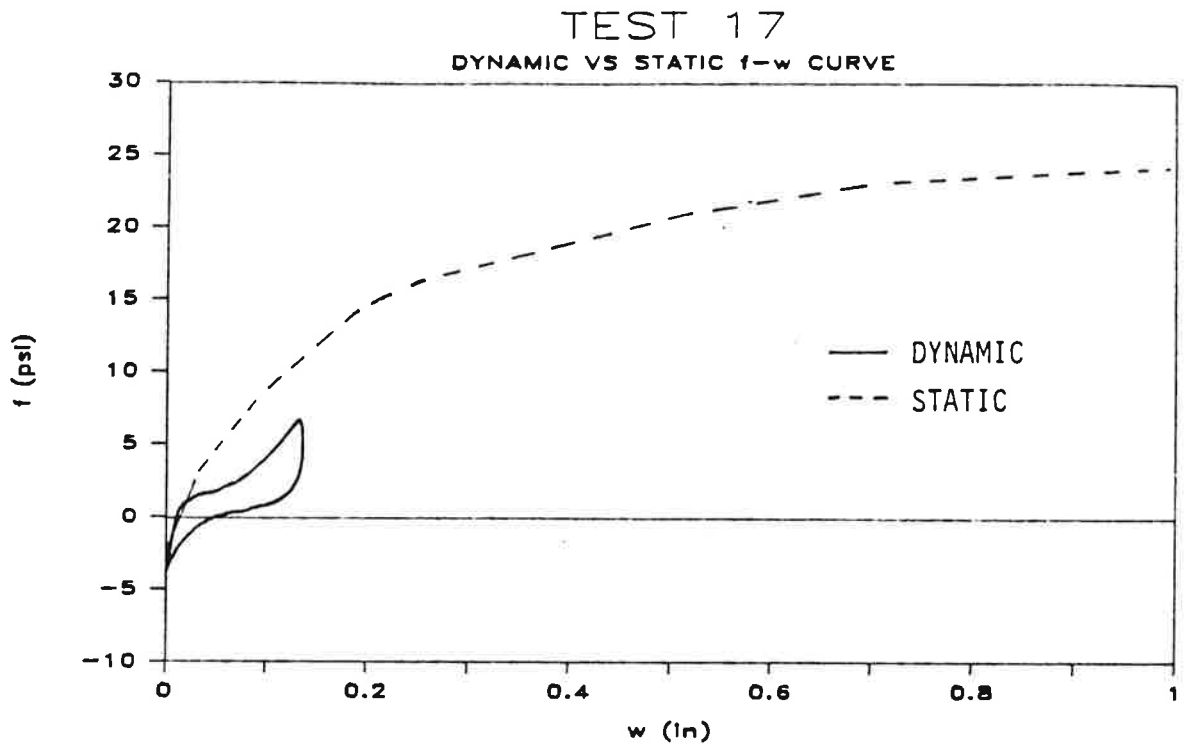

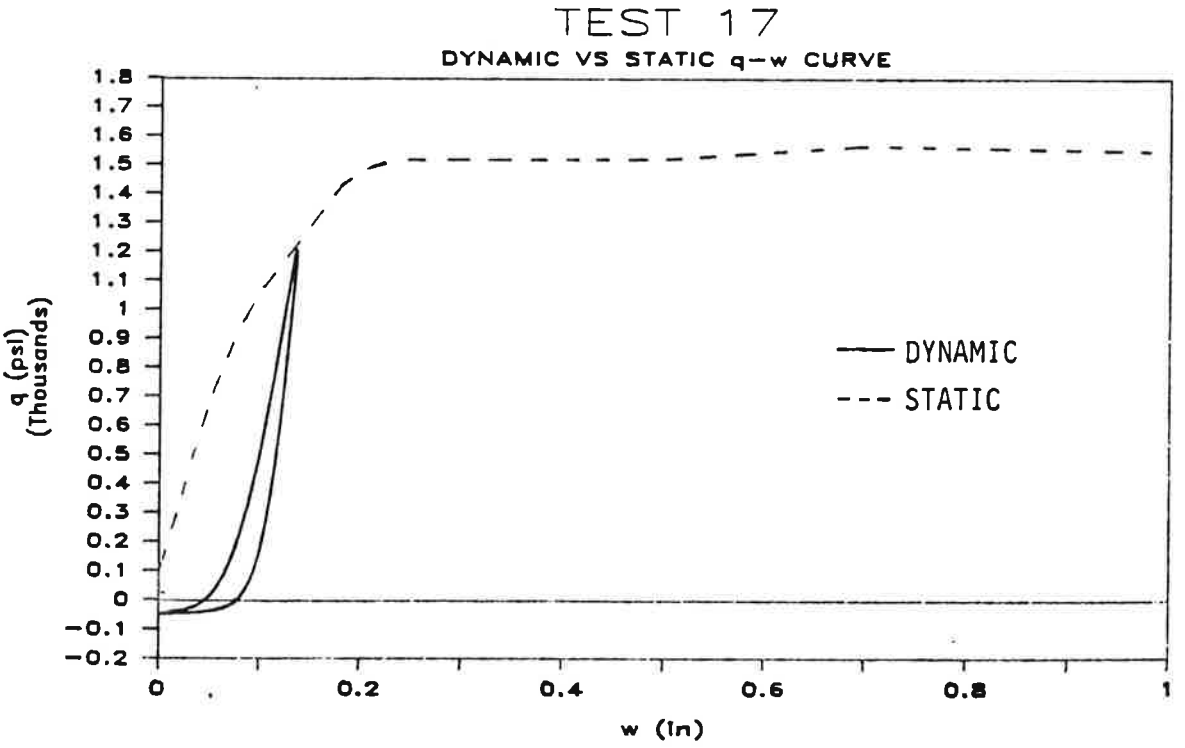

Fig. 53. Comparison of Unit Load Transfer Curves for Pile at Refusal and for Static Loading; Test 17; BLS (Coarse) Sand; 90% Relative Density; 20 Psi Effective Chamber Pressure; Pile-at-Refusal Curves for 74-Inch Penetration

the in-motion f-w relationships are for the pile as a whole, the static relationships that are shown are the average of the relationships derived for the upper and lower halves of the pile for the particular test under consideration. While much analysis can be made of the differences and similarities in these curves, it is appropriate to point out that:

a. the initial slopes of the loading branches of the in-motion ("dynamic") and static f-w curves are generally similar in SJR (fine) Sand and for 65% relative density in BLS (coarse) Sand (Figs. 47 - 50), but the in-motion curves are steeper than the corresponding static curves for very dense BLS Sand (Figs. 51 - 53);

b. the maximum slopes of the loading branches of the in-motion ("dynamic") q-w curves (corresponding to the completion of seating in the sands of high relative density) are smaller than than the corresponding slopes of the static curves for effective chamber pressures of 10 psi but are equal to or greater than the corresponding static slopes for effective chamber pressures of 20 psi;

c. the peak value of f was always less in the in-motion f-w curves than in the static curves;

d. the peak value of q was always less in the in-motion q-w curves than in the static curves, but it appeared that had it been possible to apply more energy to the pile to the pile per cycle in such a way as to produce greater toe deflection, the peak in-motion q values may have eventually become equal to or greater than the peak static values for all conditions.

These observations have important connotations with respect to how damping is viewed in vibro-driven piles. First, Figs. 15 - 18 indicate that peak velocities are small in the vibro-driven piles, generally less than about 1.5 ft/sec. This value is smaller than that which occurs in driven piles by a factor of perhaps 5, so that viscous damping is probably less important in vibro-driven piles than in impact-driven piles. For discussion purposes, damping may be viewed as equivalent Smith damping, or the increase in unit static shaft or toe resistance that is proportional to pile velocity

(Appendix O), in which the baseline zero-velocity relations are taken as the static relations in Figs. 47 - 53. From that perspective, considering the initial slopes of the in-motion unit load transfer curves, the damping coefficient appears to be nearly zero in shaft resistance, except for very dense BLS Sand, and essentially zero in toe resistance, except for effective chamber pressures of 20 psi. In fact, in several instances this view of damping suggests negative damping values, since the initial slopes of the in-motion curves are lower than those for the static curves. Low or negative Smith-type (apparent) shaft damping is believed to have been caused by soil particle motion near the interface, which lowers the effective stress at the interface and which restricts the transmission of shear waves into the soil mass, as described earlier. This reduced effective stress also reduces the available static resistance momentarily in the baseline curve, which leads to the apparent negative damping.

In toe bearing the apparent Smith-type damping appears to be near zero at low effective confining pressure, possible due to the fact that pore water pressures and/ or soil particle motion are developed locally that reduce the available static resistance momentarily, where such effects do not occur, or occur to a smaller degree, at higher confining pressure.

The clear pattern emerges that uniform, Smith-type damping constants for the shaft and for the toe defined as simple functions of soil type, as commonly used in impact-driving practice are not appropriate for vibro-driving. It appears that future mathematical models for vibro-driven piles will have to incorporate for the soil, as a minimum,

a. confining-pressure-dependent toe damping,

b. revised "static" baseline unit shaft resistance during vibration due to soil particle motion,

c. reduced radiation damping of the pile shaft due to reduced instantaneous lateral effective soil stress produced primarily by soil particle motion (not primarily by

pore water pressure generation as was demonstrated by the low pore water pressure readings that were made during the vibro-driving),

d. liftoff phenomena and distinct loading and unloading soil stiffnesses for the toe.

Phase Relationships

It is useful to describe phase relationships between motion functions at the pile head and pile toe, particularly for the reader who may want to use the information in this chapter and in the Appendices to develop or to calibrate mathematical models for vibro-driven piles. Table 21 summarizes the phase between pile-head and pile-toe accelerations. The raw, measured phase angles were relatively large; however, much of the apparent phase lead of the toe accelerometer was due to electronic phase lag in the accelerometer circuits at the pile head. Once this electronic lag was corrected, as described in Appendix G, the measured phase between the head and toe accelerations was generally ± 10° or less, with an average absolute value of 7° at 70 inches of penetration. It can be inferred from this observation that the test pile was a rigid body.

Some appropriate means to scale this phase information to the prototype is needed, since it is possible that a vibro-driven pile will behave differently if its motion everywhere along the pile is in phase, or is very nearly in phase, with that of the driver than if toe motion is out of phase with head motion. In simple single-degree-of-freedom vibrating systems, the inertial forces and forcing function are essentially in phase with one another if the operating frequency is equal to or less than about 10% of the resonsance frequency of the system. By analogy, it can also be assumed (without proof) that a full-sized pile would behave essentially as a rigid body during vibratory installation if the frequency of the vibrator is equal to or less than about 0.1 (c/2L), where c = compression wave velocity in the pile material (201,000 inches per second in steel), L = pile length, and (c/2L) = natural frequency of the pile as a freely vibrating rod. By this simple criterion, steel piles as long as 40 - 50 feet could be modelled as rigid

Table 21. Measured Phase Relationships Between Pile-Head and Pile-Toe Accelerations

Test/Condition	Penetration (in.)	Phase Lead (Toe/Head) (Degrees) Measured	Corrected
5 (S/90/10/V)**	30	26.1	0.5
	40	27.2	1.6
	50	25.4	-0.2
	60	22.1	-3.5
	70	14.9	-10.7
6 (S/90/10/VR)	30	32.2	6.6
	40	29.8	4.2
	50	21.3	-4.3
	60	17.8	-7.8
	70	16.8	-8.8
7 (S/65/10/VR)	35	15.0	-10.6
	56	18.0	-7.6
	70	19.7	-5.9
8 (S/90/K_o/VR)	30	22.7	-11.0
	40	20.6	-5.0
	50	19.8	-5.8
	60	17.2	-8.4
	70	15.2	-10.4
9 (S/90/20/VR)	30	21.1	-4.5
	40	24.2	-1.4
	45	24.7	-0.9
	50	22.9	-2.7
	55	26.4	0.8
11A/13A (B/65/10/V)	30	27.0	1.4
	40	38.0	12.4
	50	32.7	7.1
	60	32.5	6.9
	70	32.4	6.8
14 (V/90/10/V)	30	15.7	-9.9
	40	31.6	6.0
	50	28.7	3.1
	60	27.9	2.3
	70	27.7	2.1
15 (B/90/10/VR)	30	33.2	7.6
	40	34.0	8.4
	50	25.6	0.0
	60	24.1	-1.5
	70	24.1	-1.5
16 (B/65/10/VR)	40	15.7	-9.9
	50	17.7	-7.9
	70	10.0	-6.6
17 (B/90/20/VR)	30	11.8	-13.8
	40	12.5	-13.1
	50	14.1	-11.5
	60	15.3	-10.3
	70	14.6	-11.0

** S = SJR; B = Blasting / relative density (%) / effective chamber pressure (psi) ; K_o = 10 psi horiz. and 20 psi vert. / V = vibro; R = restrike

bodies when being installed by a vibrator operating at a frequency of 20 Hz, which implies that the application of the results of this study to the prototype scale may not need to include corrections for phase of motion within the pile. Such modifications may be required for longer piles or piles being vibrated at higher frequencies.

CHAPTER 3

Interpretation and Application

The objective of this chapter is to summarize those results presented in Chapter 2 and in the appendices that have potential applicability to field conditions. It should be pointed out that, while the experiments attempted to model effective stresses in the soil and provide ratios of unbalanced force and bias (quasi-static) force to pile capacity that are representative of field conditions, no assurance exists that the potential design procedures given in this chapter can be scaled directly to full-size. In fact, it will probably be found that upscaling will not be correct, because soil-pile behavior is inherently unscalable. It is believed, however, that the parameters controlling the behavior of displacement piles installed in clean sand by vibratory driving have been identified and that the relationships proposed between those parameters are generally appropriate. It remains to verify or to modify those relationships by further testing in the field and possibly in the laboratory. A suggested, general approach to field calibration of the candidate design procedure is provided in Chapter 4.

CANDIDATE DESIGN EQUATION

A practical, nondimensional, candidate design equation, derived from the analysis of the results of Tests 5, 6, 7, 9, 11a/13a, 14, 15, 16 and 17 (capacity tests) that relates the static compression capacity, Q, of a vibro-driven pile in clean, submerged

sand, to the velocity of penetration, v_p, the power delivered to the pile head, P_h, and the soil conditions, is given as Eq. (11).

$$\frac{Q\, v_p}{P_h} = \frac{0.050}{\beta_1 \beta_2 \beta_3}, \tag{11}$$

in which the factors in the denominator of the expression on the right side are defined as follows:

β_1 = horizontal effective stress coefficient = -0.486 + 0.0743 σ'_h (psi), 10 psi $\leq \sigma'_h \leq$ 20 psi;

β_2 = relative-density coefficient = 1.93 D_r (decimal) - 1.11, 0.65 $\leq D_r \leq$ 0.90; and

β_3 = grain-size coefficient = 1.228 - 0.19 d_{10}(mm), 0.2 mm $\leq d_{10} \leq$ 1.2 mm.

A frequency histogram indicating the accuracy of this method for the nine laboratory tests documented above is shown in Fig. 54.

A companion equation that relates empirically the peak pile-head acceleration a_h at the bottom of the downstroke to the velocity of penetration v_p is needed in order to apply Eq. (11) in a straightforward manner in the field. Such a relation, which was expressed in Eq. (3), was developed from an analysis of laboratory data from both parameter and capacity tests at various depths of pile penetration ranging from 12 diameters to 19.5 diameters. Equation (3) is written in a more convenient form for use in the candidate design procedure as Eq. (12).

$$a_h = \alpha_1 \alpha_2 (v_p)^{\alpha_3}, \tag{12}$$

in which

α_1 = relative density factor = - 2.186 + 3.54 D_r(decimal), 0.65 $\leq D_r \leq$ 0.90,

α_2 = grain size factor = 8.99 + 2.76 d_{10}(mm), 0.2 mm $\leq d_{10} \leq$ 1.2 mm,

α_3 = effective stress exponent = 1.71 - 0.081 σ'_h (psi), 10 psi $\leq \sigma'_h \leq$ 20 psi.

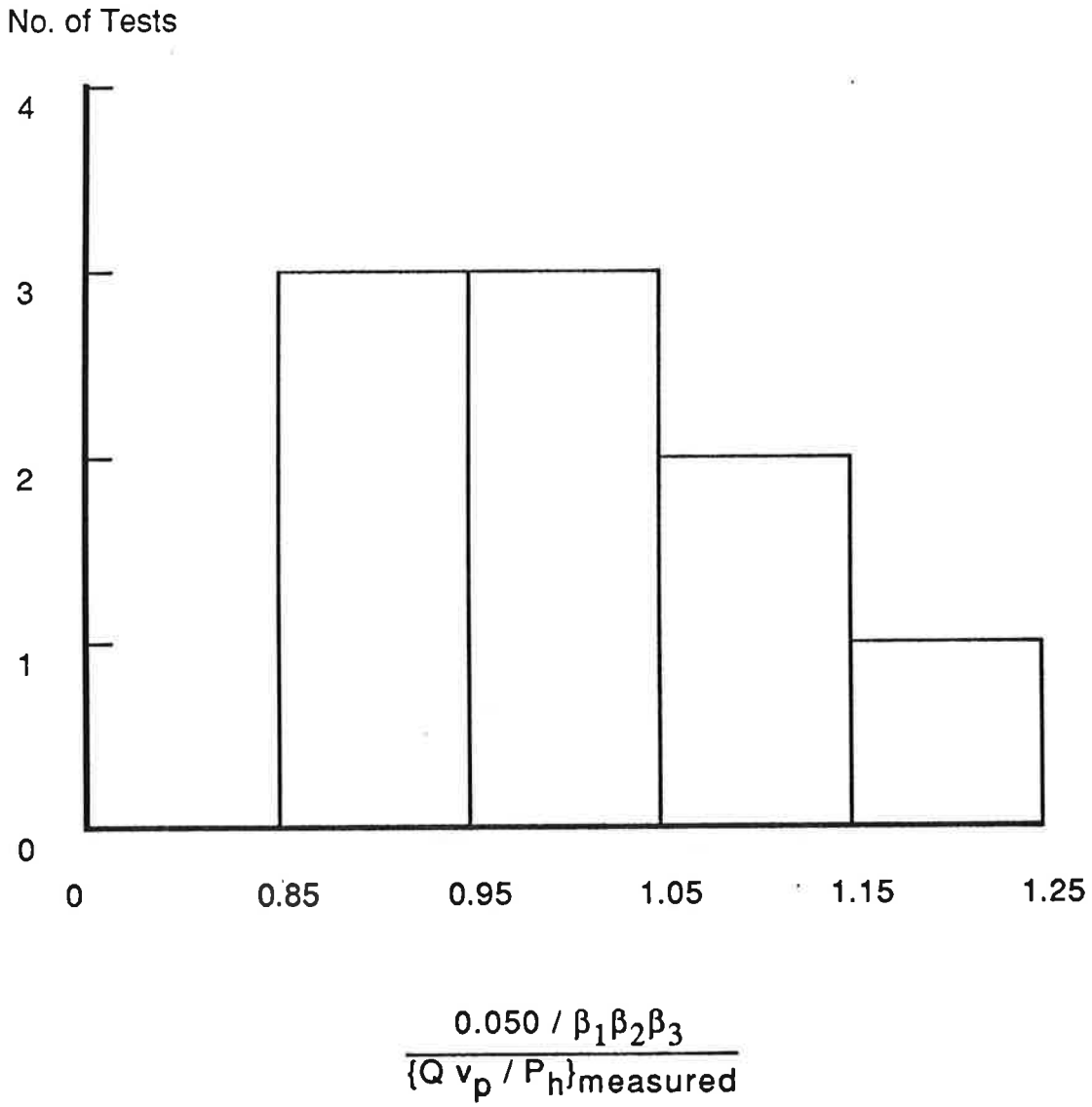

Fig. 54. Frequency Histogram of Number of Laboratory Tests vs. Ratio of Measured to Computed Normalized Static Compressive Pile Capacity

Several comments are in order regarding Eqs. (11) and (12).

a. The effect of restriking the pile is not included in Eq. (11).

b. The velocity of penetration, v_p, to be used in Eq. (11) is defined as the average velocity observed during the terminal portion of penetration equal to the diameter of the pile (incremental distance driven / time required to penetrate that incremental distance).

c. Equations. (11) and (12) are empirical. They contain implicitly the effects of the interaction of the pile, driver and soil through the power, velocity and acceleration terms and the soil coefficients and exponents. As with all empricial relationships, they must be considered to be valid only for the ranges of soil conditions described in the definition of the α and β parameters. Furthermore, they are considered valid only within the range of pile and vibrator conditions that were investigated in the study, which can be expressed in normalized form as follows, where the normalizing factor has been selected to be Q, the static compression capacity of the pile.

(1) The peak single-amplitude unbalanced force developed by the vibrator is at least 0.15 Q, and the vibrator body weight is of the order of 20% of the peak single-amplitude unbalanced driver force.

(2) The bias weight of the vibro-driver is 0.05 to 0.10 Q.

(3) The driving frequency is the optimum frequency for driving, viz., 20 Hz, and the pile is driven continuously without stopping.

(4) The pile is a full-displacement pile.

(5) The pile behaves as a rigid body during vibration (e. g., steel pile about 40 - 50 feet long or shorter).

d. The laboratory study was conducted in soils with depthwise uniform soil properties in order to obtain a clear understanding of the effects of the parameters. Although it may be reasonable to idealize sand in an entire profile as having a depthwise uniform relative density, soils with uniform lateral effective stress and

characteristic grain size are seldom found in the field. Therefore, in order to apply Eqs. (11) and (12) to common field conditions, it is suggested that weighted averages of soil properties σ'_h and d_{10} be used in evaluating the α and β factors in cases where these parameters vary with depth. It is further speculated, pending further field investigation, that the weighted values be assigned on the basis of the ratio of measured toe resistance to shaft resistance in static compression loading tests. If λ represents either σ'_h or d_{10}, then single, weighted values can be computed from Eqs. (13) and (14).

$$\lambda = 0.67\lambda_{toe} + 0.33\lambda_{middepth}, \qquad D_r = 65\%, \tag{13}$$

$$\lambda = 0.61\lambda_{toe} + 0.39\lambda_{middepth}, \qquad D_r = 90\%. \tag{14}$$

The subscript "toe" represents the value of the parameter at the level of the toe of the pile, while the subscript "middepth" indicates a value midway between the ground surface and the level of the pile toe. The coefficients represent the approximate proportions of static load distributed to toe and shaft that were measured in the laboratory during static compression loading at failure for the density conditions indicated. For relative densities between 65% and 90%, λ may be evaluated by linear interpolation.

e. Note is made of the fact that Eq. (11) requires knowledge of the lateral effective stresses in the soil, which exercise strong control of the pile behavior. Any site investigation that is undertaken must therefore include methods for evaluation of the lateral effective stress profile.

f. Other limitations may also exist that should be identified by the field verification research program outlined in Chapter 4.

APPLICATION OF CANDIDATE DESIGN PROCEDURE

Determination of Static Compressive Pile Capacity

In order to use Eq. (11) to determine pile capacity, the following step-by-step procedure should be followed, which includes the application of expressions in addition to Eq. (11) that were developed in Chapter 2. The procedure is logical, but some component relations (e. g., parameters a' and b' for Eq(7)) may need to be modified by field experiments.

a. Measure the average v_p in the last one diameter of penetration.

b. Determine the peak pile-head acceleration a_h from v_p using Eq. (12).

c. Compute P_t, the theoretical power of the hammer, from the brief procedure described in Appendix L, or obtain the information from the hammer manufacturer.

d. Determine P_h, the actual power delivered to the pile head, from a_h and P_t, using Eq. (7).

f. Finally, compute the static compressive capacity, Q, from Eq. (11).

Equations (11) and (12) require an estimation of soil grain size, relative density and mean lateral effective stresses prior to installing the pile by means of a site investigation in order to evaluate the α and β factors. The weighting expressions given in Eqs. (13) and (14) should be used where significant vertical variations occur in the relevant soil properties.

Assessment of Power Needs for Vibro-Driver

The inverse problem to computation of pile capacity from driver, penetration and soil data is that of assessing power needs for the vibro-driver to attain the necessary pile penetration to produce a pile of a given capacity (and by implication the specific vibro-driver required for installation) . A step-by-step procedure for assessing driver power needs is as follows.

a. Compute the static compressioncapacity of the pile, Q, using Eqs. (8) - (10) or some other appropriate means.

b. Select a target value of v_p at full penetration. v_p = 0.1 inches / second represents refusal.

c. Compute the required power at the pile head , P_h, at full penetration from Eq. (11).

d. Determine a_h from the selected value of v_p from Eq. (12).

e. Finally, estimate P_t , the vibrator power, from a_h and P_h, using Eq. (7), and select the driver accordingly. Verify from the manufacturer's data that the peak single amplitude force developed by the vibrator is at least 0.15 Q, that the the weight of the vibrator is on the order of 0.03 Q (20% of the single amplitude unbalanced force), that the weight of the bias mass, W, is between 0.05 and 0.10 Q, that the isolation spring constant, k, gives a natural frequency of the bias mass, $(kg/W)^{0.5}$, where g is the acceleration of gravity, of no greater than 3 Hz. Operate the vibrator at approximately 20 Hz.

CHAPTER 4

Conclusions and Recommendations

SUMMARY

The laboratory study reported herein consisted of a coordinated pile-driving testing program in which 22 large-scale model tests were conducted to identify the effects of soil and driver parameters on the behavior of vibro-driven displacement piles in submerged, clean sand, to compare the behavior of vibro-driven piles with impact-driven piles and to assess the effects of restriking vibro-driven piles. The data were analyzed, and, based on the patterns of observed phenomena, a candidate design procedure was developed.

The modelling conditions for the laboratory study were as follows:

- Soil. One-to-one model to prototype similitude was maintained in terms of average soil conditions from the ground surface to the toe of the prototype pile.

- The mean effective stress of a typical sand deposit was simulated to a nominal depth (pile penetration) of 50 feet and to a nominal depth (pile penetration) of 100 feet under conditions of isotropic effective stress (K_o = 1). The soil was contained in a saturated, pressurized test chamber that permitted drainage of water during installation to occur in a radial direction. An effective pressure of 10 psi was used to simulate a pile penetrating 50 feet. Such a value of pressure would be that which would occur in situ at a depth of approximately 25 feet (the middepth of a 50-foot-long pile) in a submerged sand of typical density. An effective pressure of 20 psi was used to simulate a pile penetrating 100 feet, in which the value of pressure would be that at the middepth

of the pile. This method of scaling presumes that the pile resists load entirely in shaft shear, and that assumption was used in developing the penetration-simulated depth values referred to throughout this report. Since the toe resistance was actually measured to be rather significant during the vibration and loading tests, however, it is likely that some weighting should have been given to the in-situ effective soil pressure at the level of the toe in a prototype, in addition to that at the middepth of the shaft, when evaluating the penetration scaling in relation to effective stresses. If a linear relation is assumed between the effective stress and depth, and if the pressure in the soil at the level of the toe of the prototype is weighted at 0.5 and that at the middepth is weighted 0.5, then the tests conducted at 10 psi effective chamber pressure would scale to a penetration of 37.5 feet rather than to 50 feet. Similarly, the tests conducted at 20 psi would scale to a pile penetration of 75 feet rather than 100 feet. Such weighting appears reasonable in retrospect, since the toe and shaft resisted about equal amounts of load during the static load tests. Therefore, the quoted scaled penetrations of 50 and 100 feet should be considered nominal values that are upper limits to the correct scaled penetrations.

- The effect of K_o was investigated by conducting some tests at $K_o = 0.5$.
- The effective grain size (d_{10}) was varied from 0.2 to 1.2 mm to assess the effects of fineness of the soil on pile and vibrator performance.
- The relative density of the soil was varied from 65% to 90%. The former value is representative of soils that contract during shear and of the general range of 50% to 70% found in many natural deposits. The latter value is representative of soils that dilate during shear and of the upper limit of relative density of sands into which piles would normally be driven.
- Pile. No formal similitude rules were followed; however, the lateral dimensions of the reusable test pile were made large enough so that the ratio of soil particle diameter to pile width would be small enough to have minimal scaling effects.

The pile was a closed-ended steel pipe, 4.00 inches in outside diameter, was installed to penetrations in the test chamber of up to 19.5 diameters, and was demonstrated during the tests to have behaved essentially as a rigid body during vibro-installation. Such behavior should be representative of relatively short prototype steel piles (40 - 50 feet in length). The weight of the pile was relatively low compared to the soil resistance that developed during vibro-installation, so that its inertial forces had a relatively minor effect on the vibro-driving process. The pile was instrumented to permit measurement of head and toe force and acceleration, force along the pile under static loading, and lateral total and pore water pressure at the pile-soil interface. All instrumentation systems were successful except for the total pressure measurement system.

- Vibro-Driver. No formal similitude rules were followed. However, several physical principles were followed, so that the behavior of the vibro-driver would be representative, at the large-model scale, of vibro-drivers in the field. Several parameters influence the driving rate. These parameters, which may interact with one another, are bias mass weight, isolation spring constant, unbalanced force magnitude and frequency, vibrator body weight, and flexibility of the connections between the driver and the pile head. Only the first two parameters were investigated explicitly during the testing program, but the ratio of the vibrator body weight to static pile capacity was established at a value that is typical of field conditions. The connection was made as rigid as feasible but was not totally rigid. Additionally,

- The operating frequency was in the low frequency range, well below the fundamental frequency of the pile itself.

- Bias (quasi-static) masses were provided that ranged from approximately 0.02 to 0.10 Q, where Q is the static compressive capacity of the pile.

- The vibro-driver was of the counterrotating-mass type. Eccentric moments produced peak vertical forces with amplitudes of approximately 0.1 to 0.2 Q.

(Higher forces were possible, but the frequency range over which the vibrator could operate at those higher force levels was not appropriate for this study.)

- The weight of the vibrator body was 780 lb., which was on the order of 3 to 5% of the static capacity of the pile.

- Impact-Driver. No formal similitude rules were followed. The driver was a single-acting, cushioned, impact hammer that delivered approximately 20 - 25 blows per minute. The hammer was designed so that the pile would be driven in such a manner as to produce a set of at least 0.1 inches per blow, which is typical of prototype hammers. The characteristics of the impact hammer were not varied during the experiments.

PRIMARY CONCLUSIONS

Vibro-Driver and Pile Parameters

- Optimum driver frequency. The optimum frequency of the driver was found to be 20 Hz over virtually all soil conditions and for all values of unbalanced and bias mass forces. Tests to evaluate pile capacity were all conducted by installing the pile at this frequency.

- Eccentric moment and vibrator weight. It was found to be necessary for the eccentric moments to produce an unbalanced force of at least 4,100 lb (0.15 Q)in order to drive the pile effectively at the optimum frequency of 20 Hz. This observation is relevant for a vibrator body weight (excluding the bias masses) of approximately 20% of the unbalanced force and for the bias mass weight documented below.

- Optimum bias mass. The optimum value of the weight of the bias mass was not established. It was observed that the larger the value of biased weight, the greater the rate of penetration. The value associated with the eccentric moment and vibrator weight described above was 2,000 lb, or 5 to 10% of the static pile capacity. It is clear

that the values of the bias mass weight, unbalanced moment and vibratory body weight are coupled with respect to their ability to produce pile penetration. Resources did not permit enough parametric tests to be conducted to establish this coupling experimentally.

- Vibrator power and power transmission. The full theoretical power developed by the vibrator was not transmitted to the pile head. The ratio of pile-head power to power produced by the vibrator appears empirically to be related to the maximum value of acceleration (more precisely, deceleration) that was observed at the pile-head on the downstroke (Eq. (7)). That acceleration could, in turn, be related to the soil parameters (Eqs. (3) and (12)). The minimum power transfer was approximately 40% of the theoretical vibrator power, which occurred at a peak pile-head acceleration of 3 g, which appears to be a practical threshold from the perspective of power. Practical refusal during vibro-driving could be consider to correspond to a rate of penetration of 0.1 inches per second.

- Comparative total energy for vibro-driving and impact-driving. The vibro-driver-installed pile required about 65% of the total energy required for the impact-driven pile at the lower relative density (65%), in terms of mechanical energy produced by the driver, for the easiest driving conditions (10 psi effective chamber pressure; i. e., simulated toe depth of 50 feet in terms of effective soil stresses) but required 200 - 500% more energy than the impact driver at the higher relative density (90%) and 20 psi effective chamber pressure (100 feet simulated toe depth). Somewhat less vibrator power was required to install the pile in coarse sand than in fine sand. For all conditions, however, vibro-driving produced considerably lower stresses in the pile than did impact driving.

Effect of Soil Parameters on Vibro-Driveability

- Relative density. The rate of penetration, v_p, decreased with increasing relative density. This parameter had the most important effect on rate of penetration.

• Horizontal effective stress (simulated depth). v_p decreased with increasing horizontal effective stress , but the effect of this parameter was less pronounced than that of relative density.

• Coefficient of earth pressure at rest. K_o had little effect on driveability. The controlling factor was horizontal effective stress.

• Effective grain size. The parameter d_{10} had a relatively small effect on driveability.

The various effects are quantified empirically in Eq. (11).

Load Transfer During Vibro-Driving

• Shaft resistance. A limiting shaft resistance was achieved during vibro-driving that was on the order of 0.30 to 0.65 times the corresponding resistance for the statically loaded pile in compression.

• Toe resistance. A limiting toe resistance was not reached during vibro-driving, during a typical stroke, but the peak soil resistances that developed were on the order of 0.50 to 0.90 times the static toe resistances at corresponding values of toe deflection. It was found that at the higher relative density a rapid impact phenomenon occurs, in which the pile toe lifts off the soil on the upstroke and impacts the soil on the downstroke. With the lower relative density this effect did not occur, probably because the pile was penetrating at a rate that was too fast to allow the toe to lose contact with the soil on the upstroke of the driver.

Residual Stresses

Residual stresses were developed at the toe and along the shaft, but their magnitude was generally minor in both impact- and vibro-driven piles, most likely due to the fact that the test pile was relatively rigid.

Effect of Vibro-Driving on Static Behavior

The most important parameter in relating comparative capacities of piles driven by vibration and by impact was found to be its relative density, and by

implication, its volume-change characteristics. Table 16 provides a general summary of the effects of the various soil parameters on static capacity, and Table 20 provides a summary of the effects of impact- versus vibro-driving with respect to relative density in terms of static design parameters..

- Soil with relative density of 65%. The impact-driven pile developed 25% higher maximum average unit shaft resistance in compression and 15 - 20% higher maximum unit toe resistance than the vibro-driven pile. This finding is in general agreement with the recent study of field tests by the Corps of Engineers (16).

- Soil with relative density of 90%. The impact-driven pile developed 20 - 30% lower maximum average unit shaft resistance in compression and approximately 30% lower maximum unit toe resistance that the vibro-driven pile.

- Pile-head stiffness. The stiffness of the pile-head, as evidenced by the load-movement relations, was not adversely affected by vibro-driving.

- Uplift resistance. The uplift resistance that developed along the shaft of both the vibro-driven pile and the impact-driven pile was approximately 75% of the corresponding resistance developed in compression. The largest reduction in shaft resistance occurred in the upper 10 diameters of the pile, while essentially no reduction occurred below 10 diameters.

Effects of Restriking the Vibro-Driven Pile

- Soil with relative density of 65%. Restriking a vibro-driven pile produced a very small increase in capacity with respect to that of a corresponding pile that was vibro-driven but not restruck. However, the restruck vibro-driven pile developed a capacity that was only about 85% of that of a corresponding impact-driven pile.

- Soil with relative density of 90%. The effect of restriking was not clearly defined by the tests, but no consistent improvement in capacity was observed. Vibrated and vibrated-restruck piles alike developed higher capacities than impact-driven piles at this relative density.

- Wave-equation parameters. Back calculation of wave-equation parameters was difficult because of the short length of the test pile. However, it appeared that the wave-equation parameters for the restruck vibro-driven pile did not differ considerably from those for the continuously impact-driven pile in fine sand. No direct comparisons were made for the pile in coarse sand. However, it was observed that the shaft and toe quake values required during restrike in the coarse sand (d_{10} = 1.2 mm) were about twice those obtained for fine sand (d_{10} = 0.2 mm) and that the ratio of toe resistance to total resistance was higher than that observed for fine sand.

CANDIDATE DESIGN METHOD

A candidate design method based on an analysis of the laboratory data was outlined concisely in Chapter 3. Further research is needed to verify and/or modify the candidate procedure due to potential differences in laboratory and field conditions and due to the fact that the laboratory study could not cover all possible combinations of parameters. The candidate procedure, however, is believed to contain all of the important variables in an appropriate framework. A three-phase approach is proposed in order to verify or modify the candidate design method to assure the proper prediction of the behavior of full-scale piles under field conditions. The first two phases should ideally be conducted in parallel, while the third involves continuing acquisition of data from the field and would be conducted over a prolonged period of time.

- Phase A. Conduct field tests specifically for research purposes. It is recommended that at least two field sites be chosen, one in which the average relative density of the soil is 50 - 70% (with verification that the soil contracts during shear), and one in which the average relative density of the soil is 80 - 100%. It is also recommended that the soils at both sites possess some fines, perhaps 5 - 12%, because totally clean soils (the type used in the laboratory study) are less common than sands

containing some fines. Sites having soils with excessive fines (greater than 12%) should not be chosen because experience dictates that vibro-drivers are not usually successful in such soils.

The objectives of the field tests should be to investigate the following effects:

- Power transmission ratio from driver to pile. This ratio must be evaluated in the design procedure. It is thought that it depends on the mechanical characteristics of the vibrator, the weight of the bias mass and its vibrational amplitude during pile driving, the details of the connection between the vibrator and the pile head and the peak accelerations of the pile head on the downstroke. The general ratios of unbalanced force, vibrator body weight and bias mass weight to static pile capacity should be maintained in the order of the values achieved in the laboratory, but some variations in either the relative body weight of the vibrator or of the unbalanced force could be investigated, and a few tests should include significant variations in bias mass in order to expand Eq. (7) to any likely range of bias mass energy absorption that could occur in the field, permitting a' and b' to be defined in terms of bias mass weight and static pile capacity or other convenient parameters.

- Pile scale. The scale of the pile [width and (particularly) pile material and length] should be investigated with the objective of determining what characteristics will allow the pile to be treated as a rigid body and what characteristics will require the pile to be modelled as a flexible body, which will require a modification of the procedure described herein. Length effects are also important to verify that the procedure developed herein assuming that the relevant value of soil effective stress is the mean lateral effective stress (or weighted mean according to Eqs. (13) and (14)) can be applied to prototype piles.

- Pile volume. The tests reported here were exclusively for a full-displacement pile. Field tests should also include the effects of non-displacement (or partial-displacement) piles such as H piles or open-ended pipe piles. It is likely that

some of the parameters in the candidate design method will have to be modified for this effect.

- Group action. Neither the laboratory study nor any of the studies surveyed in the literature addressed the issue of group action. For impact-driven piles it has been clearly established that group efficiencies are greater than unity when groups of piles are driven by impact or are jacked into sands. It is possible that the opposite effect occurs when piles are vibrated into position. Since most vibro-driven bearing piles will likely be driven in relatively close proximity to other piles, the effect of vibrating adjacent piles into place on pile capacity should be investigated.

The following may constitute a typical set of tests at one test site:

- Install and test to compression failure with one vibro-driver:
  - one isolated 35-50-foot-long full-displacement pile
  - one isolated 35-50-foot-long non-displacement pile
  - one isolated 75-100-foot-long full-displacement pile
  - one isolated 75-100-foot-long non-displacement pile

  These piles should be instrumented in a manner similar to the laboratory test pile.
- Install four to six 35-50-foot-long, isolated, full-displacement piles using a variety of connections, unbalanced forces, bias masses and vibrator body weights. It is not necessary to perform static loading tests on these piles, but measurements should be made of the pile-head power, and the power transmission ratio should be determined near full penetration.
- Install one closely spaced group of at least three piles, in a linear arrangement. The middle pile should be installed first, subjected to a compression loading test; then, the remaining piles should be installed

and the middle pile tested again. The middle pile should be instrumented in a manner similar to the laboratory test pile.

Some of these substudies, such as those to investigate non-displacement piles and those to investigate group effects, could be performed in a test chamber similar to that employed in this study or in a centrifuge prior to or in lieu of field testing. Neither companion impact-driving tests nor restrike tests are recommended for inclusion in the field test program, as it is believed that the laboratory study established their effects relative to vibro-driven piles with sufficient accuracy for field use. Such tests could be considered in a secondary test program, however, if resources permit.

The minimum information that should be acquired at each site are:

- Physical properties of the pile (weight, length, section properties, modulus),
- Vibrator characteristics, including unbalanced force amplitude, frequency, weight of vibrator body, weight of bias mass and value of spring constant between the bias mass and the vibrator body.
- Pile-head power versus toe penetration,
- Pile-head acceleration versus time and toe penetration,
- Velocity of pile penetration versus penetration,
- Static compression head load vs. head settlement up to a well-defined failure load, with concurrent measurement of toe load and toe settlement, for those piles requiring static loading tests.
- Soil properties, including distribution of vertical and lateral effective stresses, location of the piezometric surface, and profiles of relative density, unit weight, indices (such as Atterberg limits) and grain-size distribution. Representative samples of the soil should also be subjected to tests that establish their volume-change characteristics and friction angles.

The field test results should be analyzed in a manner similar to that employed to analyze the laboratory data, and the candidate design method verified for further field use or modified, as appropriate.

Phase B. Since no field experimental program can properly quantify the effects of all of the parameters, it is recommended that a new mathematical model be developed for the simulation of the vibro-installation process and, possibly, the static load-movement performance of vibro-driven piles. A rigid-body- or wave-equation-type analogy might be an appropriate point of departure for this model. Emphasis should be placed on development of an appropriate soil model, since the conventional model used for the analysis of impact-driven piles (the Smith model) appears from an analysis of the laboratory test data not to be appropriate for vibro-driven piles. The mathematical model should also be capable of modelling the physical properties of the driving system, including the bias mass, isolation springs, vibrator body weight, the vibrator forcing function, the connection between the vibrator and pile head, and the inertial effects of the pile itself. Once a comprehensive model is developed, the interaction of the many components of the driving system, pile and soil can be studied systematically. Such a systematic analytical study may point to possible changes in the candidate design procedure that are not discovered in Phase A but which could be evaluated later by proper study of appropriate tests in Phase C. One important application of the Phase B study would be to construct different relations between power ratio, P_h/P_t, and peak pile-head acceleration, a_h, (Eq. (7)) for varying values of pile capacity, pile mass, bias mass, isolation spring constant, connector flexibility, vibrator frequency and unbalanced moment, and mechancial efficiency of the vibrator.

Phase C. Due to the lack of a general body of appropriate field data on vibro-driven piles, it is recommended that the driving, soil and loading test information outlined above be collected from future production projects that employ vibro-driven piles and compiled in a data base that would be analyzed periodically with a view

toward improving and generalizing the candidate design procedure, as verified or modified in Phases A and B. In this phase it may be possible to employ stress-wave analyses of restrike operations in lieu of static testing in some of the static loading tests.

References

(1) Rodger, A.A., and Littlejohn, G.S., "A Study of Vibratory Driving on Granular Soils." Geotechnique, Vol. 30, No. 3 (1980) pp. 269-293.

(2) Jeyapalan, J.K., "Axial Capacity of Vibro-driven Piles." Unpublished Internal Report, U. S. A. E. Waterways Experiment Station (1986).

(3) Barkan, D.D., "Foundation Engineering and Drilling by Vibration Method." 4th Int. Conf. on Soil Mech. and Found. Eng., London, Proc. Vol. 2 (1957) pp. 3-7.

(4) Shekhter, O.J., "The Amplitude of Force Vibrations of Piles as a Function of Vibrator Characteristics." Science Research Institute Foundations, Proc. No. 27 (1955).

(5) Mao, T.E., Discussion, Session 6, 4th Int. Conf. on Soil Mech. and Found. Eng., London, Proc. Vol. 3, (1957) pp. 192-193.

(6) Mao, T.E., "The Yangtze River Bridge at Hankow, China." Civil Engineering, Vol. 28, No. 12 (1958) pp. 54-57.

(7) Huck, R.W., and Hall, J.R., "Resonant Driving in Permafrost." Foundation Facts, Vol. 7, No. 3 (1971) pp. 11-15.

(8) Szechy, C., "The Effects of Vibration and Driving upon the Voids on Granular Soil Surrounding a Pile." 5th Int. Conf. of Soil Mech. and Found. Eng., Proc. Vol.2 (1961) pp. 161-164.

(9) Hunter, A.H., and Davisson, M.T., "Measurements of Pile Load Transfer." STP 444, American Society for Testing and Materials (1968) pp.106-117.

(10) Bernhard, R.K., "Pile-Soil-Interactions During Vibro-Pile Driving." Journal of Materials, Vol. 3, No. 1 (1968) pp. 178-209.

(11) Schmid,W. E., "Driving Resistance and Bearing Capacity of Vibro-Driven Model Piles." STP 44, American Society for Testing and Materials (1968) pp. 362-375.

(12) Larnach, W. J., and Al-Shawaf, N.A., "The Vibratory Driving of Piles in Sand." Ground Engineering, Vol. 5, No. 5 (1972) pp. 22-24.

(13) Gardner S., "Analysis of Vibratory Driven Pile." NCLE Technical Note, No. TN-1779, (1987) 29 pp.

(14) Preliminary Report on Hunter's Point Vibro-Driving Test, Texas A and M University (1988) (report in preparation at time of submission of this draft report).

(15) "Vibratory Hammer Study: Field Measurements," Preliminary Report Prepared for Deep Foundations Institute by Goldberg-Zoino & Associates, Inc., Newton Upper Falls, Massachusetts, File No. B-7946 (1987) 42 pp.

(16) Mosher, R. L., "Comparison of Axial Capacity of Vibratory Driven Piles to Impact Driven Piles." USAEWES Technical Report ITL-87-7 (1987) 36 pp.

(17) Steffanof, G., and Boshinov, B., "Bearing Capacity of Hollow Piles Driven by Vibration." 9th Int. Conf. on Soil Mech. and Found. Eng., Tokyo, Japan, Proc. Vol. 2 (1977) pp. 753-758.

(18) Davisson, M.T., "BRD Vibratory Driving Formula." Foundation Facts, Vol. 6, No. 1 (1970) pp. 9-11.

(19) Schmid, W.E., "Low Frequency Pile Vibrators." Conference on Design and Installation of Pile Foundation of Cellular Structures, Lehigh University, Bethlehem, PA, Proc. (1970) pp. 257-265.

(20) Chua, K.M., Gardner, S., and Lowery, L.L., Jr., "Wave Equation Analysis of a Vibratory Hammer-Driven Pile," Offshore Technology Conference, Proc. Vol. 4 (1987) pp. 339- 345.

(21) Wong, D.,"Design and Analysis of An Apparatus to Simulate Density and Stresses in Deep Deposits of Granular Soils," M.S. Thesis, Department of Civil Engineering, University of Houston (1985) pp. 53-55.

(22) Annual Book of ASTM Standards, American Society for Testing and Materials, Soil and Rock/Building Stones, Vol. 04.08 (1988) pp. 554-572.

(23) Hirsch, T.J., Carr, L., and Lowery, L. L., Jr.,"Pile Driving Analysis - Wave Equation Users Manual,TTI Program," FHWA Report No. IP-76-13.2. (1976).

(24) Goble, G.G, and Rausche, F., "Wave Equation Analysis of Pile Foundations; WEAP 86 Program," FHWA Report No. IP-86/21 (1986).

(25) Tucker,L., Program APILE, Notes from a Short Course on " Compute Programs for Geotechnical Engineers," Texas A and M University (1987)

(26) Fellenius, B.H., "Test Loading of Piles and New Proof Testing Procedure," Journal of the Geotechnical Engineering Division, ASCE, Vol. 101, No. GT9, (1975) pp. 855-869.

(27) Fuller, F.M., and Hoy, H. E., "Pile Load Tests, Including Quick Load Test Method, Conventional Methods and Interpretation," Highway Research Record No. 333, Highway Research Board, National Academy of Sciences (1970) pp. 74-86.

APPENDIX A

Literature Review

Research into vibratory driving of piles began in 1930 in Germany, and the first commercial application was carried out in 1932. At the same time, studies on vibration of foundations were carried out in the USSR. Pavyluk began his work on footing vibrations in 1931, and Barkan in 1934 demonstrated that the vertical vibration of a pile markedly decreased the shaft shearing resistance between the pile and the soil (1). In 1946, Rusakov and Khokhevich studied the mechanisms of low-frequency vibratory drivers and observed impact between the pile and the soil. Commercial application of low-frequency vibratory drivers in the USSR was demonstrated at the Gordy hydroelectric development project, where a vibratory driver operating between 38 and 45 Hz, drove a total of 3700 sheet piles to depths ranging from 29.5 to 39.4 feet in saturated sand and taking about 2 to 3 minutes per pile. The vibratory driver drove 60% more sheets and consumed only 25% of the power compared to a pneumatic impact hammer (2).

In 1953, high-frequency vibratory drivers with resiliently mounted surcharge (bias masses) were used to drive piles weighing 2.2 tons to depths of 65 feet in saturated sand (2). In 1955, Tatarnikov was able to apply the vibratory method to piles having large toe resistance using low-frequency drivers (7-16 Hz). It was found that at low-frequency of vibration, penetration is enhanced by a large displacement amplitude, and the repeated impacts which occur due to the separation of the pile toe and the soil. In

1956, a vibrocorer working at 42 Hz with a 0.1-inch displacement amplitude and a 35 KW electric motor was used to install casings for exploratory boreholes.

In 1957, Barkan (3) investigated many parameters that influence the vibratory pile driving method. These include oscillator peak acceleration, displacement amplitude, frequency, non-inertia load (bias mass), pile cross-sectional area, soil grain size and angle of internal friction, and shaft resistance. This study concluded that, at constant amplitude and frequency, penetration speed decreased with pile cross-sectional area, while the toe resistance increases and hence limits penetration and thereby the practical application of the vibration method of pile driving. The inertial and non-inertial loads acting on the driver element influence the speed of penetration and maximum driving depth. The toe resistance of the pile increases in direct proportion to vibratory frequency, and hence driving at a high frequency is not recommended. There is an optimum value of the driving force at which penetration speed and penetration depth reach a maximum, and the non-inertial loads help in increasing both the speed and maximum penetration. This study also concluded that linear oscillation theory may be used for the calculation of necessary vibratory parameters when the amplitudes are less than 0.4 inches. This observation agrees with the conclusion of Shekhter (4). When the driving is carried out with large eccentric moments on the vibrator and vibrator displacement amplitudes are greater than 0.4 inches, linear oscillation theory is inadmissible.

In a follow-up discussion to Barkan's paper (3), Mao (5) described successes with vibratory drivers in fine, coarse and gravelly sand and even clays. Vibrators were very effective in sinking piles into more than 33 feet of soil. Various vibrators had vibrating forces of 17.5 to 120 tons, frequencies of 6.7 to 16.7 Hz, unbalanced moments of 720 to 2740 ft-lb, and static weights of 4.5 to 11.25 tons. During the construction (1955 to 1957)

of the Yantzu River bridge at Hankow, China, vibratory drivers were used to drive 16-foot-diameter hollow concrete caissons though soft material to a depth of 1000 ft (6).

In 1959, Barkan attempted to increase the capacity of vibratory driven piles by using the concept of soil-pile resonance. At the same time, Albert G. Bodine, Jr., developed the sonic pile driver, which vibrates the pile near the pile's second harmonic frequency. In 1961, the C.L. Guild Co. of Providence, R.I. demonstrated that the sonic (resonant) pile driver could drive a closed-end pile 71 ft, while an adjacent steam hammer drove an identical pile only 3 inches in the same time period. Furthermore, Bodine's sonic driver was found to be successful in driving piles into permafrost, while conventional impact driving often led to excessive pile damage (7). Meanwhile, German and French engineers were encouraged by the success of high-frequency machines and designed their own new generation of drivers. However, the high rates of wear in motors and bearings reduced the design frequency to 25 Hz (1).

From model tests Szechy (8) obtained valuable data describing the effects of vibratory driving and impact driving on the porosity of granular soils surrounding a pile. Fine sand with a coefficient of uniformity of 2.5, internal friction angle of 35^{o}, porosity of 0.34 and density of 1.75 t/m^3 was used. The frequency of the vibrator varied from 2,800 to 3,000 r.p.m., and the vibrator weighed 42 lb. The diameter of the seamless steel tubes used to model pipe piles varied from 1.0 inch to 3.5 inches. Changes in void ratio were measured to determine the change in relative density and the angle of internal friction of the soil. These results could be conceivably be used to include the effects of vibratory driving in the static formulae to be used to find the bearing capacity of the pile. Szechy's observations concerning the changes in void ratio can be summarized as follows. The change in porosity around vibrated open-bottom tubes differs considerably compared to the driven tubes. There is only one common

phenomenon in both, i.e. the porosity just below the ground surface undergoes a considerable reduction. A definite loosening can be found to be about the mid-height outside the vibrated tubes, whereas no practical changes occurs for the driven tubes. The greatest difference in the change in porosity occurs below the pile, where compaction occurs in the case of vibrated tubes, and where slight loosening occurs in the case of driven tubes. Based on these observations and assuming that the degree of compaction may be regarded as a measure of the inner stress conditions, it was concluded that the bearing resistance will be derived mainly from point-resistance for vibrated tubes and from shaft friction for driven tubes. Szechy then compared the volume of soil intruded into the tube, which was much greater due to vibration than driving. In the case of vibrated tubes, he observed that the height of the soil plug within the pile is on the average at the same level as the original ground surface and stands even higher in the tubes of larger diameter. The average reduction in porosity of this inner soil core ranged from 2.5 to 11 percent. On the other hand, the level of the plug was always lower in driven tubes, the difference increasing with the reduction in the inside diameter of the tube at a generic penetration. The reduction of the original porosity was observed to be about 6 to 14 percent. The study also compared the bearing capacity of the vibrated tubes with that of the driven tubes, for various diameters, and it was concluded that vibrated piles are inferior to driven piles. This inferiority was most evident for small vibration times to force the pile to the required penetration depth. This inferiority nearly disappeared when the vibration time exceeded one minute (the usual vibration time was only about 20 to 40 seconds).

Hunter and Davisson (9) studied the load transfer mechanisms of full-scale piles in medium-dense and medium-fine sand. The angle of internal friction of the sand varied from 32 to 35 degrees, and the steel-to-sand sliding friction angle was 25 degrees.

This study concluded that significant residual loads are developed in piles driven with conventional impact hammers and that the residual loads from vibratory drivers did not exceed the weight of the driver. It was also shown that the load transfer measurements made assuming zero residual loads are likely to be in error with respect to division of load between friction and point bearing. It was recommended that instrumented pile tests should be organized so as to obtain the complete stress history for the pile. They also observed that the shaft friction during compression loading was about 30 percent higher than that during tension loading and that the average value of the earth pressure coefficient was 1.1 for piles driven with a vibrator.

Bernhard (10) studied the effect of soil moisture content on model piles vibro-driven into Ottawa sand and Princeton red clay. Based on these experimental results a dynamic formula for the estimation of bearing capacity of vibro-driven piles was developed. Schmid (11) also studied the driving resistance and bearing capacity of vibro-driven laboratory model piles. Cylindrical brass tubes of 3/4-inch diameter and lengths varying up to 36 inches were used as piles. A variable-frequency electromagnetic vibrator with a maximum dynamic force of 50 lb. was used in this study, and the tests were limited to a uniform dry sand (Ottawa 30-40 sand at 0.44 void ratio). It was concluded that the peak force transmitted to the pile toe is a direct linear function of frequency and non-inertial load and that for closed-end pipe piles there appears to be a good correlation between maximum dynamic resistance and static bearing capacity. It was also observed that the maximum penetration velocity occurred only at specific optimum frequencies and that the effect of skin friction during penetration was practically negligible. Although these studies provide important insights into the performance of vibro-driven piles, there are several limitations to that preclude their direct adaptation to the field. Most important among the

limitations are scale effects (11) and inaccurate modelling of in-situ effective stresses in the soil. Larnach and Al-Showof (12) conducted some model tests on piles driven into the sand by vibrators and developed a dimensional analysis that resulted in a relationship between bearing capacity, penetration depth, dynamic force and total weight of the pile-vibrator system.

Based on a laboratory study on vibratory driving in granular soils, Rodger and Littlejohn (1) have identified two types of vibratory pile driving, termed as "slow" and "fast." The occurrence of slow or fast motion is defined by the initial soil density, pile diameter, displacement amplitude and acceleration of vibration, with slow vibro-driving being the most common method. This study also concluded that the two parameters normally used in defining the range of application of vibratory drivers are the displacement amplitude and frequency of vibration and that the choice of frequency should be related to soil type: coarse grained sand 4-10 Hz; fine to medium sand 10-40 Hz. They have also recommended ranges of values for frequency, peak displacement and peak acceleration for different pile-soil conditions. The amplitude of vibrational acceleration has been accepted as the parameter controlling the occurrence of fluidization (shear strength reduction). With reference to the effect of this parameter on the shearing strength of cohesionless soil, three distinct physical states in the soil are described as sub-threshold (elastic response), trans-threshold (compaction response) and fluidized response. During elastic response (acceleration < 0.6g), inter-particle friction does exist and the shear strength has not been found to decrease by more than 5%. In the trans-threshold state (0.7g < acceleration < 1.5g) the decrease in shear strength is governed by the exponential function of acceleration of vibration, and the parameters of this exponential are determined by the grain size, shape and magnitude of static normal effective pressure. During the fluidized response state

(acceleration > 1.5 g), shear strength reduction reaches a maximum. According to the authors, this reduction should be achieved theoretically at an amplitude of acceleration equal to that of gravity; however, in practice, due to the presence of inter-particle friction the amplitude of vibration required is approximately 1.5g. A theory has been developed for slow vibro-driving based on rigid body motion, viscous-Coulomb shaft resistance and elasto-plastic toe resistance under combined sinusoidal excitation and static surcharge force. Experimental verification of this theory has been accomplished by means of driving a fully instrumented 1.5-inch-outside-diameter, closed-ended steel pile into a bed of dense uniform sand (C_u = 1.2, d_{10} = 0.29 mm) at a relative density of 71.5% and having an angle of internal friction of 41 degrees (1).

A full-scale field study was undertaken by the U. S. Naval Civil Engineering Laboratory using 20-inch-diameter (0.5-inch wall thickness) open-ended pipe piles and a vibro-driver with a 35-ton driving force (13). The soil at the test site consisted of very dense sand with an average total unit weight of about 127 pcf. The piles were vibro-driven in 4-foot increments, and the dynamic resistance at these depths were determined by using a diesel impact hammer. The maximum penetration that the piles were able to attain was 13 feet, and the bearing capacity varied from 40 to 53 tons for the four piles tested. The rate of penetration varied from 0.03 to 0.30 feet/minute near final penetration. A limited amount of tests were conducted using 8.63-inch-diameter closed and open ended pipe piles, but the extremely dense sand conditions in the test area limited both the type and quantity of data collected (13).

In 1986, a field study was sponsored by the U.S. Army Corps of Engineers, Lower Mississippi Valley Division, to compare the performance of vibro-driven piles to impact driven piles. In this study six H piles were driven using vibratory drivers to a depth of about 35 ft at the Hunter's Point shipyard in San Francisco, California. Two

borings at the 40 foot x 40 foot site indicated 5-6 feet of dense silty sand and gravel fill underlain by medium-dense fine-to-medium sand. The bearing capacity of the vibro-driven piles varied from 180 to 200 kips, except for one pile which had only 135 kips capacity (14). The Deep Foundations Institute also sponsored a study to investigate the performance of six vibratory drivers in driving a 33 ft long instrumented H-pile (HP 14X73) at the same site. The six vibrators selected for this study, had "free-air" frequency, amplitude and acceleration varying between 22-26 Hz, 0.12-0.19 inches and 7.7g-11.6g , respectively. The maximum rate of penetration during driving varied from 5 feet/min. to 21 feet/minute, depending on the type of vibratory driver (15).

In another study performed by the U.S. Army Corps of Engineers (16), the performance of vibro-driven piles has been compared to that of impact driven piles at different field sites. In this report five testing programs have been discussed, including two Arkansas River Locks and Dams (No. 4 and No. 3), a Crane Rail Track, Geochemical Building (Harvard University) and Wall No. 7 on I-95,Providence, Rhode Island. At Lock and Dam No.4 (also the source of some of the data of Hunter and Davisson), a double-acting steam hammer and a Bodine sonic driver were used to drive 12- to 20 inch-diameter pipe piles, 16-inch concrete piles and H piles. Comparing the load carried by the 16-inch pipe piles, impact-driven piles exhibited about 25% greater toe resistance and 2% higher shaft resistance than the vibro-driven pile. The H pile driven by the Bodine sonic driver had 11% higher bearing capacity than the impact-driven pile, with 23% higher shaft resistance but 56% lower toe resistance. Although the impact-driven, 16-inch pipe pile showed an 8% higher compression capacity, the ratio of uplift to compression capacity of 0.48 remained almost a constant between the impact-driven and vibro-driven piles . At the Arkansas River Lock and Dam No. 3 a low-frequency vibratory driver and a steam impact hammer were used. The H piles (14

BP73) driven with the impact hammer had higher capacities than the vibratory driven piles by an average of 32 tons in compression and 5 tons in uplift. The uplift to compression ratio varied from 0.25 to 0.31 for both impact- and vibro-driven piles. In another study (pile foundation for a crane rail track), prestressed concrete piles with 13 inch diameter were driven using a drop hammer with a 5-ton weight and a free fall distance of 15.8-inches, and a vibratory driver with frequency, amplitude and weight of 18.3 Hz, 0.39-inch and 5.6 tons, respectively, was also used. The bearing capacity ratio of vibro-driven to impact-driven varied between 0.25 to 0.88. It was also shown that when vibro-driven piles had their last 9 feet of penetration produced by driving with a drop hammer, the bearing capacity reaches the failure load of an impact-driven pile.

There are in existence a few static and dynamic formulae for determining the bearing capacity of piles installed with vibratory drivers. In the static formulae the internal friction angle for sand beneath the pile toe and along the pile shaft are generally modified to account for the effect of vibration. There are four pile driving formulae that were specifically derived for vibratory drivers. These relationships are summarized below.

(a) Snip (1968)

This formula was originally published in Russian in 1968 (2). According to this formula,

$$P = \lambda[(25.5N/A_o n) + Q]$$

where

P = bearing capacity of pile in kN,

N = power used by vibratory driver to drive the pile, in Kw,

A_o = vibration amplitude of pile in cm,

n = rotation frequency of vibrator eccentric weight in Hz,

Q = total weight of pile and vibration hammer in kN,

λ = coefficient considering the influence of vibration driving on the soil properties.

Stefanoff and Boshinov (17) proposed the following expression to find N for electrically powered vibratory hammers.

$$N = \eta\,(3)^{0.5}\,(IV\cos\phi/1000) - 0.25N^1,$$

where η = efficiency of vibration hammer,

N^1 = rated power of vibration hammer,

I = current intensity,

Cos ϕ = power factor, derived from three-phase electric current theory,

V = voltage.

(b) Bernhard (1968)

Bernhard (10) has proposed the following formula:

$$F_{stat} = \Pi_1{}^{max} PL/V_p{}^{ave}p$$

where

F_{stat} = static bearing capacity,

$\Pi_1{}^{max}$ = maximum efficiency factor (suggested value is 0.1),

P = power input minus the losses due to the driving mechanism,

L = length of the pile,

V_p^{ave} = average penetration velocity,

p = total penetration.

The losses due to the driving mechanism must be predetermined by operating the force generator at the pile driving frequency on a very rigid or very soft support, having a natural frequency well above or below the operating frequency of the hammer.

(c) Davisson (1970)

Davisson (18) has proposed a dynamic formula for piles driven by the Bodine resonant driver. In deriving his formula, he began with a simple relation for energy conservation, which is energy supplied = energy used + losses. This simple relation is also the basis for practically all impact pile-driving formulae. If the resistance to driving is denoted as R_u, then the above relationship can be expressed as

$$E = R_u (s + s_L)$$

where E = hammer energy,

s = final permanent set of the pile per blow,

s_L = an empirically determined set that represents all losses.

Assuming that the static bearing capacity of the pile is equal to the resistance to driving, then the static bearing capacity will be equal to $E/(s+s_L)$. This expression is applicable only for impact hammers. Davisson has extended this relation to vibratory drivers by developing an equivalence of one cycle of oscillation to one blow of impact driving, energy (E) to horsepower(H_p) divided by the frequency (f) and set (s) to rate of

penetration(r_p) divided by the frequency. Since one horsepower equals 550 foot-lb/second, R_u can be expressed as follows

$$R_u = 550\, H_p / (r_p + s_L f)$$

where R_u is in pounds, r_p is in feet/second and s_L is in feet. If the pile capacity is low and the rate of penetration is high, then another power term should be added to the numerator to account for the kinetic energy of the driver, equal to 22,000 r_p. The loss factor, s_L, varies with soil condition and the power transmission characteristics of the pile.

(d) Schmid (1970)

Schmid (19) uses an impulsive approach to the problem by considering the force acting on the pile toe as an impulsive force and integrating it over one vibratory cycle. For a one-system oscillator (i.e. one pair of eccentric masses rotating in opposite directions), the dynamic forces integrated over an entire cycle is zero. The remaining terms in the impulse equation yield

$$(B + E + Q) = \int_0^{T_c} R\, dt$$

Thus, $$R = [(B + E + Q)T] / \alpha T_c \,,$$

where R = penetration resistance,

B = weight of the bias mass,

E = weight of the vibrator,

Q = weight of the pile,

T = period of vibration,

T_c = contact time between the soil and the pile tip,

α = a coefficient between 0.5 and 1.0 and generally assumed to be 2/3.

The only unknown term in the above expression is T_c, and it is calculated as follows. To drive the pile into the ground, a minimum acceleration a_{min} is required. Therefore, only the acceleration in excess of a_{min} is used to achieve the penetration velocity, V_p. Representing the average excess acceleration over the threshold acceleration a_{min} by a_o, which is equal to (a - a_{min}) averaged over the contact period, the following expression can be written for the contact period, T_c.

$$T_c = (2x / a_o)^{0.5}$$

where x is the penetration per cycle given by the penetration rate V_p divided by the frequency. Hence, penetration resistance R can be represented by

$$R = \alpha (B + E + Q) T / (2V_p / N a_o)^{0.5}.$$

More recently, Chua et al. applied the one-dimensional wave equation, which is a widely accepted mathematical model for impact-driven piles, to the analysis of the behavior of vibro-driven piles (20). By replacing the impacting ram, cushion and capblock with a forcing function from a simple harmonic oscillator and the spring-mass system to represent bias mass above the vibrator, general agreement was found between measured force time histories along a full-scale pile that was vibrated into a sand deposit (13) and those that were computed by means of the wave equation, and the mathematical model provided a reasonable prediction of rate of pile penetration. Although the authors did not publish the wave equation parameters needed to obtain

the correlations, they demonstrated that the wave equation can be adapted to the prediction of the behavior of piles during vibratory installation, which would include the prediction of vibrator parameters on pile driveability, thereby permitting the wave equation to be used as a tool to select vibro-driver properties.